Holocene and Latest Pleistocene Paleoseismology of the Salt Lake City Segment of the Wasatch Fault Zone, Utah, at the Penrose Drive Trench Site

by Christopher B. DuRoss[1], Michael D. Hylland[1], Greg N. McDonald[1], Anthony J. Crone[2], Stephen F. Personius[3], Ryan D. Gold[3], and Shannon A. Mahan[4]

[1] Utah Geological Survey, Salt Lake City, Utah
[2] U.S. Geological Survey, retired
[3] U.S. Geological Survey, Golden, Colorado
[4] U.S. Geological Survey, Denver, Colorado

Suggested citation:

DuRoss, C.B., Hylland, M.D., McDonald, G.N., Crone, A.J., Personius, S.F., Gold, R.D., and Mahan, S.A., 2014, Holocene and latest Pleistocene paleoseismology of the Salt Lake City segment of the Wasatch fault zone, Utah, at the Penrose Drive trench site, *in* DuRoss, C.B. and Hylland, M.D., Evaluating surface faulting chronologies of graben-bounding faults in Salt Lake Valley, Utah—new paleoseismic data from the Salt Lake City segment of the Wasatch fault zone and the West Valley fault zone—Paleoseismology of Utah, Volume 24: Utah Geological Survey Special Study 149, p. 1–39, 6 appendices, 1 plate, CD.

CONTENTS

FIGURES

TABLES

PLATE

Holocene and Latest Pleistocene Paleoseismology of the Salt Lake City Segment of the Wasatch Fault Zone, Utah, at the Penrose Drive Trench Site

by Christopher B. DuRoss, Michael D. Hylland, Greg N. McDonald, Anthony J. Crone, Stephen F. Personius, Ryan D. Gold, and Shannon A. Mahan

ABSTRACT

The Salt Lake City segment (SLCS) of the Wasatch fault zone (WFZ) and the West Valley fault zone (WVFZ) comprise Holocene-active normal faults that bound a large intrabasin graben in northern Salt Lake Valley and have evidence of recurrent, large-magnitude (M ~6–7) surface-faulting earthquakes. However, at the time of this investigation, questions remained regarding the timing, displacement, and recurrence of latest Pleistocene and Holocene earthquakes on the northern SLCS and WVFZ, and whether the WVFZ is seismically independent of, or moves coseismically with, the SLCS.

To improve paleoseismic data for the SLCS, we conducted a fault-trench investigation at the Penrose Drive site on the northern SLCS. Two trenches, excavated across an 11-m-high scarp near the northern end of the East Bench fault, exposed colluvial-wedge evidence for five or six (preferred) surface-faulting earthquakes postdating the Provo-phase shoreline of Lake Bonneville (~14–18 ka). Radiocarbon and luminescence ages support earthquake times at 4.0 ± 0.5 ka (2σ) (PD1), 5.9 ± 0.7 ka (PD2), 7.5 ± 0.8 ka (PD3a), 9.7 ± 1.1 ka (PD3b), 10.9 ± 0.2 ka (PD4), and 12.1 ± 1.6 ka (PD5). At least one additional earthquake occurred at 16.5 ± 1.9 ka (PD6) based on an erosional unconformity that separates deformed Lake Bonneville silt and flat-lying Provo-phase shoreline gravel. Earthquakes PD5–PD1 yield latest Pleistocene (post-Provo) and Holocene mean recurrence intervals of ~1.6 kyr and ~1.7–1.9 kyr, respectively. Using 1.0–1.4 m of per-event vertical displacement for PD5–PD1, latest Pleistocene and Holocene vertical slip rates for the Penrose Drive site are 0.5–0.9 mm/yr. These data correspond well with the results of previous investigations: PD1–PD3b corroborate previously identified SLCS earthquakes at 4–10 ka, PD4 and PD5 occurred within an ~8-kyr (17–9 ka) time interval on the SLCS previously interpreted as a period of seismic quiescence, and PD6 possibly corresponds with a previously identified earthquake at ~17 ka (although both events have large timing uncertainties).

The Penrose Drive data, when combined with previous paleoseismic results, improve the latest Pleistocene–Holocene earthquake chronology of the SLCS, and demonstrate that the SLCS has been a consistently active source of large-magnitude earthquakes since the latest Pleistocene. At least nine surface-faulting earthquakes (S1–S9) have occurred since the highstand of Lake Bonneville (~18 ka). Where the SLCS earthquake record is most complete (since ~14 ka), per-site estimates of mean recurrence are similar for the latest Pleistocene (post-Provo) (~1.6 kyr), Holocene (~1.6–1.9 kyr), and late Holocene (~1.2–1.4 kyr). These SLCS paleoearthquake data indicate an essentially stable rate of earthquake recurrence since the latest Pleistocene and are important for understanding the earthquake potential of the SLCS, clarifying the seismogenic relation between the SLCS and WVFZ, and forecasting the probabilities of future large-magnitude earthquake in the Wasatch Front region.

INTRODUCTION

Purpose and Scope

The Salt Lake City segment (SLCS) of the Wasatch fault zone (WFZ) and the West Valley fault zone (WVFZ) comprise Holocene-active normal faults that together form a 3–12-km-wide intrabasin graben in the northern part of Salt Lake Valley (figures 1 and 2). These faults trend through the most densely populated part of Utah and have evidence of recurrent, large-magnitude (M ~6–7) surface-faulting earthquakes, but, because of urbanization, have received limited paleoseismic study. At the time of this investigation, significant questions remained regarding the paleoseismic histories of both faults, including (1) the timing of Holocene earthquakes on the northern SLCS (previous paleoseismic data were limited to the southern third of the segment), (2) the timing, recurrence, and displacement of mid-Holocene to latest Pleistocene earthquakes on both faults, and (3) whether the WVFZ is seismically independent of, or moves coseismically with, the SLCS. Understanding these fault characteristics is critical to accurately quantifying the seismic hazard of the central Wasatch Front.

To improve the quality and resolution of paleoseismic data for the SLCS and WVFZ, as well as our understanding of the seismic relation between them, we completed fault-trench investigations at two sites—one on the SLCS (Penrose Drive

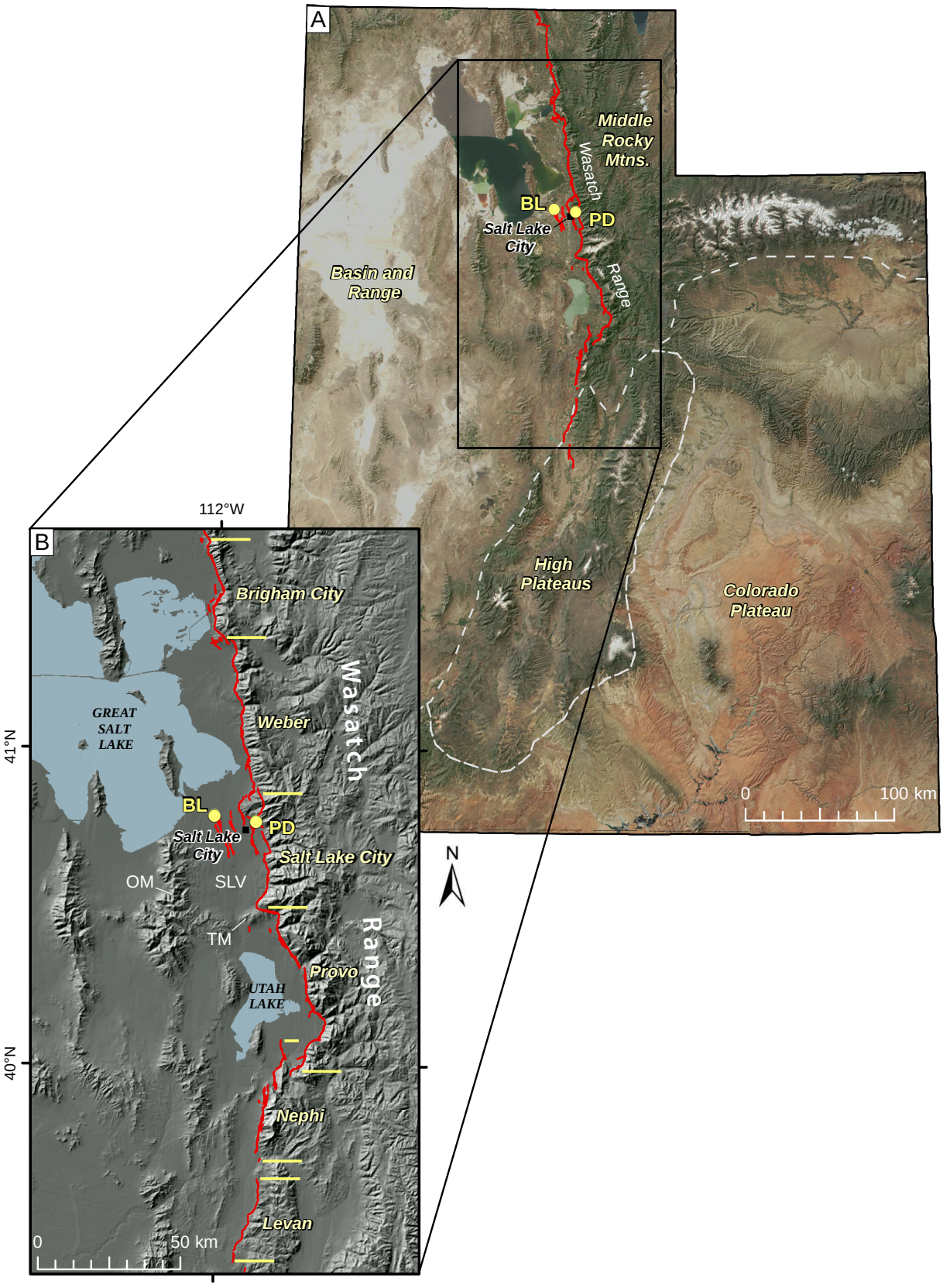

Figure 1. *(A) Physiographic provinces of Utah (gray dashed lines; AGRC, 2012), showing the Wasatch fault (red) and the general location of the Penrose Drive (PD; this study) and Baileys Lake (BL; Hylland and others, 2014) trench sites. Base map: true-color satellite image from the National Aeronautics & Space Administration (NASA, 2006; taken May 31, 2001) overlain on a 90-m digital elevation model (DEM; AGRC, 2012). (B) Central segments of the Wasatch fault zone from Black and others (2003). Horizontal yellow lines indicate segment boundaries. Base map: 90-m DEM (AGRC, 2012). OM – Oquirrh Mountains, SLV – Salt Lake Valley, TM – Traverse Mountains.*

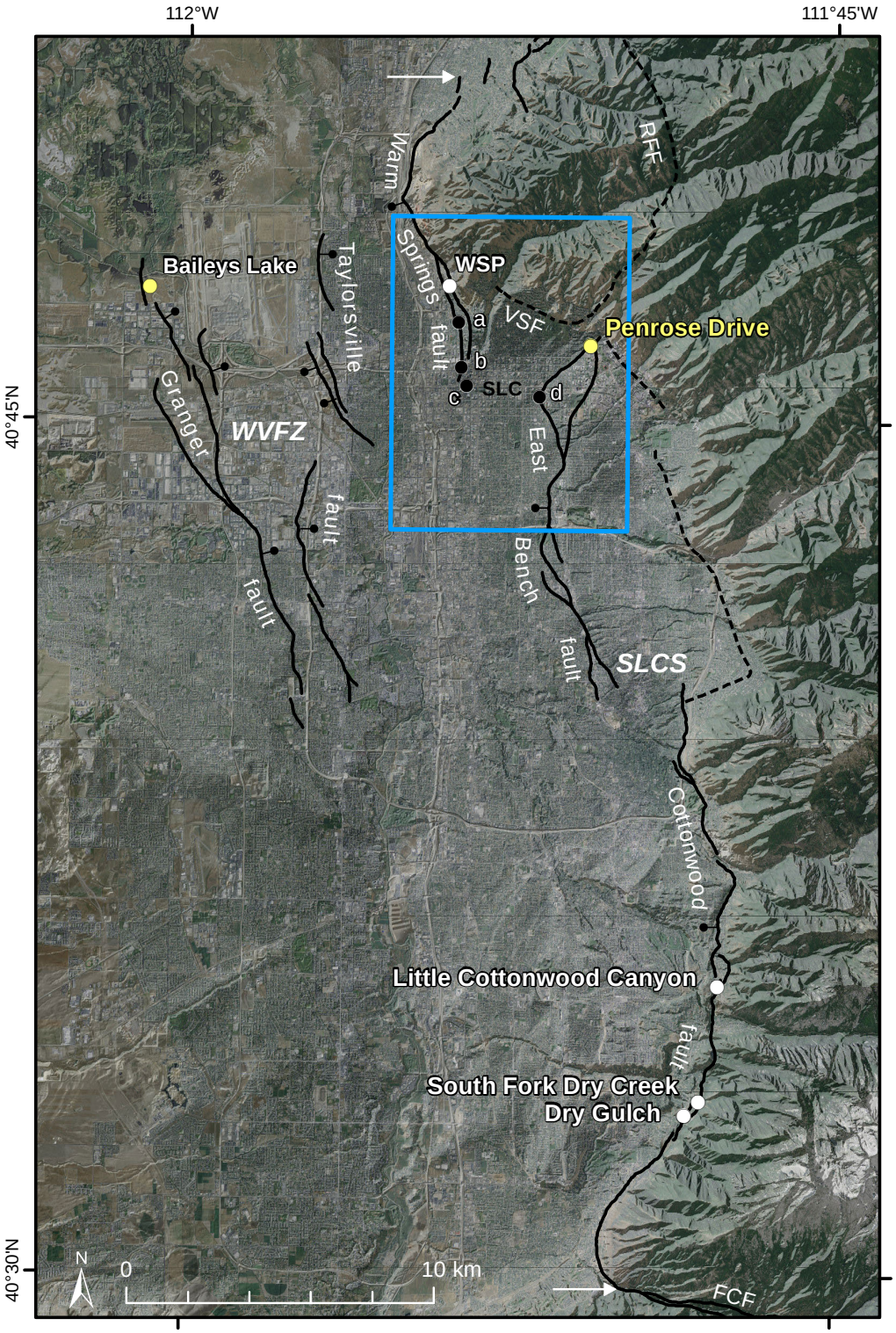

Figure 2. *Holocene-active traces of the Salt Lake City segment (SLCS) of the Wasatch fault zone and the West Valley fault zone (WVFZ) (solid black lines; Black and others, 2003; dashed lines are pre-Holocene traces), showing the Penrose Drive (this study) and Baileys Lake (Hylland and others, 2014) trench sites (yellow circles). White circles denote the Warm Springs Park (WSP) trench site (this study) and previous SLCS trench studies. Black circles indicate paleoseismic investigations that provided fault-location information, but not individual earthquake-timing data: a. Washington Elementary School (Robison and Burr, 1991), b. Salt Palace expansion project (Kleinfelder, 1999; Simon-Bymaster, 1999), c. 400 South cone penetrometer study (Leeflang, 2008), d. Dresden Place (Machette and others, 1992). FCF – Fort Canyon fault, RFF – Rudys Flat fault, VSF – Virginia Street fault. White arrows indicate the northern and southern ends of the SLCS. Base map is 2011 color aerial photography (USDA, 2012) overlain on a 2-m DEM (AGRC, 2012). Box outlined in blue shows extent of figure 3.*

site) and one on the WVFZ (Baileys Lake site). The trench investigation at Penrose Drive is the subject of this paper; for paleoseismic results from the Baileys Lake trench study, see the companion paper by Hylland and others (2014; this volume). These two reports supersede the initial release of the study results in a Final Technical Report to the USGS (DuRoss and Hylland, 2012). A separate paper (DuRoss and Hylland, in review) will integrate the results of these two investigations and include expanded discussions on the SLCS paleoearthquake history and the seismogenic relation between the SLCS and WVFZ.

Our Penrose Drive investigation included (1) detailed topographic and geologic mapping of the trench site, (2) scarp profiling, (3) excavating two trenches, (4) mapping the trench-wall exposures in detail, (5) sampling organic remains and fine-grained detrital sediment for radiocarbon and luminescence dating, respectively, (6) developing probabilistic models of earthquake times using OxCal software, and (7) determining earthquake chronologies, vertical displacement, recurrence, and fault slip rate. These data refine earthquake chronologies, mean-recurrence intervals, and slip-rate estimates for the SLCS, and, when combined with paleoseismic results from the Baileys Lake investigation, improve our understanding of how the SLCS and WVFZ interact seismogenically (Hylland and others, 2014).

Geologic Setting

Salt Lake Valley occupies one of several north-south-trending grabens at the eastern margin of the actively extending Basin and Range Province. The Wasatch Range and Oquirrh Mountains bound the valley on the east and west, respectively; Great Salt Lake lies to the north; and the east-west-trending Traverse Mountains separate Salt Lake Valley from Utah Valley to the south (figure 1). Two Quaternary geologic features that have been particularly important in producing the modern physiography of the region are the WFZ and late Pleistocene Lake Bonneville.

The WFZ, the longest active normal-slip fault in the western United States and the most active fault in Utah, forms a prominent structural boundary between the actively extending Basin and Range Province and the relatively more stable Middle Rocky Mountain and Colorado Plateau provinces to the east. Extending 350 km from southern Idaho to central Utah, the WFZ includes 10 segments, 5 of which have evidence of repeated Holocene earthquakes (Machette and others, 1992). Each segment is generally considered seismogenically independent on the basis of (1) fault structure and range-front morphology, (2) shallowly buried bedrock at fault salients, (3) geophysical data indicating separate hanging-wall basins, (4) late-Quaternary fault-trace geometries, and (5) for the central segments, unique Holocene surface-faulting earthquake chronologies (Swan and others, 1980; Schwartz and Coppersmith, 1984; Machette and others, 1992; Wheeler and Krystinik, 1992). However, available paleoseismic data permit exceptions to the traditional model of individually rupturing segments (e.g., multi-segment ruptures considered by Chang and Smith, 2002; DuRoss, 2008; and DuRoss and others, 2011). Since the mid-Holocene (~6 ka), surface-faulting earthquakes have occurred on average every 1300–2500 years per segment (Lund, 2005), and average vertical slip rates range from about 0.5 to 2.2 mm/yr using paleoseismic and geomorphic data (Machette and others, 1992; Friedrich and others, 2003; Lund, 2005).

Lake Bonneville was the most recent and largest of several pluvial lakes to occupy the eastern Great Basin during the Pleistocene (Gilbert, 1890). Details of Lake Bonneville's history are the subjects of ongoing research, but the general record of the rise and fall of the lake is well established. As summarized by Currey (1990) and Oviatt and others (1992), and recently updated by Godsey and others (2005, 2011), Oviatt and others (2005), Benson and others (2011), and Miller and others (2013), the Bonneville lake cycle began around 30 ka. Over time, the lake rose and eventually reached its highest level at the Bonneville shoreline (~1550 m [5090 ft] above mean sea level [amsl]) around 18 ka. At the Bonneville highstand, lake water overflowed the Bonneville basin threshold at Zenda in southeastern Idaho, spilling into the Snake–Columbia River drainage basin. In Salt Lake Valley, the Bonneville highstand is generally expressed as a single, prominent shoreline.

Around 17.6 ka, the Zenda threshold failed catastrophically, resulting in a rapid drop in lake level of approximately 110 m during the Bonneville Flood. The lake level stabilized when erosional downcutting was stopped by a bedrock-controlled threshold near Red Rock Pass, about 2.5 km south of Zenda, or possibly about 9 km farther south near Swan Lake (Janecke and Oaks, 2011). The lake remained at or near this level until about 14–15 ka (Godsey and others, 2005, 2011), forming the Provo shoreline (~1450 m [4760 ft] amsl). In Salt Lake Valley, the Provo shoreline is less well expressed than the Bonneville shoreline.

A climatic change to warmer and drier conditions caused the lake to regress rapidly from the Provo shoreline to near desiccation levels by the end of the Pleistocene (Eardley, 1962; Currey and others, 1988b; Currey, 1990). A small rise in lake level to an elevation of 1295 m (4250 ft) amsl marked the Gilbert phase around 12 ka (Oviatt and others, 2005; Benson and others, 2011), after which the lake regressed to near modern Great Salt Lake levels (historical average elev. 1280 m [4200 ft] amsl) (Currey, 1988a). The remarkable stratigraphic and geomorphic records of Lake Bonneville have proven extremely valuable in reconstructing the paleoseismic history of the WFZ, particularly along the central segments of the fault.

Surface Faulting in Salt Lake Valley

Salt Lake City Segment of the Wasatch Fault Zone

The 40-km-long SLCS consists of three subsections separated by left steps: the Warm Springs, East Bench, and Cottonwood faults (Scott and Shroba, 1985; Personius and Scott, 1992) (figure 2). At the northern end of the SLCS, the Warm Springs fault marks the western edge of the Salt Lake salient, a fault-bounded block of Tertiary bedrock that defines the boundary between the SLCS and the Weber segment to the north. The Warm Springs fault is at least 7.5 km long (Personius and Scott, 1992) and may extend an additional 3 km southward (e.g., Scott and Shroba, 1985; Black and others, 2003) into downtown Salt Lake City, where possible evidence of surface faulting has been exposed in construction exposures (Simon-Bymaster, Inc., 1999). At the southern end of the Warm Springs fault, the SLCS steps east about 3–4 km to the East Bench fault (figure 3), where large, prominent scarps are about 3–5 km west of the range front. The East Bench fault bounds uplifted and incised alluvial-fan surfaces and Lake Bonneville sediments, and has multiple, anastomosing traces that continue southward for 12 km. At the southern end of the East Bench fault, the SLCS steps 2–3 km eastward to the Cottonwood fault—the longest subsection of the SLCS. The Cottonwood fault is a complex fault zone that follows the range front and has large scarps, which bound prominent, but relatively narrow (<500 m wide) grabens. The Cottonwood fault extends for about 20 km to the southern end of the SLCS, where the Traverse Mountains and east-west oriented Fort Canyon fault separate the SLCS from the Provo segment (Bruhn and others, 1992).

The earliest movement on the WFZ in the Salt Lake City area likely occurred about 17.6 ± 0.7 Ma based on a K-Ar age on sericite from fault rock exhumed from ~11 km depth (Parry and Bruhn, 1987). Continued fault movement uplifted and exhumed the range along the northern SLCS at a rate of about 0.2–0.4 mm/yr over the past 5 myr, compared to 0.6–1.0 mm/yr over 2.5 Ma for the southern SLCS (Armstrong and others, 2004). The faster exhumation rate to the south is consistent with the steep range-front morphology (Armstrong and others, 2004) and the location of the greatest structural throw on the SLCS (Parry and Bruhn, 1987).

Previous paleoseismic data for the SLCS are from fault-trench investigations at Little Cottonwood Canyon (LCC) and South Fork Dry Creek (SFDC) (table 1), both at the south end of Salt Lake Valley on the Cottonwood fault (figure 2). In an early study at LCC, Swan and others (1981) found evidence of two to three Holocene earthquakes, but they were only able to determine an early Holocene minimum limiting age for the second (penultimate) earthquake. In 1999, McCalpin (2002) reoccupied the LCC site and, with a "megatrench" investigation, extended the paleoseismic record for the southern SLCS into the latest Pleistocene. McCalpin (2002) interpreted seven post-Bonneville (<18 ka) earthquakes, including four earthquakes younger than about 6 ka. Significantly, McCalpin (2002) interpreted a period of seismic quiescence on the SLCS between about 17 and 9 ka. Using the lower (western) fault zone exposed at LCC, which has colluvial-wedge evidence of the youngest four events, McCalpin (2002) estimated an average displacement of 1.8 m per event using the total displacement (~7.5 m) across the fault. This average displacement estimate does not account for possible displacement on the upper (eastern) fault and thus could be a minimum value.

At SFDC, about 5 km south of LCC, the WFZ forms a complex zone of faulting in Holocene alluvial-fan deposits. Schwartz and Lund (1988) excavated trenches across three of six scarps at SFDC, and reported maximum-limiting ages for two earthquakes. In a follow-up study at SFDC, Lund and Mayes (1995) excavated five trenches (resulting in all of the scarps at the site being trenched) and constrained the timing of four earthquakes. The SFDC data, combined with the results of a geotechnical trench excavation at Dry Gulch (Black and others, 1996), established the current chronology of four earthquakes younger than 5.3 ka on the Cottonwood fault (Black and others, 1996; Lund, 2005; table 1). Per-event displacements are about 1.5–2.5 m based on a debris-flow levee vertically offset by two and possibly three surface-faulting events (Black and others, 1996; DuRoss, 2008).

Two exploratory trenches excavated in 1986 across the East Bench fault at the Dresden Place site (Machette and others, 1992; figure 2), about 2 km southwest of Penrose Drive (figure 3), also provide paleoseismic data for the SLCS. The trenches exposed 3 m of plastic, monoclinal warping in Lake Bonneville (highstand?) laminated silt and clay. This deformation likely occurred during a single earthquake between the highstand of Lake Bonneville (about 18 ka) and dewatering of the site following the regression from the Provo shoreline (about 14 ka) (Machette and others, 1992). An additional 4 m or more of post-Bonneville (~Holocene) faulting occurred during one or more earthquakes; however, individual earthquake times were not constrained.

Table 1. *Summary of previous late Holocene earthquake-timing data for the Salt Lake City segment.*

Earthquake	South Fork Dry Creek[1] (ka)	Little Cottonwood Canyon[2] (ka)	UQFPWG Consensus[3] (ka)
Z	*shortly after* 1.3 +0.25/-0.2	~1.3	1.3 ± 0.7
Y	*shortly after* 2.45 ± 0.35	~2.3	2.5 ± 0.6
X	*shortly after* 3.95 +0.55/-0.45	~3.5	4.0 ± 0.6
W	*shortly after* 5.3 +0.45/-0.35	~5.3	5.3 ± 0.8

[1] Black and others (1996); includes the Dry Gulch trench.
[2] McCalpin (2002).
[3] SLCS consensus earthquake timing (and estimated 5th–95th percentile uncertainty) of the Utah Quaternary Fault Parameters Working Group (UQFPWG; Lund, 2005), rounded to the nearest century.

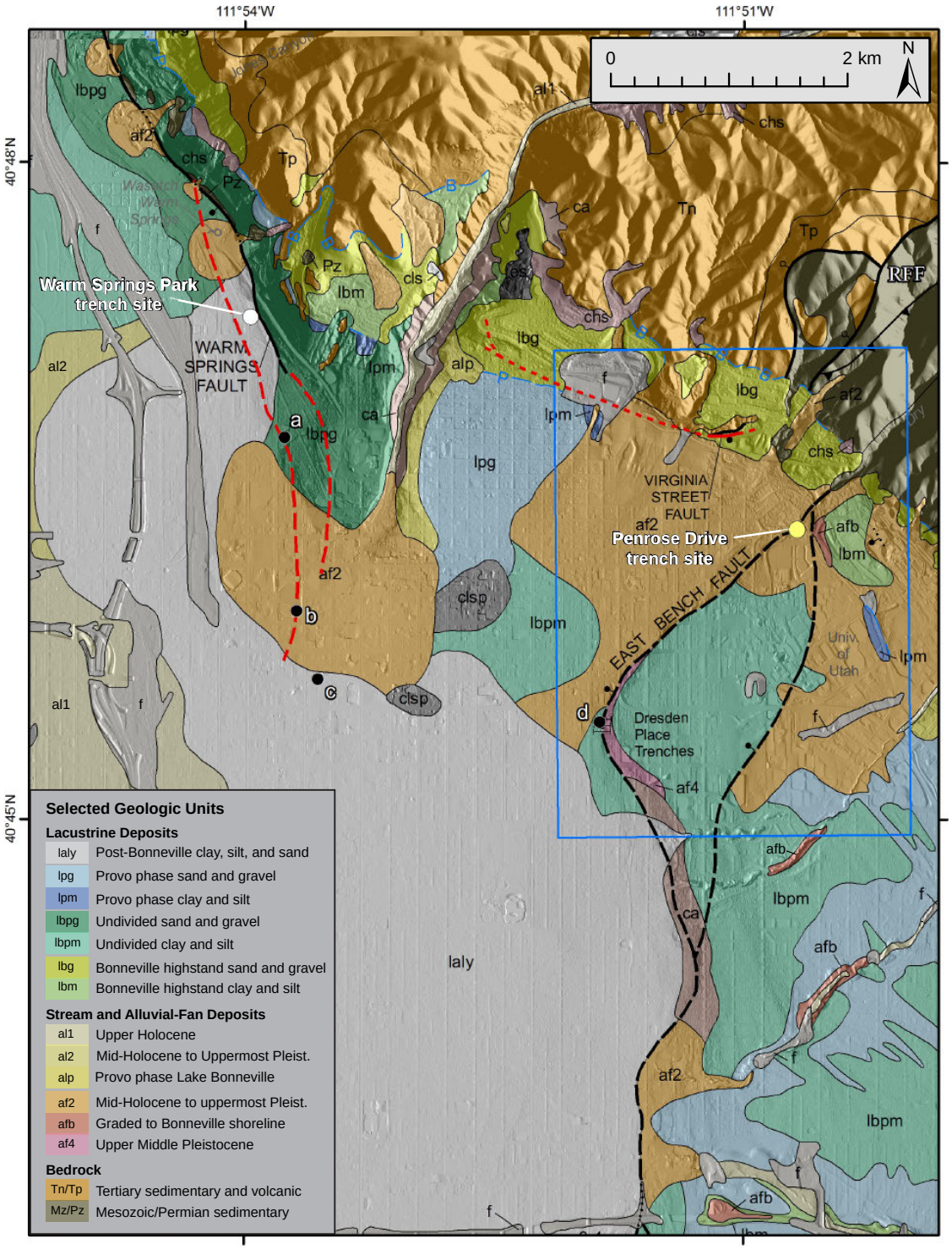

Figure 3. *Surficial geologic map of the northern East Bench fault and southern Warm Springs fault modified from Personius and Scott (1992; GIS data from Personius and Scott, 2009). Heavy black lines are normal faults, dashed where inferred; ball and bar on down-thrown side; RFF – Rudys Flat fault. Red dashed lines show trace of the Warm Springs fault based on Scott and Shroba (1985; data from Black and others, 2003); red solid and dotted lines show trace of the Virginia Street fault from Van Horn and Crittenden (1987). Blue lines are Bonneville highstand (B) and Provo-phase (P) shorelines. For a complete description of map units, see Personius and Scott (1992). Black circles correspond with those on figure 2. Base map is 2-m DEM (AGRC, 2012) with hillshade illumination from the east. Box outlined in blue shows extent of figure 5.*

Geotechnical studies of the Warm Springs fault offer valuable information on the location, style, and relative timing of faulting on the SLCS, but provide only limited earthquake-timing data. For example, trenches on the southern Warm Springs fault (Washington Elementary School site; figure 2) indicated 12 m of displacement since about 15 ka, but the timing of individual earthquakes is unknown (Robison and Burr, 1991). At the Salt Palace Convention Center in downtown Salt Lake City (figure 2), construction excavations and exploratory trenches revealed complex fault zones and grabens likely related to at least one surface-faulting earthquake (Simon-Bymaster, 1999; Simon and Shlemon, 1999). Two radiocarbon ages for bulk-soil sediment limit the timing of faulting in one of several trenches to a maximum of ~9.0 ka (no mean-residence-time correction applied). Charcoal from a different trench limited the timing of a presumably younger earthquake to before ~7.4 ka (Kleinfelder, 1999; Simon-Bymaster, 1999). The location of the Salt Palace faults coincides with the inferred southern extent of the Warm Springs fault mapped by Scott and Shroba (1985). However, Kleinfelder (1999) and Korbay and McCormick (1999a) interpreted the complex fault zone as a liquefaction-induced lateral spread in post-Bonneville sediments, relying on cone-penetrometer (CPT) data (contoured in Simon-Bymaster, 1999) that show minimal (less than ~1 m) vertical offset in Lake Bonneville sediments across the grabens. However, we note that the CPT data (1) were irregularly distributed across the Salt Palace site and that few points extended west, beyond the grabens; and (2) have poor vertical accuracies due to surveying errors (Korbay and McCormick, 1999b). Finally, the CPT data considered did not include ~3 m of vertical offset in Bonneville sediments measured in sounding CP-9 as the location was not surveyed (Simon-Bymaster, 1999). To address these fault versus lateral-spread interpretations, Leeflang (2008) completed a 1.7-km long, east-west CPT line along 400 South (about 0.5 km south of the Salt Palace) across the projected trace of the Warm Springs fault (figure 2). Leeflang (2008) interpreted tectonic displacement near the projected trace of the fault due to (1) 10.4–11.8 m of vertical offset in pre-Bonneville alluvium and transgressive (basal) Lake Bonneville sediments based on three CPT soundings over a horizontal distance of 460 m (soundings to the east and west show flat-lying Lake Bonneville sediments), (2) an increase in the thickness of the transgressive deposits on the down-thrown side of the inferred fault zone (from about 4–7 m to 12 m thick), (3) differential offset between transgressive (basal) and regressive (upper) Lake Bonneville sediments, which indicate multiple surface-faulting earthquakes at the site, and (4) liquefaction analysis using the CPT data that only supports minor settlement and lateral-spread displacements.

West Valley Fault Zone

The WVFZ consists of intrabasin normal faults that span an area 16 km long by 1–6 km wide in the northern part of Salt Lake Valley (figure 2). The two subparallel, northwest-trending main traces and their associated subsidiary traces are known as the Granger fault (western traces) and Taylorsville fault (eastern traces). Both faults have scarps on post-Bonneville lake cycle (latest Pleistocene to Holocene) lacustrine and alluvial deposits, and previous paleoseismic studies (Keaton and others, 1987; Keaton and Currey, 1989) have documented multiple Holocene surface-faulting earthquakes. The scarps are typically about 0.5–1.5 m high, but have a maximum height of 6 m near the southern end of the Granger fault. Scarps on the Granger fault face east, and scarps on the Taylorsville fault face both east and west. As a whole, the WVFZ is considered an antithetic structure to the west-dipping SLCS master or controlling fault (e.g., Bruhn and Schultz, 1996).

Previous studies have produced a long-term (140 kyr) slip history for the WVFZ, but timing and displacement data for individual surface-faulting earthquakes have been lacking. For example, Keaton and others (1987) and Keaton and Currey (1989) mapped parts of the fault, excavated trenches, and drilled numerous boreholes. Boreholes on the Granger fault indicate 0.7–3 m of displacement in post-Bonneville sediments (<12 ka) and 5–7 m in Bonneville lake-cycle deposits (12–28 ka), but no evidence of individual surface-faulting events. Trenches excavated by consultants have yielded earthquake-timing information for the WVFZ where the Utah Geological Survey (UGS) was able to sample organic sediment for radiocarbon dating. Radiocarbon ages from these trenches indicate surface faulting earthquakes on the Granger fault at about 1.3–1.7 ka (unpublished UGS data) and Taylorsville fault at about 2.2 ka (Solomon, 1998), which correspond well with the timing of the youngest SLCS earthquakes (table 1). However, the context of the samples and their relation to earthquake timing is not well understood owing to brief site visits that precluded detailed logging and the nature of the bulk-soil (apparent mean residence time [AMRT]) ages, which are difficult to interpret (Machette and others, 1992).

Why Trench the Salt Lake City Segment?

Because of extensive development in Salt Lake Valley, limited paleoseismic data are available for the SLCS. Previous research trenches on the SLCS define several Holocene surface-rupturing events; however, these studies have been limited to the Cottonwood fault on the southern part of the SLCS, which is about 15 km southeast of the southernmost scarps on the WVFZ. In addition, important questions remain regarding the mid-Holocene to latest Pleistocene earthquake record for the SLCS, including whether earthquakes occurred between 17 and 9 ka. Finally, previous investigations of the SLCS relied on AMRT radiocarbon ages, which are problematic in that they are composite ages that reflect the total age distribution of carbon in the sampled soil and require a mean-residence-time (MRT) correction based on the assumed age of the soil at the time of burial (Machette and others, 1992). Because of these limitations, the previously available data are insufficient to understand the timing and rupture extent of earthquakes on both the northern and southern SLCS, as well as their relation to earthquakes on the WVFZ.

OVERVIEW AND METHODS

Trench Investigations

We identified trench sites on the SLCS using (1) fault-trace and surficial-geologic mapping by Scott and Shroba (1985) and Personius and Scott (1992); (2) our interpretation of 1937 (Agricultural Stabilization and Conservation Service, 1937) and 1970s (low-sun-angle) aerial photographs (Cluff and others, 1970; included in Bowman and others, 2009) and 2006–2009 orthophotography from the National Agricultural Imagery Program (NAIP) (U.S. Department of Agriculture [USDA], 2012; Utah Automated Geographic Reference Center [AGRC], 2012); (3) 2-m-posting LiDAR data for Salt Lake Valley (AGRC, 2012); and (4) field reconnaissance of prospective sites. We also considered the discussions and analyses of SLCS paleoseismic data by the Utah Quaternary Fault Parameters Working Group (UQFPWG; e.g., Lund, 2005, 2007) prior to selecting preferred sites. We found only three potential sites on the SLCS, and we excavated trenches at two of them: the Warm Springs Park site on the southern Warm Springs fault and the Penrose Drive site on the northern part of the East Bench fault (figures 2 and 3).

Warm Springs Park Site

Warm Springs Park is close to the southern end of the Warm Springs fault (figure 3) where Gilbert (1890) documented evidence of Holocene surface faulting. However, at the time of our study, virtually the entire Warm Springs fault had been modified by extensive development or aggregate mining. As a result, the Warm Springs Park site provided the only opportunity to conduct a paleoseismic trench investigation. We excavated three trenches at the site in May 2010 (figure 4), but only exposed cultural fill and extensively modified sediments. Two northern trenches, which were 8 and 21 m long, exposed cultural fill to a depth of about 4–5 m. About 0.4 km south, an 8-m-long and about 2-m-deep southern trench encountered rotated blocks of probable Tertiary Salt Lake Formation that are likely landslide deposits, but no evidence of faulting. Because we did not encounter in-place native deposits or expose the WFZ, we did not clean or map these trench exposures. Thus, we show the site and trench locations on figure 4, but do not discuss the Warm Springs site further.

Penrose Drive Site

The Penrose Drive site is near the northern end of the East Bench fault (figures 3 and 5), north of the University of Utah campus (near the intersection of Penrose Drive and Military Way in Salt Lake City), where a northwest-facing scarp crosses Lake Bonneville sediments and post-Bonneville alluvial-fan deposits (Personius and Scott, 1992). This site was one of only a few possible trench sites on the East Bench fault that had not been fully developed. We chose the site because of the simple geometry and moderately large height of the fault scarp, and because the site had minimal evidence of cultural disturbance based on examination of the 1937–2009 aerial photographs (figure 6).

Figure 4. *Warm Springs Park trench site on the southern Warm Springs fault. Because we exposed only manmade fill or landslide blocks of Tertiary Salt Lake Formation and did not expose the Wasatch fault, we did not clean or map these trenches. Base map is 2009 NAIP data (USDA, 2012; AGRC, 2012). Red shaded areas show excavated trenches.*

We excavated two trenches at Penrose Drive in May 2010: a 36-m-long western trench and, 20 m to the northeast, a 14-m-long, parallel eastern trench (figure 7). The western trench was generally less than 4 m deep, whereas the eastern trench reached depths of about 5 m. To map the exposures, we used an electronic distance meter (Trimble TTS 500) to measure the positions of markers (e.g., nails and flagging) along stratigraphic contacts and structures and projected those points to a vertical plane that represented the average orientation of the trench wall. We then mapped the points for each wall at 1:20 scale on gridded drafting film and sketched in additional detail in the fault zones. The total station and averaged vertical plane were also used to set up a 1-m square grid on the trench walls, which we used as a reference grid to construct 1:20-scale photomosaics of the walls. We mapped the northeast-facing wall of the west trench, and the entire southwest-facing wall and uppermost northeast-facing wall of the east trench. Plate 1 includes maps and photomosaics of the exposures with a single

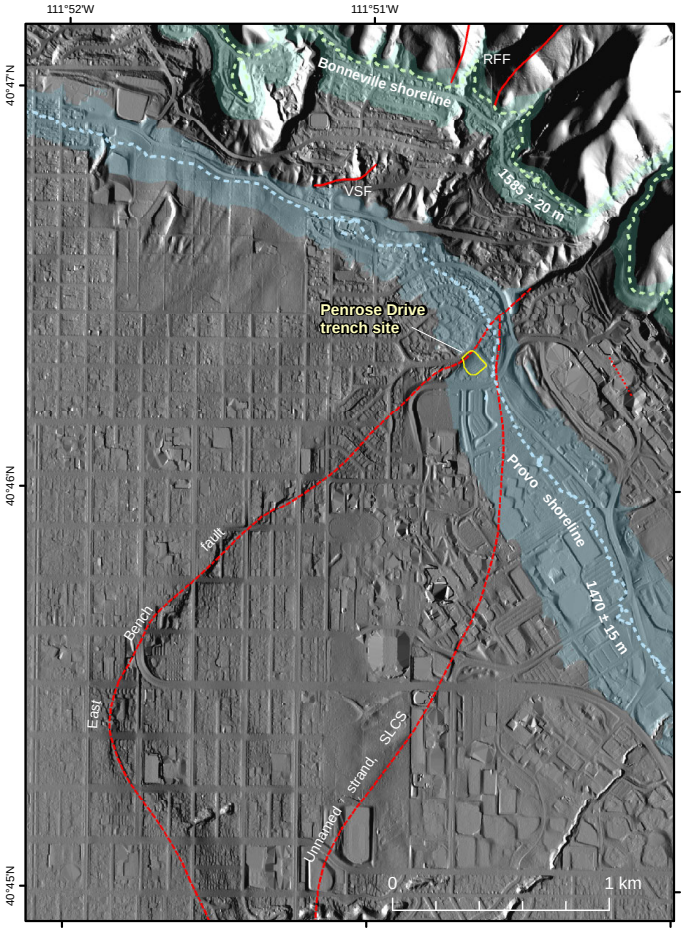

Figure 5. *Northern part of the East Bench fault, showing the Penrose Drive trench site and the approximate elevations of the Bonneville-highstand and Provo-phase shorelines of Lake Bonneville (shoreline elevations based on Currey, 1990; see text for discussion). Wasatch fault traces, including the Virginia Street fault (VSF) and Rudys Flat fault (RFF), are from Personius and Scott (1992, 2009). Yellow outline shows the Penrose Drive trench site (figure 7). Base map is 1-m DEM (AGRC, 2012) with hillshade illumination from the east.*

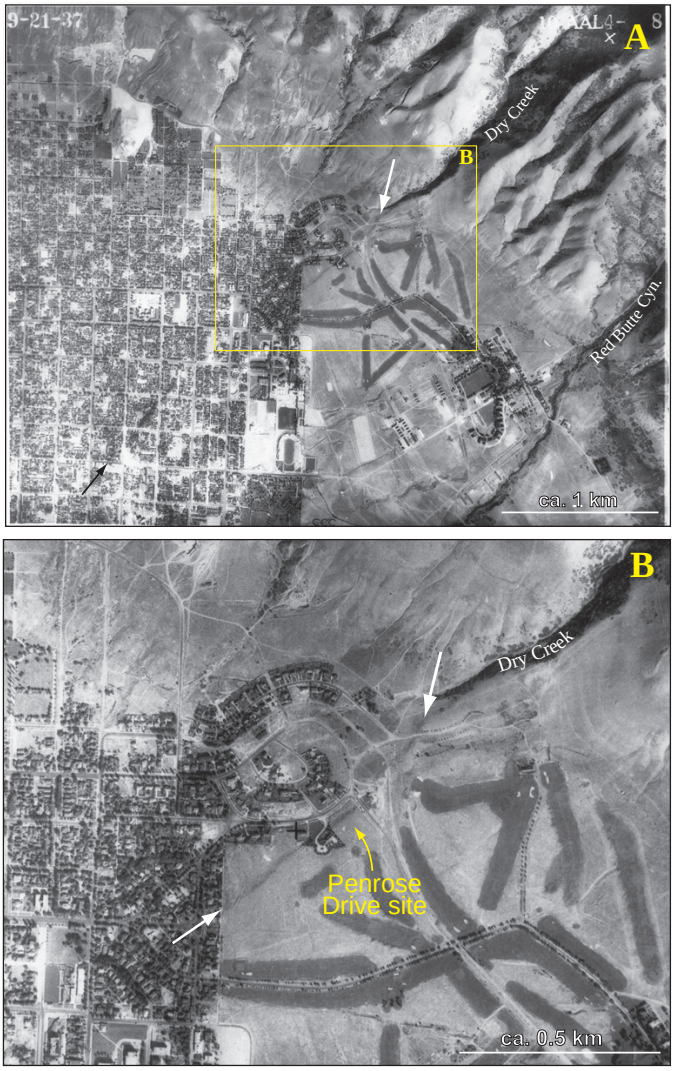

Figure 6. *(A) 1937 aerial photograph (AAL 4-8; Agricultural Stabilization and Conservation Service, 1937) showing the Penrose Drive trench site and the prominent expression of the East Bench fault scarps (denoted by black and white arrows). Yellow box shows area of figure 6B. (B) Detail of 1937 aerial photograph, showing the northernmost East Bench fault scarps (white arrows) and location of the Penrose Drive site.*

coordinate system for both trenches referenced using horizontal (h-) and vertical (v-) meter marks. For example, the fault zone exposed in the west trench is h-21.5 m, v-5.0 m, west trench; plate 1. Stratigraphic units are described in appendix A and summarized on plate 1.

Numerical Dating

Radiocarbon Dating

We sampled bulk soil A-horizon sediment (appendix B) and radiocarbon (^{14}C) dated discrete fragments of charcoal recovered from the horizons (appendix C) to estimate the ages of buried soil and to limit the timing of paleoearthquakes. For discussions of common sources of uncertainty in ^{14}C dating and paleoseismic studies, see Nelson and others (2006) and DuRoss and others (2011). To increase the likelihood of dating locally derived charcoal (e.g., sagebrush) rather than non-local (detrital) charcoal (e.g., conifer transported from higher elevations), PaleoResearch Institute (Boulder, Colorado) separated and identified by genus (if possible) charcoal fragments from bulk A-horizon sediment samples. Locally derived charcoal fragments are more likely burned in place or very close by, and therefore less likely to have an inherited, older age (Puseman and Cummings, 2005). Four of 20 individual charcoal samples from Penrose Drive could be identified (e.g., *Artemisia*—flowering plants such as sagebrush, and *Quercus*—oak; appendix B) and were likely locally derived. The remaining Penrose Drive samples only produced collections of small, unidentified charcoal fragments. For each sample, these unidentified fragments were recombined into samples of at least ~0.5 mg, which yielded composite charcoal ages.

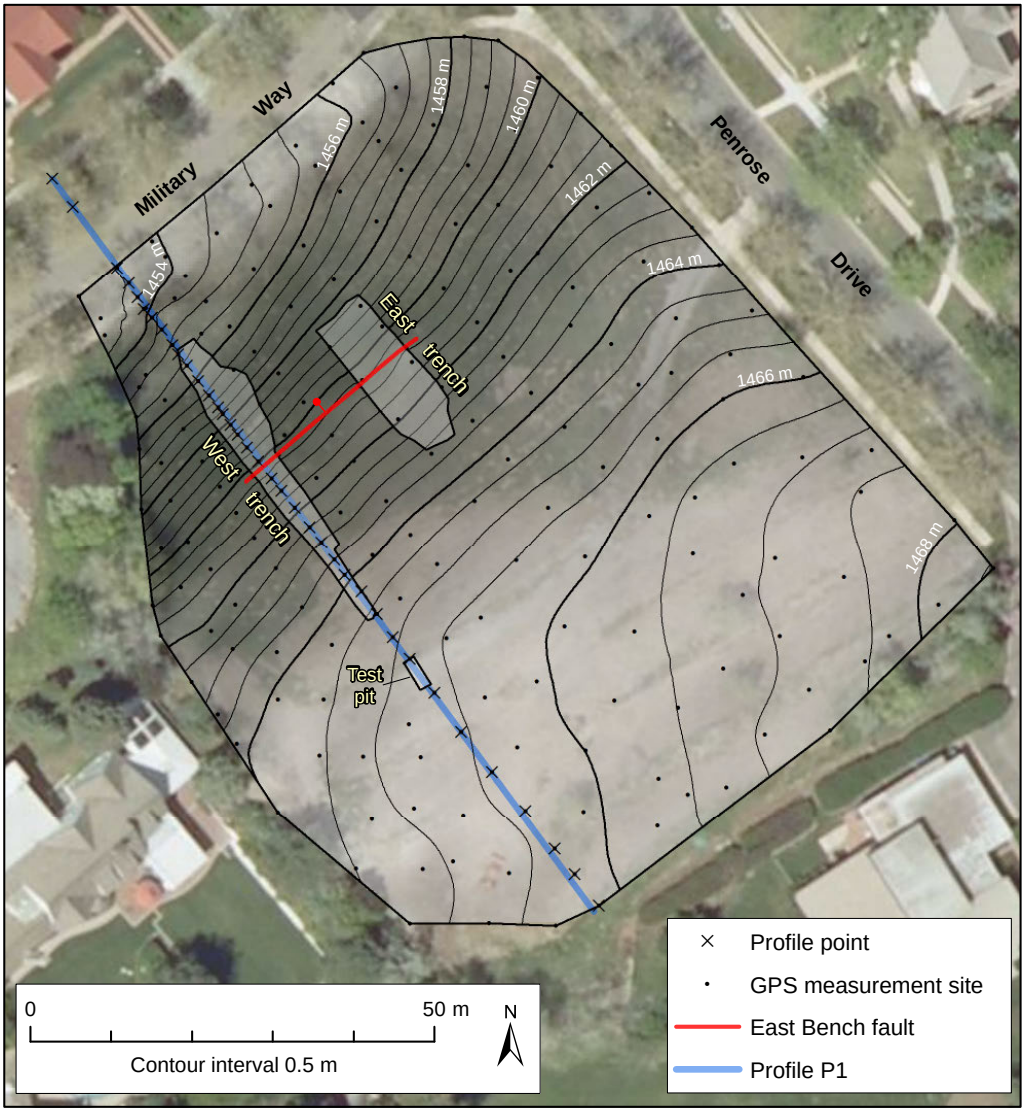

Figure 7. *Topographic map (0.5-m contours) of the Penrose Drive site based on survey-grade GPS data measured May 5–25, 2010. Traces of the East Bench fault exposed in the west and east trenches (and projected between them) are shown in red; ball and bar on down-thrown side. Blue line indicates scarp profile (figure 8). Contours interpolated using kriging method; hillshade illumination from the east. Base map is 2009 high resolution (25-cm) orthophotography (AGRC, 2012).*

Although detrital charcoal could have been present in either the unidentified or identified samples, the stratigraphic consistency of the ages and the similar ages between the unidentified and identified charcoal fragments (from the same A horizons) indicate minimal age uncertainty related to a detrital signal or post-depositional modification of the dated material.

We submitted the charcoal samples to the National Ocean Sciences Accelerator Mass Spectrometry (NOSAMS) Facility of the Woods Hole Oceanographic Institution (Woods Hole, Massachusetts) for accelerator mass spectrometry (AMS) ^{14}C dating. We report the radiocarbon ages as the mean and two-sigma (2σ) uncertainty rounded to the nearest century in thousands of calendar years before 1950 (ka) using the Reimer and others (2009) terrestrial calibration curve applied in OxCal (Bronk Ramsey, 1995, 2001).

Luminescence Dating

We used optically stimulated luminescence (OSL) dating to estimate burial ages of lacustrine and colluvial-wedge sediments at Penrose Drive (appendix D). OSL dating relies on the cumulative dose of in situ natural radiation in sediment (e.g., quartz grains) to estimate the time when the sediment was last exposed to sunlight prior to final deposition (Huntley and others, 1985). Ideally, the sunlight exposure was sufficiently long (about 10 minutes) during erosion and transport to fully reset or "zero" any preexisting luminescence signal in the grains, and thus the luminescence age should represent the time when the sediment was deposited (Aitken, 1994). If the sediment's exposure to sunlight was not long enough (e.g., because of rapid deposition, a short travel path, or filtered light in turbid water) to fully zero the sediment, then the sediment may re-

tain an inherited luminescence signal (Duller, 2008), which results in an overestimated (maximum) age for the deposit. In contrast, underestimated (minimum) ages result if the luminescence signal becomes saturated, where the signal does not increase despite continued exposure of the sediment to radiation (Duller, 2008). Saturation results in a maximum age limit for OSL dating of ~75–300 ka, depending on the radiation dose rate and mineral dated (Duller, 2008; Rhodes, 2011).

Luminescence ages for the Penrose Drive site (appendix D) include OSL ages on quartz grains (quartz-OSL) and in some cases, infrared-stimulated luminescence (IRSL) ages on feldspar grains measured as a complement to the OSL ages. We generally prefer the quartz-OSL ages because the IRSL signal takes longer to zero than the OSL signal—after sunlight exposure durations of about tens of seconds to minutes, there is a 1–2 order-of-magnitude difference in the remaining OSL and IRSL signals (Duller, 2008). However, OSL and IRSL ages that overlap within error provide an additional degree of confidence that partial bleaching (insufficient sunlight exposure) is not a problem in the sediments.

Our luminescence samples were processed at the U.S. Geological Survey Luminescence Dating Laboratory (Denver, Colorado). Background radiation from potassium, uranium, and thorium was measured in the field using a portable gamma-ray spectrometer; however, field moisture was measured in the laboratory. We report OSL ages (appendix D) as the mean and one-sigma uncertainty rounded to the nearest decade. However, where discussed in the text, the error is doubled (2σ rounded to the nearest century) for continuity with the calendar-calibrated ^{14}C ages and the modeling of earthquake times in OxCal. In discussing the OSL ages, we report the ages in thousands of years before the sample processing date (2010) (ka) and do not account for the 60-year difference in the OSL sample date (2010) versus the reference standard for ^{14}C (1950). This difference is minor compared to the large OSL age uncertainties (generally ~1–3 kyr at 2σ), and is accounted for in later modeling of earthquake times in OxCal (discussed below).

OxCal Modeling Methods

To evaluate earthquake timing and associated uncertainties, we used OxCal ^{14}C calibration and analysis software (version 4.1; Bronk Ramsey, 1995, 2001; using the IntCal09 calibration curve of Reimer and others, 2009). OxCal probabilistically models the timing of undated events (e.g., earthquakes) by weighting the time distributions of chronological constraints (e.g., radiocarbon and OSL ages and historical constraints) included in a stratigraphic model (Bronk Ramsey, 2008). The program generates a probability density function (PDF) for each event in the model, or the likelihood that an earthquake occurred at a particular time, using the chronologic and stratigraphic constraints and a Markov Chain Monte Carlo (MCMC) sampling method (Bronk Ramsey, 2008, 2009). For more detailed discussions of the application of OxCal modeling to paleoseismic data, see discussions by Lienkaemper and Bronk Ramsey (2009) and DuRoss and others (2011).

OxCal depositional models for the Penrose Drive site (appendix E) use stratigraphic ordering information, radiocarbon and OSL ages, and a historical constraint that no large surface-faulting earthquakes (M ~6.5+) have occurred since about 1847 to define the time distributions of earthquakes identified at the site. We correlated depositional units between the west and east trenches and constructed a single OxCal model for the site. Where necessary, we removed numerical-age outliers using geologic judgment (knowledge of sediments, soils, and sample contexts), the degree of inconsistency with other ages in the model for comparable deposits (e.g., stratigraphically inverted ages), and an agreement index between the original (unmodeled) and modeled numerical ages (Bronk Ramsey, 1995, 2008). For the SLCS, we also constructed OxCal models for the previously studied paleoseismic sites using available data. Because these previous investigations used bulk-soil-sediment (AMRT) ages, we used the Delta_R command to correct for the estimated residence time of the soil at the time of burial (see DuRoss and others [2011] for discussion). We report earthquake time ranges for each site as the mean and 2σ uncertainty in thousands of calendar years B.P. (ka) rounded to the nearest century.

PENROSE DRIVE TRENCH SITE, SALT LAKE CITY SEGMENT

Surface Faulting and Geology

The Penrose Drive site is at the northern end of the East Bench fault, where the Holocene trace of the SLCS trends 230° (N. 50° E.) for about 3 km before terminating at the mouth of Dry Creek (Personius and Scott, 1992; figures 3 and 6). The northern East Bench fault is separated from the Warm Springs fault to the west by a 3–4-km-wide overlapping left step (figure 2). No known Holocene faults span the step-over zone between these faults; however, a short, less than 0.5-km-long (Personius and Scott, 1992) to ~2.5-km-long (Van Horn and Crittenden, 1987), west-northwest trending normal fault (Virginia Street fault [VSF]; figures 2 and 3) with a pre-Holocene time of most-recent movement partly bounds the southern extent of Tertiary bedrock in the northern part of the step-over zone. Although the Holocene trace of the SLCS steps west, the pre-Holocene Rudys Flat fault (RFF; figures 2 and 3) continues north, juxtaposing Paleozoic and Tertiary bedrock and forming the eastern boundary of the Salt Lake salient (Personius and Scott, 1992). The RFF has no evidence of late Quaternary movement; however, surficial deposits are limited (Personius and Scott, 1992). Although we cannot preclude a subsurface connection between the East Bench and Rudys Flat faults, it is more likely that the Warm Springs fault, which bounds the western edge of the Salt Lake salient and has clear evidence of Holocene surface faulting (Gilbert, 1890; Personius and Scott, 1992), is the active trace of the WFZ to the north of the East Bench fault.

Surficial geology near Penrose Drive is dominated by Lake Bonneville lacustrine sediments and geomorphic features, and both pre- and post-Bonneville alluvial-fan deposits (figure 3). Deposits associated with the Lake Bonneville highstand generally include laminated silt and fine sand below the shoreline and sand to coarse gravel forming wave-built terraces in the shorezone. Close to the site (within about 5 km), the highstand shoreline is mapped at about 1570–1585 m elevation (Personius and Scott, 1992), which compares well with a measurement of 1586 ± 1 m made by Currey (1982) (shoreline elevations in this discussion are not corrected for isostatic rebound; e.g., Oviatt and others, 1992). Similar deposits are associated with the Provo-phase shoreline, which spans an elevation range of about 1465–1475 m (Personius and Scott, 1992) and is less well expressed than the Bonneville shoreline. The Penrose Drive site spans an elevation of 1454–1466 m, which is well below the elevation of the Bonneville highstand (~1585 m), but very close to the elevation of the Provo shoreline (~1470 m). Alluvial-fan deposits in the area consist of overland (sheet) and debris flows emanating from Dry Creek and Red Butte Canyon, which are cut into Paleozoic to Mesozoic bedrock east of the SLCS. Post-Bonneville alluvial-fan sediments are most prevalent; however, southwest of Penrose Drive, pre-Bonneville alluvial-fan remnants are exposed in the footwall of the East Bench fault (Personius and Scott, 1992).

Wasatch Fault Scarp and Surface Offset

At the Penrose Drive site, the East Bench fault is expressed as a single 11-m-high, northwest-facing scarp at about 1455–1465 m elevation (figures 7 and 8). Above the elevation of the scarp (1465–1468 m), the upper surface slopes downward gently to the west to northwest and has likely been modified by Provo-phase shorezone processes and possibly cultural disturbance related to the historical use of the site as an orchard. Below the scarp, the lower surface has been partly developed, but based on the trench exposures (discussed below), may be underlain by Provo-phase shorezone sediments. We estimate 11.0 m of vertical surface offset using projections of the upper and lower surfaces along a northwest-oriented profile (figures 7 and 8).

Trench Stratigraphy and Structure

Our two Penrose Drive trenches served to (1) locate the East Bench fault and expose fault-related sediments (west trench; figure 9), and (2) maximize the exposure in the fault zone (east trench). We exposed four distinct packages of sediment in both trenches: (1) pre-Bonneville alluvial-fan deposits, (2) Lake Bonneville sediments, (3) scarp-derived colluvium (colluvial wedges), and (4) cultural (manmade) fill (figures 9, 10, and 11). We also exposed the pre-Bonneville sediments in a test pit about 9 m southeast of the west trench (figure 12). Because we exposed very similar fault geometries and packages of sediment in both trench exposures, including nearly identical individual colluvial-wedge deposits, and given the close (about 20 m) horizontal distance between the trenches, we describe a single set of sedimentary units for the entire site in appendix A.

Pre-Bonneville Alluvial-Fan Deposits

We exposed pre-Bonneville alluvial-fan gravel (unit 1, plate 1) in the eroded footwall of the East Bench fault. The gravel consists of vertically aggraded stream- and debris-flow deposits likely derived from Dry Creek and (or) Red Butte Canyon to the east. The texture of the gravel within individual (intra-unit) subunits varies laterally along the exposures, but generally unit 1 includes massive to well-bedded, clast-supported, fine to coarse gravels in an oxidized red-orange sand matrix. The red-orange color is likely related to post-depositional oxidation of the alluvial-fan gravel, rather than being primary in origin (e.g., derived from a single iron-stained bedrock unit exposed in the Wasatch Range). Individual subunits are less than about 1.5–1.9 m thick, together reach a thickness of at least 6–7 m in the east trench, and have bedding contacts with apparent dips of zero to about 5–8° NW.

A soil consisting of an A horizon and a well-developed calcic Bkt horizon has formed on the pre-Bonneville alluvial-fan gravels (soil S6; h-1.0–4.0 m, v-11.1–11.2 m; west trench; plate 1). In the southeast part of the west trench, the carbonate in this soil is generally diffuse (only locally weakly laminated), but it cements gravel clasts in a 0.2–0.7-m-thick B horizon (soils 2Bk and 2Btk; plate 1). We exposed similar Bk and Btk horizons on pre-Bonneville alluvial-fan deposits in the test pit (figure 12). Soil S6 also includes a 0.2–0.3-m-thick A horizon, which overlies and locally overprints the soil carbonate. The A horizon is best expressed at the end of the west trench and in the test pit and is less developed on the slope of the scarp face.

Unit-1 fan gravels are best exposed in the footwall of the west trench, where we mapped several individual stream or debris-flow deposits and found lenses of fine sand, which we sampled for quartz-OSL dating. Samples PD-L1 to -L3, from a sandy upper part of a debris-flow deposit near the top of the package of fan gravels, yielded mean ages of 64.4 ± 8.0 ka (sample PD-L3; all ages are ±2σ), 69.3 ± 8.1 ka (PD-L2), and ~77 ka (PD-L1). Another OSL sample from the base of the flow yielded a mean age of 58.8 ± 3.4 ka (PD-L4). IRSL ages on feldspar grains yielded ages of 134.7 ± 13.7 ka (PD-L1) and 220.8 ± 19.8 ka (PD-L4) (appendix D). The significantly older IRSL ages could indicate that the quartz-OSL ages are saturated, and are thus minimum ages. Alternatively, the IRSL ages could be too old (maximum ages for unit 1) if the feldspars were only partially bleached, which is likely the case for PD-L4. We favor the quartz-OSL ages as representing the age of the fan gravel because the OSL samples have consistent mean ages and relatively small (6–12%) uncertainties. Only one sample (PD-L1) yielded a poorly defined age, which could be a function of poor sample luminescence or a saturated age. The PDF of the sum of the four OSL ages (PD-L1–L4) indicates a mean age of 67.3 ± 14.4 ka (2σ) for the pre-Bonneville fan gravels.

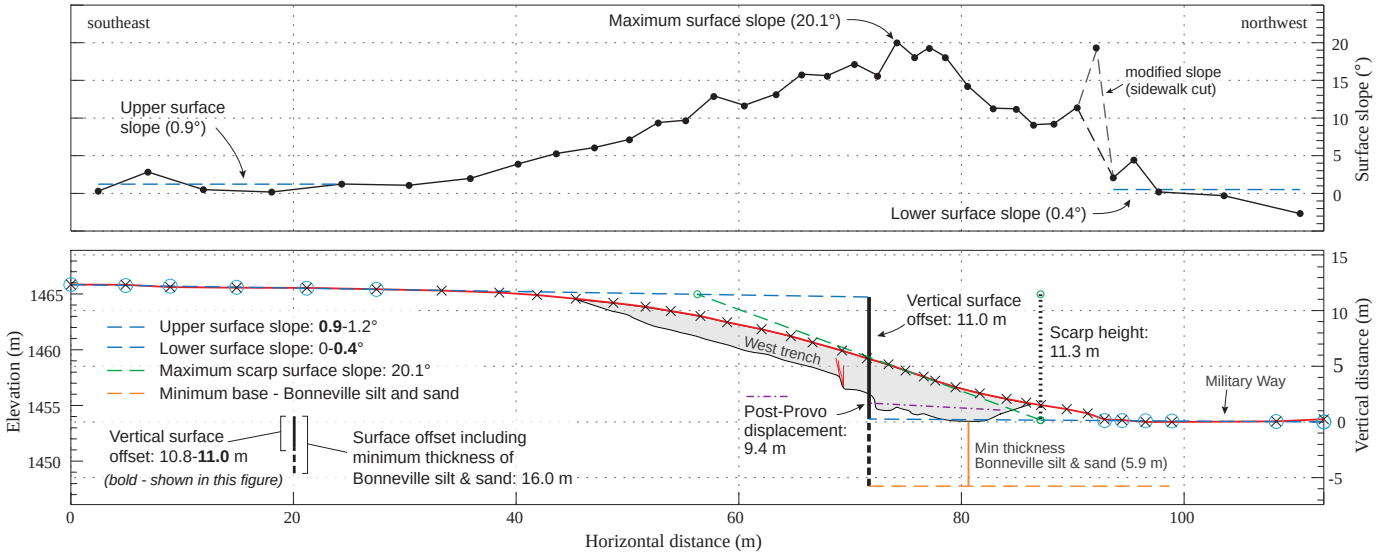

Figure 8. *Scarp profile P1 (red line) measured across the Penrose Drive site (May 5, 2010). Profile points (X's) measured using high-precision GPS; elevation is relative to mean sea level; vertical distance is relative to minimum surface elevation (1453.5 m). Black dots show surface slope at midpoint distances between profile points. Blue circles indicate profile points selected for upper and lower surface-slope measurements (horizontal blue dashed lines in upper figure). The ranges of surface slopes and vertical offsets reflect the selection of alternate profile points; bold values correspond with this figure. Scarp height is the vertical distance between the intersections of the maximum scarp slope with the upper and lower surface-slope projections (green circles). Orange dashed line is horizontal projection of the minimum base of Bonneville highstand silt and sand (unit 2) from a hand-auger hole at 33.1 m horiz., 1.0 m vert. (west trench), which met refusal in unit 2 at 5.9 m below the bottom of the west trench (vertical orange line). Gray shaded area shows extent of the west trench; red lines are faults corresponding with plate 1.*

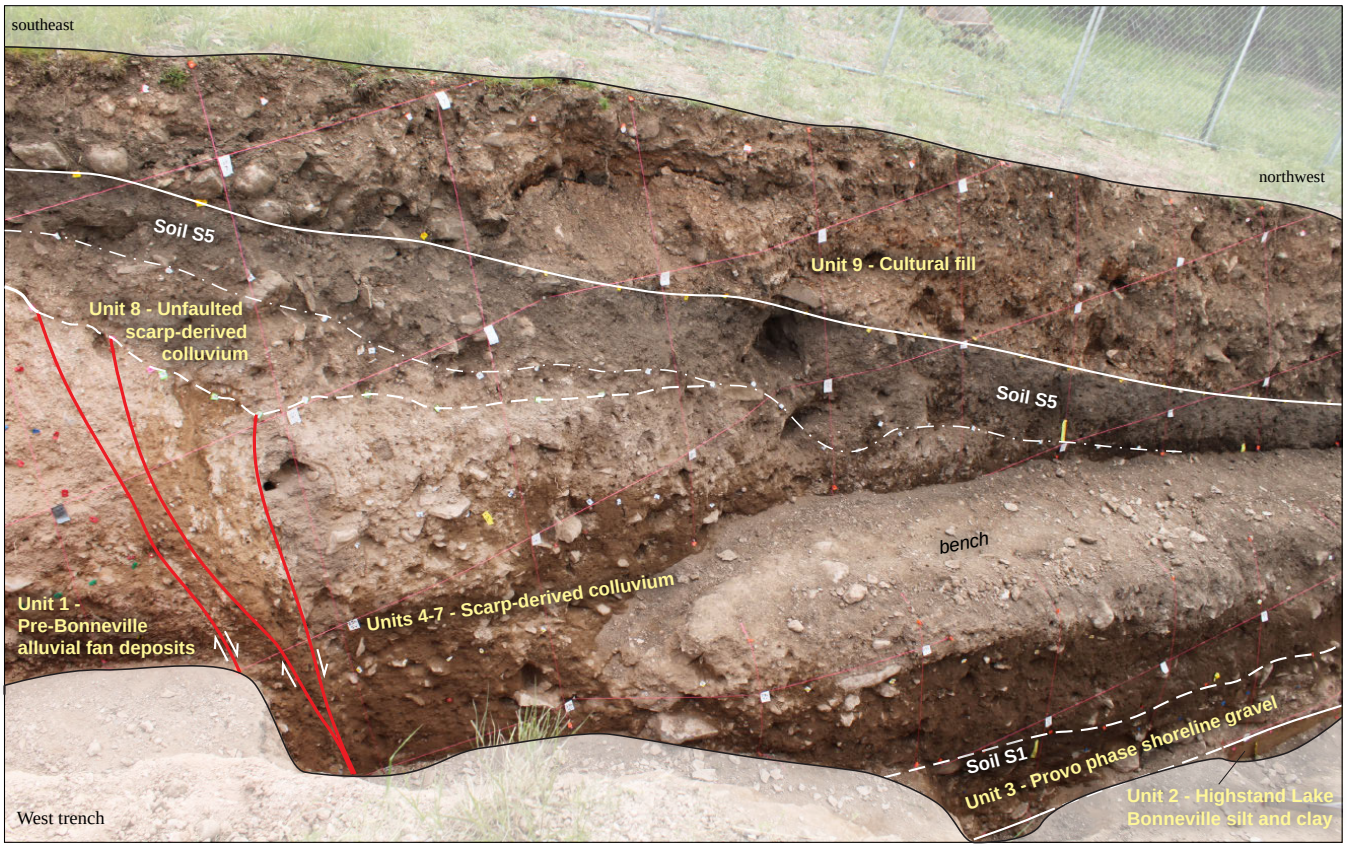

Figure 9. *East Bench fault of the Wasatch fault zone (red lines) and scarp-derived colluvium (units 4–8) exposed in the northeast-facing wall of the west trench at the Penrose Drive site. S1 and S5 (buried by cultural fill) indicate prominent soil A horizons formed in Provo-phase boulder gravel and scarp-derived colluvium, respectively. See plate 1 for additional stratigraphic contacts and soils mapped in the west trench. Pink level lines form 1-m squares.*

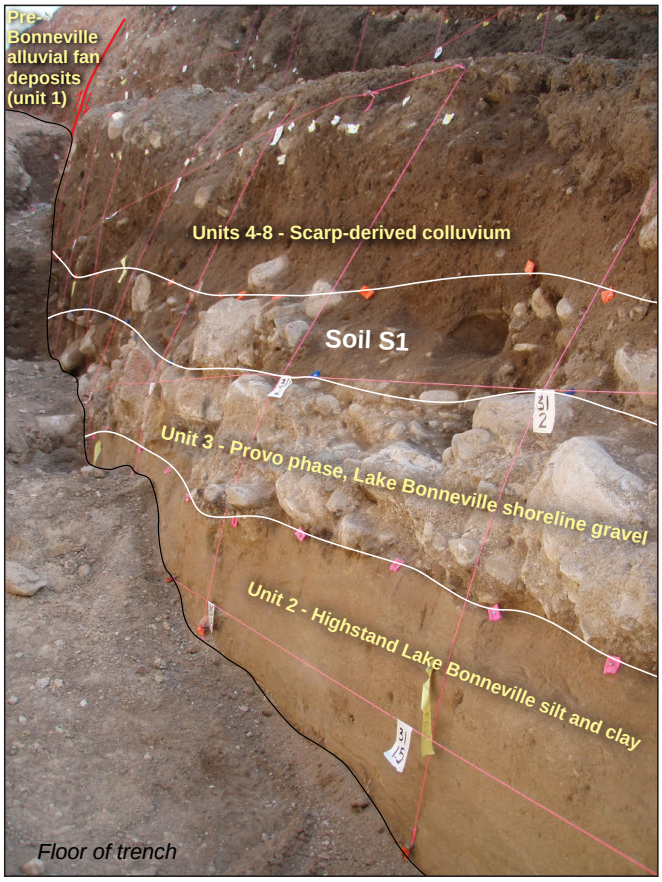

Figure 10. *Lake Bonneville highstand sediments (unit 2), Provo-phase boulder gravel (unit 3), and scarp-derived colluvium (units 4–8) exposed on the hanging wall of the East Bench fault (red line) in the northeast-facing wall of the west trench at the Penrose Drive site. S1 is prominent soil A horizon developed within the Provo-phase boulder gravel. Pre-Bonneville alluvial-fan deposits (unit 1) in the footwall of the East Bench fault are in the upper-left part of the figure. See plate 1 for additional stratigraphic contacts and soils mapped in the west trench. Lowest two horizontal level lines are 0.5 m apart, all other level lines (horizontal and vertical) form 1-m squares.*

Lake Bonneville Sediments

Lacustrine sediments related to Lake Bonneville are the oldest units exposed on the hanging wall of the East Bench fault at this site and include fine silt and sand deposited during the Bonneville highstand (unit 2; plate 1). The silt and sand are overlain by coarse boulder-cobble gravel (unit 3; plate 1) that was likely deposited during formation of the Provo-phase shoreline. A well-developed soil A horizon is present on unit 3 (soil S1; plate 1; figure 10). Units 2 and 3 are not present in the footwall of the fault in the trenches.

In the west trench, unit 2 consists of massive to thinly and subhorizontally bedded silt with little variability in its texture over an 8-m-long exposure (figure 10). Two OSL samples of fine silt from the uppermost part of unit 2 yielded ages of 17.0 ± 1.4 ka (PD-L5) and 17.8 ± 0.7 ka (PD-L6). These ages correspond well with the age of the latest highstand occupation (Bonneville flood) of 14,500 ^{14}C yr B.P. (Oviatt, 1997), which we calendar calibrated to 17.6 ± 0.3 ka (2σ) using OxCal.

We also exposed Lake Bonneville sediments in the 2-m-wide lowermost exposure of the east trench (figure 11) immediately adjacent to the fault plane. In this exposure, unit 2 is slightly coarser than in the west trench and contains abrupt, linear contacts that separate silt and fine sand laminae. The bedding in unit 2 dips steeply to the northwest. We measured apparent dips of 30–45° NW on several contacts and a true dip of 53° N (275° strike, using right-hand rule and 12° declination) for one contact based on a three-dimensional exposure. We attribute the dip of these beds to monoclinal folding associated with movement on the East Bench fault (at least one surface-faulting earthquake), rather than to primary depositional dip (e.g., foreset beds of a delta or onlap of beds onto a preexisting scarp). In addition, we do not consider subaqueously deposited colluvium as a likely origin for the inclined beds because of the fine, well-sorted sediment and planar interbed contacts. This pattern of deformation is similar to the monoclinal, fault-related warping of Lake Bonneville silt and clay described at the Dresden Place site (2 km to the south) on the East Bench fault by Machette and others (1992). However, at Penrose Drive, the folded Lake Bonneville sediments are eroded and unconformably overlain by flat-lying Provo-phase shoreline gravel (h-7.5 m, v-1 m, east trench; plate 1). We interpret the folded Bonneville highstand beds and angular unconformity with the overlying Provo gravel as evidence of at least one surface-faulting earthquake that occurred after deposition of Bonneville highstand silt at the site (~17–18 ka based on OSL ages for unit 2; appendix D), but before the regression from the Provo shoreline (~14.5 ka) (figure 13).

We drilled an 8-cm-diameter hand-auger hole in the bottom of the west trench in an attempt to locate the pre-Bonneville fan gravel on the fault hanging wall (h-33; plate 1). The borehole penetrated 5.9 m of silt and sand prior to refusal; however, no pre-Bonneville fan gravels were encountered. Based on this hole, we conclude that deposits from the Lake Bonneville transgression and highstand (unit 2) have a minimum thickness of 6.5 m at the base of the scarp at the Penrose Drive site. In contrast, correlative Bonneville sediments were not observed on the fault footwall, including in the test pit 9 m south of the west trench.

We offer several possible explanations for the thick Bonneville highstand deposits on the hanging wall but no highstand deposits on the footwall. One explanation is that Bonneville sediments were deposited on the footwall but later eroded in the Provo-phase shorezone. However, we find it unlikely that at least 6.5 m of fine-grained Bonneville sediment has been completely eroded from the footwall since the lake dropped to the Provo level at about 18 ka. A second explanation is that pre-Bonneville topography, either from a north- to west-sloping alluvial-fan surface or a sublacustrine fault scarp (greater than a few meters high), enhanced deposition of highstand fine sediment on the hanging wall. Finally, fault movement

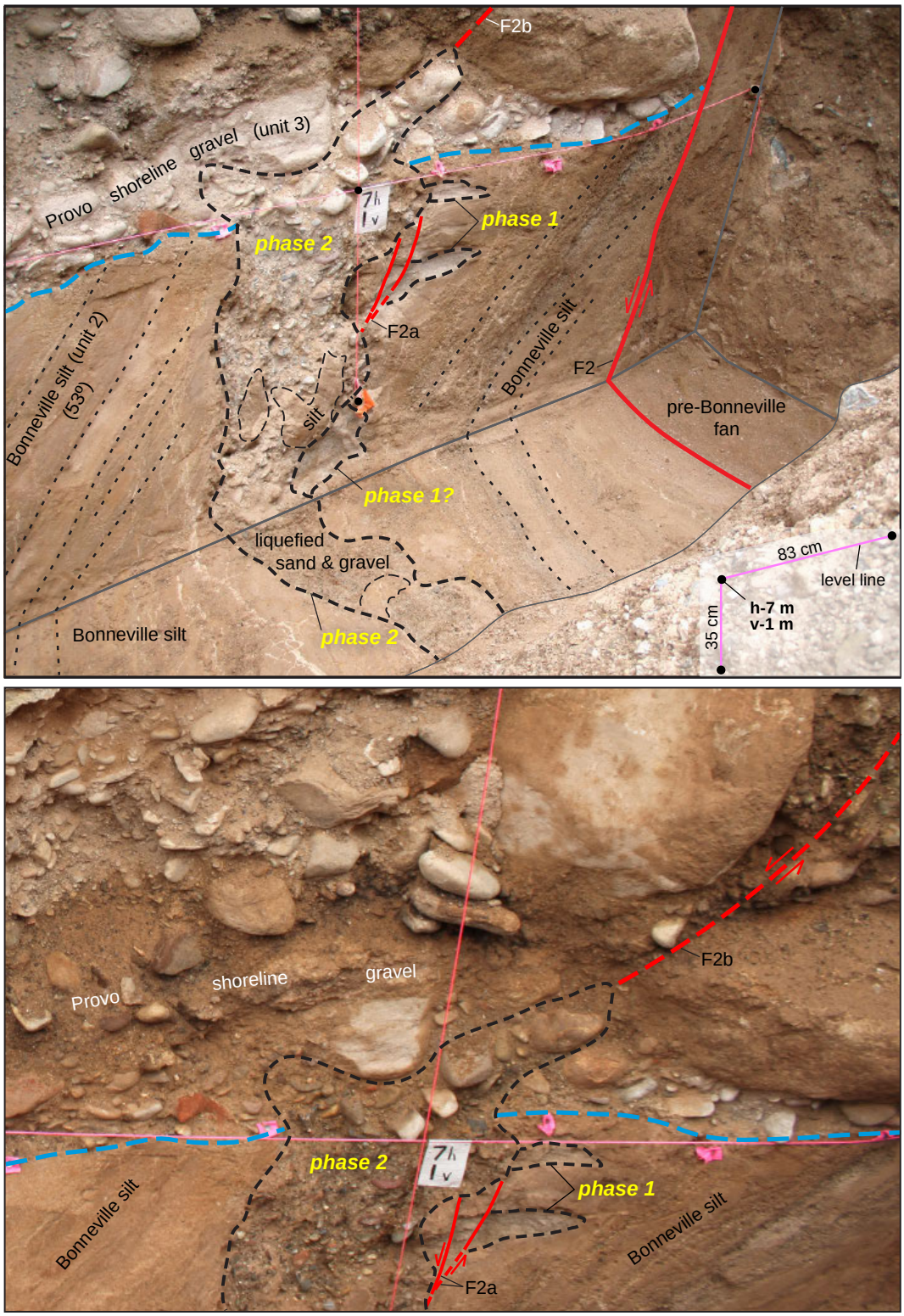

Figure 11. *Upper photo shows monoclinal folding in Lake Bonneville silt (unit 2) in the base of the east trench that predates an angular unconformity formed during the Provo-shoreline occupation (flat-lying Provo shoreline gravel) and provides evidence of at least one surface-faulting earthquake (PD6). Red lines show traces of the East Bench fault, including subsidiary traces (short solid and dashed lines) that are partly obscured by liquefied sand and gravel. Phase-1 liquefaction denotes sand horizontally injected into Bonneville highstand silt (possibly during earthquake PD6). Possible upward termination of subsidiary faults at the unit angular unconformity could be evidence of an older event (predating PD6); however, later-phase liquefaction has obscured this possible cross-cutting relation. Phase-2 liquefaction marks liquefied sand and pebble gravel extending into the lower Provo shoreline gravel that occurred during PD5 or possibly a later earthquake. See figure 13 for conceptual models of the faulting and liquefaction observed in the East Trench. View is to the southeast. Lower photo shows detail near grid intersection 7 m horizontal and 1 m vertical.*

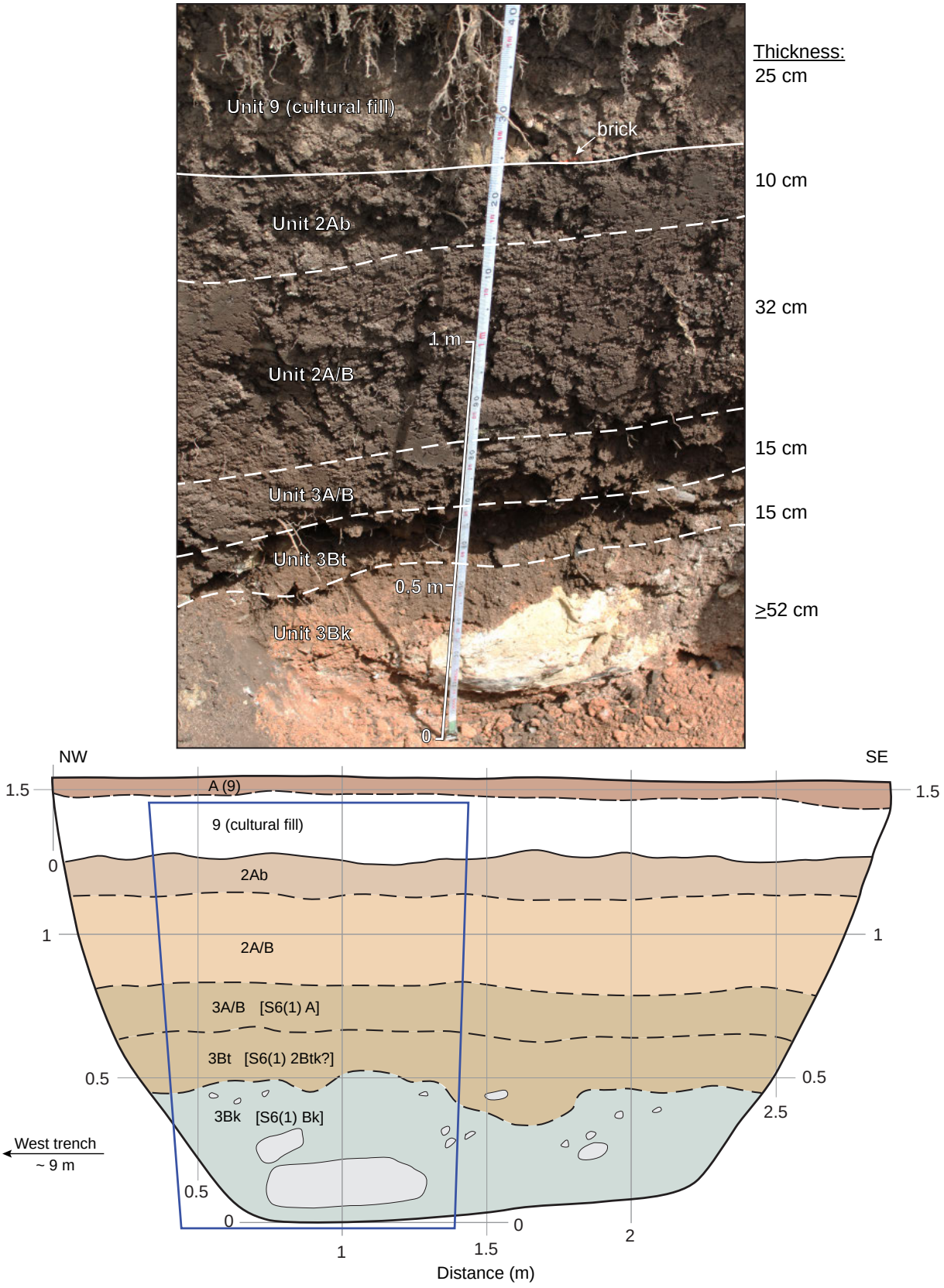

Figure 12. *Soil profile exposed in the test pit excavated on the footwall of the East Bench fault, about 9 m southeast of the south end of the west trench at the Penrose Drive site. Soil description on annotated image and map is for this exposure only; a possible correlation of soil horizons with those exposed in the west trench is shown in brackets. Photograph taken May 12, 2010; box outlined in blue shows location of photograph relative to map of exposure.*

could have played a role in the preservation and erosion of the highstand sediments. For example, vertical fault movement during the highstand and Provo-phase occupations would have dropped and preserved sediments on the hanging wall and uplifted and exposed sediments on the footwall (figure 13). If strike-slip motion occurred (discussed below), then local variations in sediment thickness could be juxtaposed at the site. We favor a combination of these explanations to explain our observations: preexisting topography and fault movement likely enhanced deposition and preservation of fine-grained Bonneville highstand sediment on the fault hanging wall, whereas erosion of these (relatively thinner) sediments on the footwall likely occurred as they were uplifted and exposed in the Provo shorezone.

Unit 3 consists of carbonate-cemented coarse sand and boulder gravel unconformably (east trench; figure 11) to conformably (west trench; figure 10) overlying the highstand silt and sand of unit 2. The boulder gravel is 0.5 m thick in the east trench (where undisturbed by liquefaction) and about 0.6–1.1 m thick in the west trench, and includes numerous gastropod shells (and fragments), which we sampled but did not date. At a distance greater than about 3 m from the East Bench fault, a well-developed, 0.2–0.5-m-thick soil A horizon is present in unit 3 (soil S1; west trench; plate 1). Within about 3 m of the fault, soil S1 is formed on scarp colluvium that postdates the boulder gravel (east trench; plate 1).

We sampled macrocharcoal from the A horizon of soil S1 and also collected a bulk sample of the A-horizon for ^{14}C dating. Two unidentifiable macrocharcoal fragments from the east trench yielded ages of 11.4 ± 0.3 ka (PD-R1) and 10.9 ± 0.2 ka (PD-R3), compared to an age of 10.6 ± 0.1 ka (PD-R2) for *Rosaceae* (flowering plant) charcoal from the west trench. The slightly younger age from the west trench could be related to the location of PD-R3, which sampled the uppermost part of soil S1. However, it is also possible that PD-R3 sampled distal colluvial-wedge sediment (and organics) which directly overlies soil S1 in the sample area. Unidentified charcoal fragments separated from the S1 soil (sample PD-R13; west trench) yielded an age of 11.5 ± 0.3 ka, which agrees well with the 10.9–11.4-ka age for PD-R1 and -R3.

Liquefied Sand and Gravel

In the basal exposure of the eastern trench, a prominent liquefaction vent (h-7 m, v-1 m; plate 1; figure 11) injected sand and gravel into the silty Bonneville sediments (unit 2) and the overlying Provo shoreline deposits (unit 3) along lower (F2a) and upper (F2b) splay faults that parallel the main trace of the East Bench fault. The feature records at least two phases of liquefaction: an initial event that injected fine sand vertically and horizontally into unit 2 (phase 1; figure 13), and a later event that injected a much larger volume of sandy pebble gravel vertically into unit 2 and the lower part of unit 3 (phase 2; figure 13). Liquefied sand and gravel in both phases likely correspond with the splay faults; however, the later event has obscured the expression of discrete faulting in much of the exposure. Evidence of shearing and unit displacement and truncation includes (1) displacement of phase-1 fine-sand injection features in unit 2 by fault F2a (h-7.1 m, v-0.8 m, east trench; plate 1), (2) shearing and clast rotation in the upper part of unit 3 along fault F2b (h-7.4 m, v-1.5 m, east trench; plate 1), (3) a ~10-cm step in the unit 3/unit 4 contact coincident with upward termination of fault F2b (h-7.4 m, v-1.7 m; plate 1), and (4) apparent offset (~4–5 cm) of the base of unit 3 across the later-phase liquefaction event (inferred location of splay fault F2b). Although it is possible that fault F2a, which cuts the initial-phase injection features, terminates at the unit 2–3 contact; the later-phase liquefaction has obscured this possible cross-cutting relation (figure 11) (h-7.1 m, v-0.9 m; east trench; plate 1).

The spatial association of liquefaction features with the splay faults indicates that these features are likely the result of seismic shaking from at least two surface-faulting earthquakes on the East Bench fault, rather than from earthquakes elsewhere in the region. The timing of these "liquefaction" earthquakes can be roughly estimated by stratigraphic relations with the lacustrine sediments: the earlier liquefaction event postdates the deposition of Bonneville transgressive and highstand silts and may be related to the earthquake that resulted in the monoclinal folding of these sediments, and the later event postdates the Provo shoreline. Termination of the lower splay faults (F2a)—which displace the initial-phase injection features—at the unit 2–3 contact would be evidence of a third earthquake in the later stages of the Bonneville transgression; however, this possible upward termination is obscured by later-phase liquefaction (figure 11) and we cannot preclude the possibility that faults F2a and F2b in units 2 and 3, respectively, moved contemporaneously (models A and B; figure 13). We observed another liquefaction feature in the west wall of the east trench, where a deposit of fine sand is injected into scarp colluvium (unit 6) subparallel to the main fault zone (h-8.2 m, v-3.1 m; plate 1). Given its height in the stratigraphic section and the relations described above, this feature likely was formed during a younger, separate earthquake that postdated the deposition of unit 6.

Scarp-Derived Colluvium

We identified five and possibly six deposits of scarp-derived colluvium (units 4, 5, 6a, 6b, 7, and 8; plate 1), each providing evidence of an individual surface-faulting earthquake on the SLCS. The colluvial units have similar wedge-shaped geometries, and with the exception of unit 6a, have soil A horizons developed on them. The youngest scarp-colluvial wedge (unit 8) is not faulted, whereas units 4–7 have been faulted down to the northwest along the East Bench fault. In general, the colluvial deposits reflect an evolving depositional environment in which the oldest wedges have a limited lateral extent of 3–6 m away from the fault compared to the younger wedges, which extend about 11 m from the

Model A: One Lake Bonneville Highstand to Provo Phase Earthquake

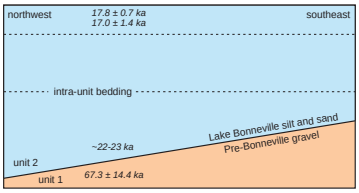

Initial Condition

Transgressive and highstand silt and fine sand (unit 2) deposited between about 22-23 ka and 18 ka (Bonneville Flood) on possibly west-to north-sloping pre-Bonneville alluvial fan surface (unit 2).

Bonneville Flood *(17.6 ± 0.3 ka)*

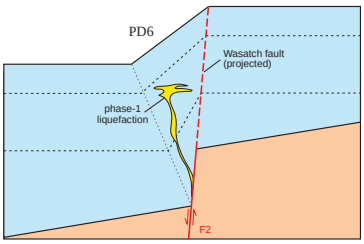

Earthquake PD6

Earthquake PD6 occurs during Provo-phase (14-18 ka) occupation, resulting in subaqueous scarp and folding in cohesive highstand sediments (unit 2).

Liquefied fine sand injected vertically and horizontally into folded unit 2 (phase 1).

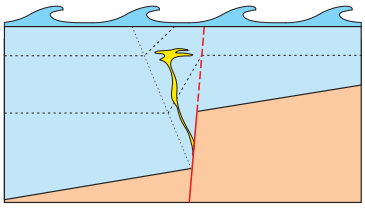

Erosion During Provo Shoreline

Bonneville sediments in footwall and near fault zone eroded during Provo-phase of Lake Bonneville (~18-14 ka).

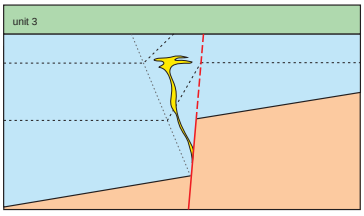

Deposition of Provo Shoreline Gravel

Provo-phase boulder gravel (unit 3) deposited on folded and eroded Bonneville highstand sediments (unit 2).

Lake Bonneville regresses from site by about 14 ka.

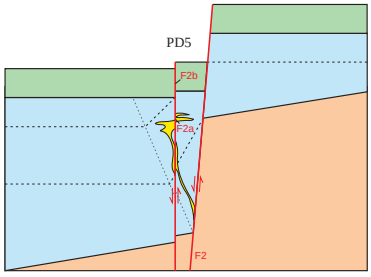

Earthquake PD5

Provo shoreline boulder gravel (unit 3), folded Bonneville highstand sediments (unit 2), and phase-1 liquefied sand faulted in earthquake PD5.

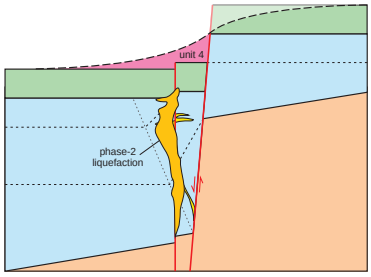

Scarp-Colluvium Deposition and Liquefaction

Colluvial-wedge (unit 4) deposited following earthquake PD5.

During a later earthquake (PD4-PD1), liquefied sand and gravel (phase 2) injected into units 2 and 3, overprinting synthetic faulting and phase-1 liquefaction.

EXPLANATION

- Erosion related to Provo-shoreline occupation of site
- Unit 4. Scarp-derived colluvium eroded from fault scarp formed in earthquake PD5.
- Phase-2 liquefaction. More extensive sand and gravel (compared to phase-1) vertically injected into Bonneville highstand and Provo-phase sediments along synthetic fault.
- Phase-1 liquefaction. Fine sand vertically and horizontally injected into Bonneville highstand sediments (unit 2); limited extent.
- Unit 3. Lake Bonneville Provo-phase boulder gravel. Carbonate-cemented coarse sand and boulders about 0.5-1.1 m thick deposited in near-shore environment.
- Unit 2. Lake Bonneville highstand silt and sand. Massive to subhorizontally bedded silt with fine sand interbeds deposited during Lake Bonneville highstand occupation.
- Unit 1. Pre-Bonneville alluvial-fan gravel. Massive to well-bedded, clast supported, fine to coarse gravels in an oxidized red-orange sand matrix

Model B: Two Lake Bonneville Highstand to Provo Phase Earthquakes

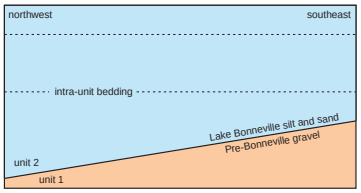

Initial Condition

Transgressive and highstand silt and fine sand (unit 2) deposited between about 22-23 ka and 18 ka (Bonneville Flood) on possibly west- to north-sloping pre-Bonneville alluvial fan surface (unit 2).

Bonneville Flood *(17.6 ± 0.3 ka)*

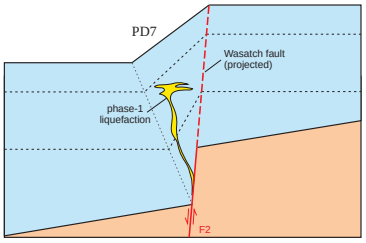

Earthquake PD7

Earthquake PD7 occurs during Provo-phase (14-18 ka) occupation, resulting in subaqueous scarp and folding in cohesive highstand sediments (unit 2).

Liquefied fine sand injected vertically and horizontally into folded unit 2 (phase 1).

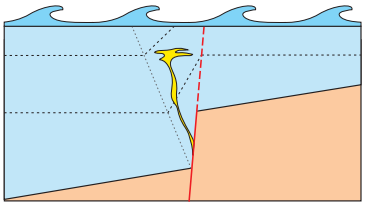

Erosion During Provo Shoreline

Bonneville sediments in footwall and near fault zone eroded during Provo-phase of Lake Bonneville (~18-14 ka).

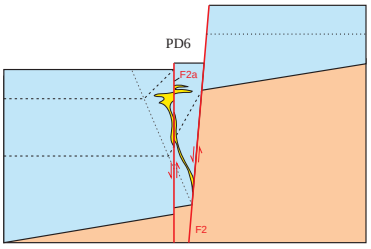

Earthquake PD6

Folded and Bonneville fine sand and silt and phase-1 liquefied sand faulted by earthquake PD6.

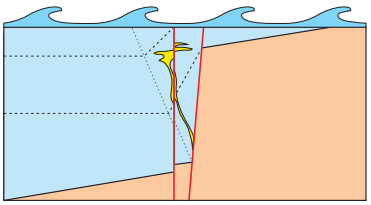

Erosion During Provo Shoreline

Bonneville sediments in footwall and near fault zone eroded during Provo-phase of Lake Bonneville (~18-14 ka).

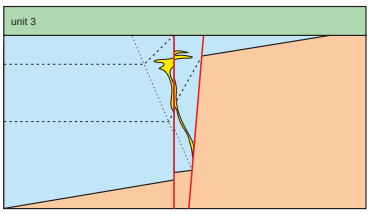

Deposition of Provo Shoreline Gravel

Provo-phase boulder gravel (unit 3) deposited on folded and eroded Bonneville highstand sediments (unit 2).

Lake Bonneville regresses from site by about 14 ka.

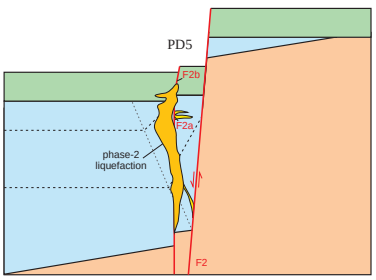

Earthquake PD5

Provo shoreline boulder gravel and folded Bonneville fine sand and silt faulted in earthquake PD5.

Liquefied sand and gravel (phase 2) obscures overprints phase-1 liquefaction.

Colluvial-wedge (unit 4) deposited following earthquake PD5 (not shown).

fault, equal to the horizontal length of the scarp. In addition, the basal contacts of the wedges steepen as they become younger, reflecting a growing scarp that has progressively influenced scarp-colluvium deposition. In the west trench, the basal contacts steepen upward from 13° to 25°, in increments of 2°–4° over distances of 1–6 m from the trace of the East Bench fault. In the east trench, the basal contacts steepen upward from 6° to 25°, in more irregular 0°–11° increments over distances of 0–4 m from the fault.

Unit 4—the oldest scarp-colluvial wedge—contains a distinct mixture of subrounded boulders that were likely derived from unit 3 and orange-red sand and gravel of unit 1 (h-7.4 m, v-1.8 m; east trench; plate 1). Unit 4 tapers from 1.0 to 0.7 m thick over a distance of about 3 m and, adjacent to the East Bench fault, has slope-parallel clast fabric. Because soil S1 is developed on unit 4 and no soil is present on the Provo boulder gravel, we suspect that this earthquake occurred shortly after the Provo shoreline regressed from the site. Calibrated ^{14}C ages from charcoal in soil S1 indicate that unit 4 was deposited before about 10.9–11.5 ka (PD-R1, -R3, -R13; appendix C; plate 1). We did not expose unit 4 in the west trench, which did not extend deep enough adjacent to the fault zone.

Unit 5 consists of a mixture of silt, sand, and gravel clasts, and soil organics that is about 0.8 m thick adjacent to the fault (in both trenches) and pinches out over a horizontal distance of about 6 m. Although locally massive, unit 5 includes fine gravel that defines slope-parallel lenses and stone lines. The A horizon of soil S2 is developed on unit 5 and is 0.2–0.3 m thick. We could not clearly identify soil S2 within about 1 m of the fault, possibly because of fault-related disturbance, or because the deposition of scarp colluvium continued close to the fault at the time of soil S2 development. OSL sample PD-L7 constrains the age of the uppermost part of unit 5 (below soil S2) to 11.0 ± 1.2 ka. This age agrees well with two radiocarbon ages of 10.6 ± 0.1 ka (PD-R6a) and 10.1 ± 0.2 ka (PD-R6b) on unidentified charcoal fragments from a bulk sample of soil S2.

Two distinct packages of scarp colluvium, separated by a prominent stone line, compose unit 6 (6a-lower, 6b-upper; plate 1). Units 6a and 6b consist of a mixture of mainly fine sand, silt, and soil organics with interspersed pebble to small cobble clasts that form slope-parallel lenses and stone lines. Unit 6 is locally massive and, in the east trench, fines to the northwest. Unit 6a tapers from about 0.8 m thick to zero over a horizontal distance of about 5 m, and unit 6b tapers from about 0.7–0.8 m thick to zero over a distance of 4–5 m. The maximum (combined) thickness of units 6a and 6b is 1.6 m. A prominent pebble and cobble stone line marks the boundary between units 6a and 6b, but no soil is present at the contact. This stone line is best expressed in both walls of the east trench (h-7.0 m, v-3.6 m; plate 1) and is visible (but more subtle) in the west trench (h-22.5 m, v-4.8 m; plate 1). Two OSL samples of unit 6 yielded ages of 7.4 ± 0.9 ka (unit 6a; PD-L8) and 8.4 ± 1.3 ka (unit 6b; PD-L9). Although PD-L9 is stratigraphically inverted with PD-L8, the two ages have about 67% overlap at one sigma (appendix B) and PD-L9 likely represents a maximum constraint for unit 6b. We also sampled a moderately well-developed, 0.2–0.4-m-thick soil A horizon (soil S3) developed on unit 6b. Two microcharcoal samples and a charred *Prunus*-type (similar to Cherry) seed fragment yielded ages of 6.3 ± 0.1 ka (PD-R8), 6.3 ± 0.1 ka (PD-R10b), and 6.6 ± 0.2 ka (PD-R10a), respectively. An additional sample of unidentified charcoal from soil S3 yielded an age of 3.8 ± 0.1 ka (PD-R5); however, we dismiss this age because it differs greatly from the concordant PD-R8 and PD-R10 ages. The anomalously young age for S3 is likely related to mixing of organic-rich sediment from the overlying younger soil S4 (well dated to ~4 ka; discussed below) with S3 through burrowing.

Our favored interpretation is that units 6a and 6b are evidence of two separate surface-faulting earthquakes based on the prominent stone line and their individual maximum thicknesses of 0.8 m, which are nearly identical to those for units 4, 5, 7, and 8. Because no soil is present between units 6a and 6b, we cannot dismiss the possibility that units 6a and 6b represent two pulses of scarp colluvium following a single large-displacement earthquake. We address both of these alternative interpretations in two separate OxCal models (appendix E).

Unit 7 consists of silt and sand mixed with soil organics and interspersed pebble and cobble clasts, which form slope-parallel lenses within about 4 m of the East Bench fault. At greater distances from the fault, unit 7 is finer grained and massive. Unit 7 tapers from 0.7 m thick adjacent to the fault to zero over a distance of about 11 m. Soil S4 is an A horizon soil developed on unit 7 that reaches a maximum thickness of about 0.2 m, but is locally only weakly developed. Beyond about 2–3 m from the fault, unit 7 and soil S4 are locally overprinted by soil S5. Soil S4 is locally burrowed, but it is best expressed in the west trench, where we collected two samples of the A horizon. Unidentified charcoal fragments from soil S4 (PD-R14a) and two microcharcoal samples (PD-R14b and -R9b) yielded ages of 4.2 ± 0.2 ka, 4.4 ± 0.1 ka, and 4.4 ± 0.2 ka, respectively. An additional charcoal sample (PD-R9a) was too small to date. As discussed previously, sample PD-R5 (~3.8 ka) likely dates charcoal derived from soil S4.

Figure 13. *(opposite page) Conceptual models of faulting in Lake Bonneville sediments. Model A shows monoclinal folding related to at least one earthquake (PD6) between the Bonneville flood and the regression from the Provo shoreline, and younger splay faulting (contemporaneous movement of faults F2a and F2b) in earthquake PD5. Model B includes at least two earthquakes (PD7 and PD6) between the Bonneville flood and Provo regression that predate earthquake PD5. In this model, fault F2a is active in PD6 and F2b in PD5. In both models, phase-1 liquefaction occurs during monoclinal folding of unit 2 and phase-2 liquefaction occurs after deposition of unit 3.*

Scarp colluvium in unit 8 includes a poorly sorted mixture of silt, sand, soil organics, and gravel that bury an eroded scarp free face and the faulted soil A horizon S4. The unit is mostly massive, but locally the clasts define a weak slope-parallel fabric. Unit 8 has a maximum thickness of 1.0 m, and thins to about 0.7 m within 2–3 m from the East Bench fault before being completely overprinted by soil S5. Soil S5 varies in thickness from about 0.3 to 0.6 m where developed on unit 8 in the center of the fault scarp to about 0.7–0.8 m in the northwestern part of the west trench. S5 is extensively burrowed, but locally very well developed. We separated charcoal fragments from two samples of the S5 A-horizon sediment. A fragment of *Quercus* (oak) charcoal yielded an age of 0.5 ± 0.05 ka (PD-R11) and *Artemisia* (herbs and shrubs of the daisy family Asteraceae) charcoal provided an age of 0.5 ± 0.04 ka (PD-R12).

Cultural Fill

A deposit of cultural (manmade) fill (unit 9; plate 1; figure 9) overlies soil S5 on the hanging wall of the East Bench fault. Unit 9 is distinctive as it includes fragments of brick and metal. The cultural fill has a maximum thickness of 1.6 m, which coincides with the base of the East Bench fault scarp (h-30 m; plate 1) in the west trench. At the northwest end of the west trench, unit 9 is at most 0.5 m thick where it overlies colluvial unit 8. Unit 9 may be the result of site excavation and grading (above the elevation of the west trench) for a fruit orchard. We found no evidence of cultural disturbance or manmade fill below soil S5.

East Bench Fault of the Wasatch Fault Zone

The East Bench fault (fault F2; plate 1) is characterized by a sharp, steeply dipping zone of sheared sediment consisting of carbonate-rich silt, sand, and gravel in which clasts are rotated parallel to one of several fault planes. In the west trench, two faults dipping 79°–90° NW bound a 0.3–0.7-m-wide zone of sheared sediment. In the east trench, a narrow, ~0.1-m-wide shear zone is bounded by two subparallel, linear faults dipping 83°–85° NW. In a three-dimensional exposure of fault gouge at the base of the east trench, we measured a fault striking 229° and dipping 88° NW; in the same location, a flat, ~0.1-m-wide rotated clast was striking 227° and dipping 79° NW. In the base of the west trench, the southeastern fault bounding the sheared sediment has an orientation of 229°/90°. Where projected to the surface and shown on our site topographic map (figure 7), the fault strike is 229°. Based on these measurements, we prefer a strike of 229° and dip of 85 ± 5° NW for the East Bench fault.

Partly because of the planar and steeply dipping character of the East Bench fault, the contacts of stratigraphic units have only been slightly rotated (flattened) or dragged (steepened) adjacent to the fault zone. The progressive decrease in the dips of the bases of the colluvial wedges could be interpreted as evidence of fault rotation; however, we interpret these decreasing dips to be depositional and the result of colluvial wedges being deposited on the sloping surface of a progressively growing scarp. In the west trench, a slight upward inflection in the contact between units 2 and 3 within about 7.5 m of the fault (from subhorizontal to dipping 4° NW at h-29.5 m; plate 1) could be related to fault drag, but not rotation. Averaged over several earthquakes, the 4° change in dip indicates that only a very small amount of fault drag has occurred since the time of the Provo shoreline. One exception is unit-2 interbeds that dip 30–50° adjacent to the fault in the base of the east trench. We interpret these inclined beds as related to monoclinal folding of saturated highstand sediments during at least one surface-faulting earthquake that occurred between the Bonneville highstand and Provo-shoreline occupation (figure 13).

We measured vertical displacement on the East Bench fault using the minimum offset of the pre-Bonneville fan gravel, surface-slope information from the scarp profile, the inferred stratigraphic offset of the Provo-phase shoreline, and the maximum thicknesses of colluvial wedges. Because Lake Bonneville highstand sediments were not exposed in the footwall, we cannot measure the cumulative displacement that has occurred since the Bonneville highstand. To estimate the minimum displacement on the East Bench fault since deposition of the pre-Bonneville fan gravel, we used the thickness of augered Lake Bonneville highstand sediments (unit 2) on the hanging wall. Using the 6.5-m thickness of unit 2, and a 0.9° sloping upper surface from the scarp profile, the minimum vertical displacement of the pre-Bonneville fan gravel is 16 m (figure 8).

Our estimates of post-Provo-phase displacement assume that the upper surface from the scarp profile (~1466 m amsl; figure 8) corresponds with the Provo shoreline elevation and thus the Provo shoreline boulder gravel (unit 3) exposed in the trenches. The basis for this assumption is the absence of Lake Bonneville highstand sediments on the footwall (likely eroded while in the Provo shorezone) and the Provo shoreline elevation near the site (~1470 m amsl; figure 5). Using a 0.9° sloping upper-surface projection, a 3° slope for the top of the Provo-phase boulder gravel (top of soil S1 where best expressed from h-29–33 m; plate 1), and an 85° fault dip, the displacement is 9.4 m (figure 8). We consider this to be a maximum displacement because (1) it is possible that the top of unit 3 is not correlative with the upper surface (~1466 m amsl) and could be a shoreline from a lower, later Provo phase (e.g., P9 of Godsey and others, 2005), and (2) there may have been a preexisting scarp at the site, as discussed above.

To estimate total post-Provo displacement as well as displacement per event, we use maximum colluvial-wedge thickness as a proxy for fault displacement (DuRoss, 2008). As described above, the maximum thicknesses of colluvial wedges are as follows: unit 4–1.0 m, unit 5–0.8 m, unit

6a–0.8 m, unit 6b–0.8 m, unit 7–0.7 m, and unit 8–1.0 m. The sum of these is 5.1 m, which represents the minimum vertical displacement that occurred after deposition of the Provo gravel. Using this estimate, and the vertical displacement from the scarp profile, our preferred post-Provo-phase displacement is 5.1–9.4 m. The maximum thicknesses of individual wedges have only minor variations and indicate a mean per-event displacement of 0.9 m (0.7–1.0-m range). Increasing the per-event displacements by 84% to account for a total upper-bound displacement of 9.4 m, suggests that the mean per-event displacement could be 1.6 m (1.3–1.8-m range). Our preferred per-event displacement is 1.2 m (the midpoint between the 0.9 and 1.6 m mean displacements), with a possible range of 0.7–1.8 m.

We mapped three minor-displacement subsidiary faults in the west trench. Two down-to-the-northwest faults about 1–3 m southeast of the main East Bench fault trace (F2; plate 1) dip 74–78° NW (faults F1a and F1b; plate 1). Fault F1a has less than 0.1 m of vertical displacement; we were unable to correlate intra-unit gravel beds in unit 1 to determine F1b displacement. We also identified a poorly expressed (possibly reverse) fault about 1.5 m northwest of the main fault trace that dips 81° SE (fault F3; plate 1). F3 corresponds with a minor down-to-the-northwest inflection in the top of soil S3; however, the contact between units 6a and 6b suggests little to no displacement.

Subsidiary faults in the east trench consist of down-to-the-northwest splay faults in Lake Bonneville highstand silt and Provo-phase shoreline gravel (figure 11). Fault F2a (h-7.1 m, v-0.9 m; plate 1) displaces liquefied sand injected into folded Lake Bonneville highstand silt (unit 3). Because F2a has been disturbed by a later liquefaction event (figure 11), we were unable to measure the total displacement in unit 2. F2a may terminate at (predate) the unit 2–3 contact; however, this relation has been obscured by liquefaction. Fault F2b (h-7.4 m, v-1.5 m; plate 1) displaces Provo-phase shoreline gravel (unit 3) down to the northwest about 5–10 cm based on the apparent offset of the unit 2–3 contact (about 4–5 cm) and a northwest-down step in the unit 3–4 contact (about 10 cm). Because liquefaction has removed evidence of faulting near the base of unit 3, the geometry of fault F2b in unit 2 is poorly constrained.

The steeply dipping, planar, and simple fault zone exposed at Penrose Drive is unusual compared to other trenches that have exposed the Wasatch fault (e.g., see Machette and others, 1992; DuRoss and others 2009, 2012). The near-vertical planar fault may indicate that a component of strike-slip motion occurs on this part of the fault. The Penrose Drive site is on a part of the East Bench fault where the fault's strike is subparallel to the general extension direction for the Salt Lake City segment as a whole. The northern 3 km of the East Bench fault strikes about 230° (N. 50° E.), which is essentially identical to the 229° strike of the fault exposed at Penrose Drive. Bruhn and others (1992) show that the general direction of slip for all sections of the SLCS is 230–250° based on slickenlines measured on bedrock fault planes, or 240° based on a paleostress analysis for the Salt Lake City–Provo segment boundary. Comparably, the geodetic extension direction for the Wasatch Front is 266°, using data in a 65-km-wide zone across the Wasatch fault (Chang and others, 2006). Given this geometry, it is possible that both normal and strike-slip faulting occurs on the northernmost East Bench fault. Thus, while normal faulting is likely the main slip direction at the Penrose Drive site (based on the significant vertical surface offset), a component of strike-slip motion may help explain the unusual subsurface fault geometry.

Paleoseismology of the Penrose Drive Site

Chronology of Surface-Faulting Earthquakes

We interpret at least six and possibly seven surface-faulting earthquakes at the Penrose Drive site (PD1–PD6; table 2) after deposition of Lake Bonneville highstand silt (unit 2) at about 17.0–17.8 ka (figures 13 and 14). Monoclinal folding in unit 2 that predates an angular unconformity formed during the Provo-shoreline occupation provides evidence of at least one surface-faulting earthquake (PD6), whereas earthquakes PD5–PD1 are based on distinct scarp-colluvial deposits and soil A horizons. The timing of these earthquakes is based on two OxCal models: a preferred model that includes seven earthquakes (accounting for units 6a and 6b; OxCal model 4b; appendix E; figure 14), and an alternative model that includes six earthquakes (a single earthquake for unit 6; OxCal model 4c; appendix E). We report earthquake times from the seven-earthquake OxCal model as the mean and 2σ uncertainty; however, for earthquakes having asymmetrically distributed timing PDFs (i.e., where the mean and modal times differ by several hundred years or more), the modal times and 5^{th}–95^{th} percentile ranges (table 2; appendix F) may better approximate the earthquake times. Per-event vertical displacements for PD1–PD5 range from about 0.7 to 1.8 m based on colluvial-wedge thickness and the total post-Provo displacement at the site (tables 2 and 3).

Earthquake PD6 occurred at 16.5 ± 1.9 ka based on an angular unconformity between folded Bonneville highstand silt beds (unit 2) and relatively flat-lying Provo-phase boulder gravel (unit 3). Considering the ductile deformation and elevation of the site close to the Provo-shoreline elevation, earthquake PD6 likely produced a subaqueous scarp that was later modified and eroded by Provo-phase shorezone processes. Liquefied sand injected into the steeply dipping highstand silt beds along a fault splay synthetic to the East Bench fault may be evidence of PD6 or an earlier earthquake (figure 13). Two OSL ages (PD-L5 and -L6) provide maximum-limiting times of 17.0–17.8 ka, whereas ^{14}C ages from Provo-shoreline environments at similar elevations in the Bonneville basin provide a minimum time constraint for this earthquake. Using a Provo-shoreline elevation range of 1430–1450 m (adjusted for isostatic rebound) for Penrose Drive, 13 ^{14}C ages compiled by Godsey and others

Table 2. *Timing and displacement of surface-faulting earthquakes at the Penrose Drive site.*

Event[1]	Mean[2] (cal yr)	±2σ[2] (yr)	5th [2] (cal yr)	50th [2] (cal yr)	95th [2] (cal yr)	Mode[2] (cal yr)	Displacement[3] (m)	Unit[4]
PD1	4000	500	3530	4070	4250	4100	1.0–1.8	8
PD2	5890	700	5140	6010	6250	6210	0.7–1.3	7
PD3a	7510	760	6890	7520	8150	7520	0.8–1.5	6b
PD3b	9700	1110	8390	9910	10,190	10,160	0.8–1.5	6a
(PD3)	*(9370)*	*(1540)*	*(7820)*	*(9680)*	*(10,170)*	*(10,150)*	*(1.6–2.9)*	*(6)*
PD4	10,870	240	10,680	10,870	11,060	10,920	0.8–1.5	5
PD5	12,080	1590	11,400	11,810	13,830	11,620	1.0–1.8	4
PD6	16,470	1910	14,580	16,680	17,660	17,140	unknown	-

[1] Earthquakes identified at Penrose Drive and modeled in OxCal (figure 14; appendices E and F). Events in bold are included in our preferred seven-event OxCal model 4b, including PD3a and PD3b. An alternative 6-event OxCal model (4c) includes a single earthquake PD3 in place of PD3a and PD3b.
[2] Mean earthquake times, 2σ ranges, and 5th–50th–95th percentile ranges, and modal times are based on OxCal models 1 and 2 (appendix E; see text for discussion).
[3] Per-event vertical displacement. Ranges are based on the maximum colluvial wedge thickness and an upper-bound displacement using the wedge thickness adjusted for a maximum post-Provo displacement (see text for discussion).
[4] Map unit for scarp-derived colluvium associated with the event (plate 1, appendix A).

Table 3. *Vertical slip rates at the Penrose Drive site.*

Event[1]	Mean[2] (ka)	Disp.[3] (m)	Total Displacement[4] (m)	Elapsed Time[5] (kyr)	Slip Rate[6] (mm/yr)
PD1	4.0	1.0–1.8	-	-	-
PD2	5.9	0.7–1.3	1.0–1.8 (PD1)	1.9 (PD2–PD1)	0.5–0.9
PD3a	7.5	0.8–1.5	1.7–3.1 (PD2–PD1)	3.5 (PD3a–PD1)	0.5–0.9
PD3b	9.7	0.8–1.5	2.5–4.6 (PD3a–PD1)	5.7 (PD3b–PD1)	0.4–0.8
PD4	10.9	0.8–1.5	3.3–6.1 (PD3b–PD1)	6.9 (PD4–PD1)	0.5–0.9
PD5	12.1	1.0–1.8	4.1–7.6 (PD4–PD1)	8.1 (PD5–PD1)	0.5–0.9
PD6	16.5	unknown	5.1–9.4 (PD5–PD1)	12.5 (PD6–PD1)	0.4–0.8

[1] Earthquakes identified at Penrose Drive and modeled in OxCal model 4b (figure 14; appendix E).
[2] Mean earthquake times from OxCal model 4b (table 2; appendix E).
[3] Per-event vertical displacement (see table 2 and text for description).
[4] Total displacement equal to sum of per-event displacements for earthquakes in parentheses.
[5] Elapsed time between events in parentheses, using the mean earthquake times.
[6] Vertical slip rate, based on total displacement divided by elapsed time.

(2005)—ranging from 17.4 ka (~14,300 ^{14}C yr B.P.) to 13.8 ka (~11,900 ^{14}C yr B.P.)—fall within this elevation range. We determined the minimum elevation range of the Provo shoreline at the site by (1) taking the elevation of the Provo boulder gravel where it is projected into the fault (1455 m; figure 8), (2) accounting for a (minimum) fault displacement of 5 m (1460 m), (3) correcting for isostatic rebound using the methods of Oviatt and others (1992) (1440 m adjusted elevation), and (4) adding an uncertainty of ±10 m as recommended by Oviatt and others (1992) (1430–1450 m elevation). When summed, the age ranges of Godsey and others (2005) have a midpoint of 15.6 ka, 2σ uncertainty of 2.7 kyr, and a 5th to 95th percentile (5–95%) range of 13.7–17.5 ka. To model the minimum constraint in OxCal, we include a single "calendar date" ("C_Date" in model) of 15.6 ± 2.7 ka. Although this results in a peak probability at 15.6 ka (compared to peaks in the summed PDF at 13.8 and 16.8 ka) for the age of the Provo shoreline, PD6 has a 5–95% range of 14.4–18.0 ka, which is consistent with our interpretation that the earthquake occurred after the Bonneville flood (~17.6 ka) but before regression of the Provo shoreline from the site (~14.5 ka).

Earthquake PD5 occurred at 12.1 ± 1.6 ka, during a time of very low lake level following regression from the Provo shoreline. Evidence for this event includes scarp-derived colluvium (unit 4) derived from both lacustrine and alluvial-fan sediments (units 1–3). A splay fault that displaces Provo-shoreline gravel (unit 3), but not the scarp colluvium (unit 4), also provides evidence of PD5. A prominent sand- and gravel-filled liquefaction vent that extends through unit 2 and into unit 3 and coincides with the splay fault (figure 11) is likely related to PD5. However, it is also possible that this liquefaction occurred during a later earthquake (possibly PD3a) based on fine sand injected into younger scarp-colluvium (unit 6) (h-8.1 m, v-3.2 m; west wall of east trench; plate 1). The Provo-shoreline age of 15.6 ± 2.7 ka described above provides a maximum constraint for the

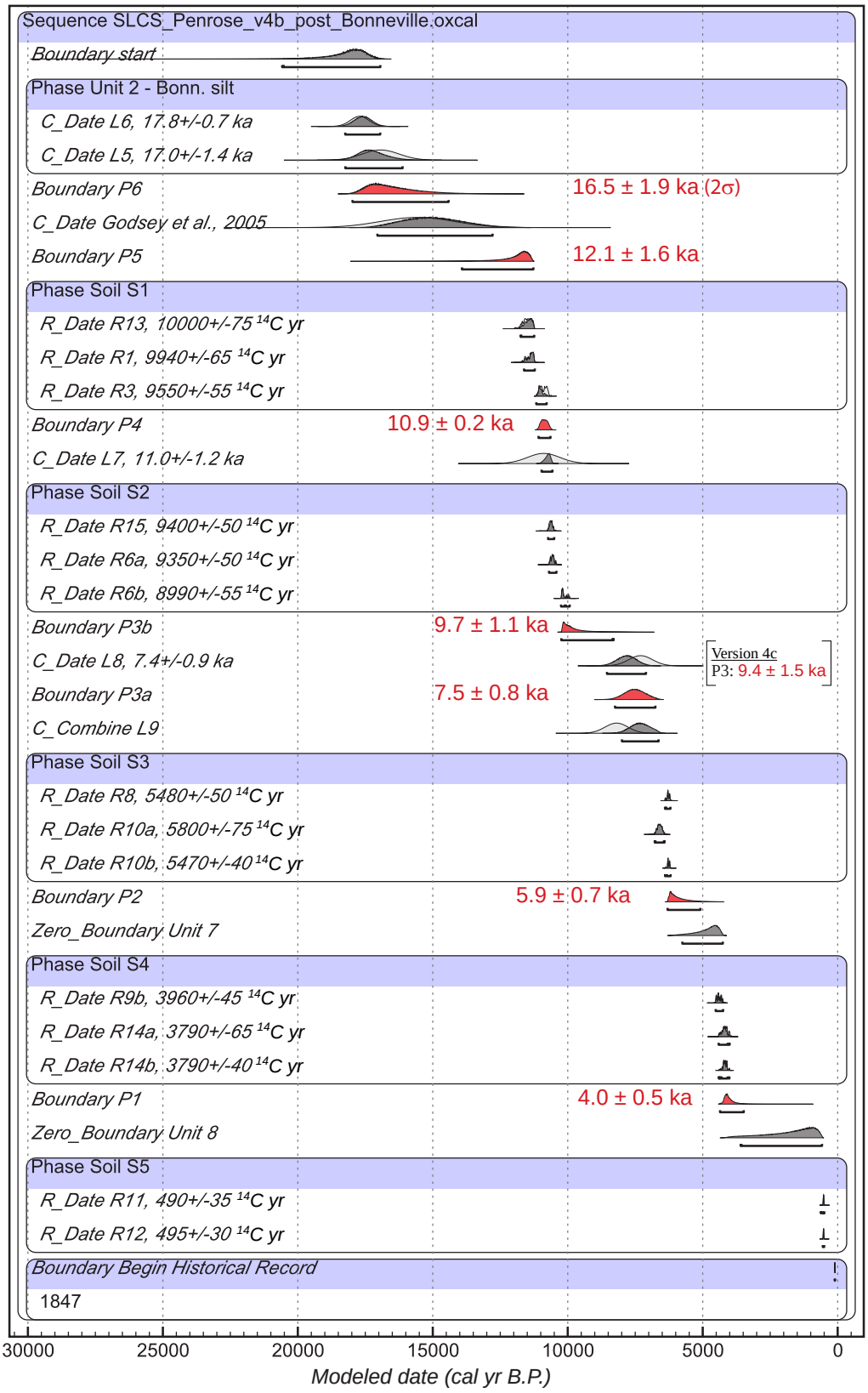

Figure 14. *OxCal model 4b for the Penrose Drive site, showing stratigraphic ordering of numerical data (appendices C and D) and probability density functions (PDFs) for earthquakes PD1–PD6. The models include* ***C_Date*** *for luminescence ages,* ***R_Date*** *for radiocarbon ages,* ***Phases*** *for groups of ages where the relative stratigraphic ordering is unknown, and* ***Boundary*** *for undated events (e.g., earthquake PD1) (see appendix E and DuRoss and others [2011] for discussion). Our preferred model of seven earthquakes is shown; an alternate, six-event model 4c is included in appendix E. Model constructed using OxCal version 4.1 (Bronk Ramsey, 1995, 2001) and the IntCal09 radiocarbon calibration curve (Reimer and others, 2009). Brackets below PDFs indicate 2σ time ranges.*

time of PD5. Soil S1 on unit 4 contains a well-developed A horizon and provides minimum time constraints of 10.9–11.5 ka (PD-R1, -R3, and -R13). An additional age (PD-R2) constrains soil S1 to 10.6 ka; however, this age is likely a poor minimum constraint on the timing of PD5 as the dated soil is developed on Provo boulder gravel (unit 2) away from the main scarp colluvium (several meters southwest of fault F2), where soils S1, S2, and S3 coalesce. Therefore, PD-R2 could potentially postdate earthquake PD4 (be contemporaneous with soil S2) as well as PD5. PD-R2 (10.6 ka) agrees better with the age of soil S2 (10.1–10.6 ka) than soil S1 (10.9–11.5 ka), and thus we do not use PD-R2 to constrain the time of earthquake PD5. We estimate 1.0–1.8 m of vertical displacement in PD5 (table 2).

The time of earthquake PD4 is well constrained to 10.9 ± 0.2 ka. Evidence for PD4 includes scarp colluvium (unit 5) that postdates soil S1 and predates soil S2. Soil S1 ages of 10.9–11.5 ka provide a maximum constraint on PD4 timing, whereas ages from soil S2 of 10.1–10.6 ka (PD-R6; east trench) and 10.6 ka (PD-R15; west trench) provide minimum constraints. An OSL age for unit 5 of 11.0 ± 1.2 ka (L7) is also a minimum timing constraint, and within its 1σ uncertainty, is consistent with the soil S2 ages. We estimate that earthquake PD4 had a vertical displacement of about 0.8–1.5 m (table 2).

The lower (unit 6a) and upper (unit 6b) colluvial wedges of unit 6 can be interpreted as either evidence of two earthquakes at 9.7 ± 1.1 ka (6a–PD3b) and 7.5 ± 0.8 ka (6b–PD3a), or a single earthquake at 9.4 ± 1.5 ka (PD3) (table 2). We prefer the two-earthquake interpretation, PD3a and PD3b, based on the distinct stone line between units 6a and 6b and because, individually, the two earthquakes have per-event displacements of 0.8–1.5 m, which is similar to the 0.7–1.8 m displacements estimated for PD1, PD2, PD4, and PD5. However, the absence of a soil between units 6a and 6b prevents us from dismissing the possibility of a single earthquake (PD3) having 1.6–2.9 m of vertical displacement. PD3b (and PD3) timing is based on maximum constraints of 10.1–10.6 ka for soil S2 and a minimum constraint of 7.4 ka (PD-L8) for unit 6a. PD3a occurred after deposition of unit 6a at about 7.4 ka, but before unit 6b and the formation of soil S3 within it. Unit 6b has OSL and IRSL mean ages of 8.4 and 8.1 ka (PD-L9), respectively, that are stratigraphically inverted with PD-L8 (7.4 ka); however, all three ages agree within their 1-kyr 2σ uncertainties. Because the IRSL age (8.1 ka) for PD-L9 is younger than the OSL age (8.4 ka), we combined both in the OxCal model. Radiocarbon ages for soil S3 provide a minimum constraint of 6.3–6.6 ka (PD-R8 and -R10) on the timing of PD3a. We disregard an additional age for soil S3 of 3.8 ka (PD-R5), which likely dated burrowed sediment.

Earthquake PD2 occurred at 5.9 ± 0.7 ka, after formation of soil S3 within unit 6b and before deposition of scarp colluvium from this earthquake (unit 7). A possible fault termination at the soil S3–unit 7 contact (h-23.3 m, v-5.1 m, west trench; plate 1) is also evidence of this earthquake. The ages from soil S3 of 6.3–6.6 ka provide a maximum constraint on the time of PD2, whereas ages of 4.2 ka (PD-R14a and -R14b) and 4.4 ka (PD-R9) from soil S4 developed on unit 7 provide minimum constraints. Earthquake PD2 had a vertical displacement of 0.7–1.3 m (table 2).

Earthquake PD1—the most recent earthquake—occurred at 4.0 ± 0.5 ka and had a vertical displacement of about 1.0–1.8 m. Evidence for PD1 includes unfaulted scarp colluvium (unit 8) that unconformably overlies sheared sediment and an eroded fault-scarp free face. Unit 8 also buries soil S4, which we estimate to have an age of 4.2–4.4 ka. Because unit 8 is extensively burrowed, we could not find a suitable place to sample it for dating. Soil S5 is developed on unit 8, and our two ages (PD-R11 and -R12) from S5 are both about 0.5 ka, which provides a poor minimum constraint on the time of PD1. We prefer a time for earthquake PD1 that is close to the ~4-ka maximum ages from soil S4, given the thick, strongly developed A horizon (several times thicker than soils S2–S4) on unit 8; this well-developed A horizon likely indicates a relatively long elapsed time since earthquake PD1. Furthermore, PD-R9 and PD-R14 sampled soil S4 less than 2 m from the fault zone; because of the preexisting scarp and easily erodible scarp colluvium and alluvial-fan soil, soil S4 in this area was likely buried by colluvium shortly after surface faulting during earthquake PD1.

Earthquake Recurrence and Fault Slip Rate

We calculated inter-event and mean recurrence intervals between individual Penrose Drive earthquakes using the mean earthquake times (table 2). Inter-event recurrence is the elapsed time between two successive earthquakes (e.g., S9–S8); mean recurrence is the mean over several seismic cycles based on the elapsed time between the oldest and youngest earthquakes (e.g., S9–S1) divided by the number of closed inter-event intervals.

Inter-event recurrence intervals vary from 1.2 kyr for PD5–PD4 and PD4–PD3b to 4.4 kyr between PD6 and PD5. However, additional earthquakes may have occurred in the ~4-kyr time between PD6 and PD5, which roughly corresponds with the time window during which the Provo shoreline could have occupied the site (~18–14 ka). If these earthquakes occurred during the Provo-phase occupation, such is likely the case for PD6, the sublacustrine colluvial wedges may have been removed by erosion. For example, 53° dipping Bonneville silt beds that we describe as evidence of PD6 could have been deformed by two events if the splay fault F2a, which displaces older, phase-1 liquefied sand (likely generated in PD6), is truncated at the angular unconformity between Bonneville silt and Provo gravel (unit 2–3 contact) (figure 11). Thus, we consider the PD6–PD5 recurrence interval poorly constrained.

Mean recurrence intervals for Penrose Drive earthquakes range from about 1.6 to 2.1 kyr, depending on the time interval (table 4). Including all events (PD6–PD1), the

Table 4. *Mean recurrence intervals for Salt Lake City-segment paleoseismic sites.*

	Penrose Drive[2]			Little Cottonwood Canyon[3]			South Fork Dry Creek[3]		
Time Period (To Present)[1]	Events	Time (kyr)/ int.	Mean RI (kyr)	Events	Time (kyr)/ int.	Mean RI (kyr)	Events	Time (kyr)/ int.	Mean RI (kyr)
Post-Bonneville Highstand	PD6–PD1 (S9–S3)	12.5/6	2.1	T–Z (S9–S1)	15.2/6 15.2/8	2.5 1.9	-	-	-
Post-Provo phase	PD5–PD1 (S8–S3)	8.1/5	1.6	-	-	-	-	-	-
Holocene	PD4–PD1 (S7–S3)	6.9/4	1.7	-	-	-	-	-	-
Holocene	PD3b–PD1 (S6–S3)	5.7/3	1.9	U–Z (S6–S1)	8.2/5	1.6	-	-	-
Late Holocene	-	-	-	W–Z (S4–S1)	4.2/3	1.4	A–D (S4–S1)	3.7/3	1.2

[1] Latest Pleistocene time periods are based on the Bonneville highstand (~18 ka) and Provo shoreline (~14 ka) datums. Holocene and mid-Holocene indicate time periods younger than ~10–11 ka and 5–6 ka, respectively.

[2] Penrose Drive mean recurrence intervals are based on the mean times shown in tables 2 and 5.

[3] Little Cottonwood Canyon and South Fork Dry Creek mean recurrence intervals are based on the mean times shown in table 5.

mean recurrence since the Bonneville highstand is 2.1 kyr; however, this estimate includes the long (~4-kyr), and possibly incomplete record between PD6 and PD5, and is thus poorly constrained. Considering the more complete post-Provo-shoreline record, the mean recurrence between earthquakes PD5 and PD1 is 1.6 kyr. Holocene mean recurrence estimates vary from about 1.7 to 1.9 kyr based on earthquakes PD4–PD1 and PD3b–PD1, respectively. Because the most recent Penrose Drive earthquake occurred at about 4.0 ka, there is insufficient data to calculate a late Holocene mean recurrence interval.

The post-Provo vertical slip rate for the East Bench fault at Penrose Drive ranges from 0.3 to 0.9 mm/yr; however, we prefer an estimate of 0.5–0.9 mm/yr based on 4.1–7.6 m of displacement in the 8.1-kyr span between PD5 and PD1 (table 3). This slip rate is nearly identical to those calculated using shorter time periods, such as PD4–PD1 (table 3). If we include the poorly constrained PD6–PD5 recurrence (and PD5 displacement), then 5.1–9.4 m of displacement occurred in the 12.5 kyr between PD6 and PD1, yielding a rate of 0.4–0.8 mm/yr. Alternatively, an open-ended post-Provo slip rate, which accounts for the 4-kyr elapsed time since PD1, is 0.3–0.7 mm/yr using 5.1–9.4 m of displacement and a Provo-shoreline age of 15.6 ± 2.8 ka. Because Lake Bonneville highstand sediments have likely been eroded from the footwall of the fault, we have insufficient data to calculate a post-Bonneville highstand slip rate.

A poorly constrained, long-term vertical slip rate is based on the minimum displacement of the pre-Bonneville alluvial-fan gravel. A minimum of 16 m of vertical displacement divided by the mean age of unit 1 (67.3 ± 14.4 ka) yields a slip rate of greater than 0.2–0.3 mm/yr.

PALEOSEISMOLOGY OF THE SALT LAKE CITY SEGMENT

Correlation of Earthquakes

Surface-faulting earthquake histories for the East Bench and Cottonwood faults indicate that at least nine earthquakes (S1–S9; table 5) have occurred on the SLCS since the latest Pleistocene. At Penrose Drive, at least seven earthquakes occurred between about 16.5 ka and 4.0 ka, postdating the highstand of Lake Bonneville (~18 ka) (figure 15; table 2). Similarly, seven post-Bonneville earthquakes occurred at LCC (events T–Z; McCalpin, 2002; figure 16); however, of these, we only correlate five earthquakes between the sites (figure 17). Black and others (1996) identified four late Holocene earthquakes at SFDC (W–Z; Black and others, 1996; renamed earthquakes A–D for clarity), two of which likely correlate with the youngest two Penrose Drive events (figure 17). Because each site only exposed a subset of the nine SLCS earthquakes, important questions remain regarding the extent of individual fault ruptures during these earthquakes.

We constructed OxCal models for the LCC and SFDC sites (appendix E) to compare with our Penrose Drive results. Our OxCal models use previously published data, rely heavily on the original interpretations of the authors, treat the AMRT ages consistently, calendar calibrate the radiocarbon ages, and yield internally consistent models of the earthquake times (see DuRoss and others, 2011, for further discussion). Our OxCal results (figure 16 and appendix F) are similar to the previously published earthquake times, with minor differences related to AMRT corrections and the treatment of numerical-age and earthquake-timing uncertainties.

Table 5. *Correlation of surface-faulting earthquakes on the Salt Lake City segment.*

Earthquake	Penrose Drive[1] (ka)	Little Cottonwood Canyon[2] (ka)	South Fork Dry Creek[3] (ka)
S1	no evidence	1.3 ± 0.04 (Z-1.3)	1.3 ± 0.2 (D)
S2	no evidence	2.1 ± 0.3 (Y-2.3)	2.2 ± 0.4 (C)
S3	4.0 ± 0.5 (PD1)	4.4 ± 0.5 (X-3.5)	3.8 ± 0.6 (B)
S4	5.9 ± 0.7 (PD2)	5.5 ± 0.8 (W-5.3)	5.0 ± 0.5 (A)
S5	7.5 ± 0.8 (PD3a)	7.8 ± 0.7 (V-7.5)	not exposed
S6	9.7 ± 1.1 (PD3b)	9.5 ± 0.2 (U-9)	“
S7	10.9 ± 0.2 (PD4)	no evidence	“
S8	12.1 ± 1.6 (PD5)	no evidence	“
S9	16.5 ± 1.9 (PD6)	16.5 ± 2.7 (T-17)	“

[1] Penrose Drive earthquake timing (mean ± 2σ) based on OxCal model 4b.
[2] Little Cottonwood Canyon (LCC) earthquake timing (mean ± 2σ) based on OxCal model (appendix E) using paleoseismic data from McCalpin (2002). The earthquake times as published by McCalpin (2002) are included in parentheses. The timing uncertainty for LCC event T is based on the minimum-maximum possible range rather than 2σ standard deviation (see text for discussion).
[3] South Fork Dry Creek (and Dry Gulch) earthquake timing (mean ± 2σ) based on OxCal model (appendix E) constructed using paleoseismic data from Black and others (1996).

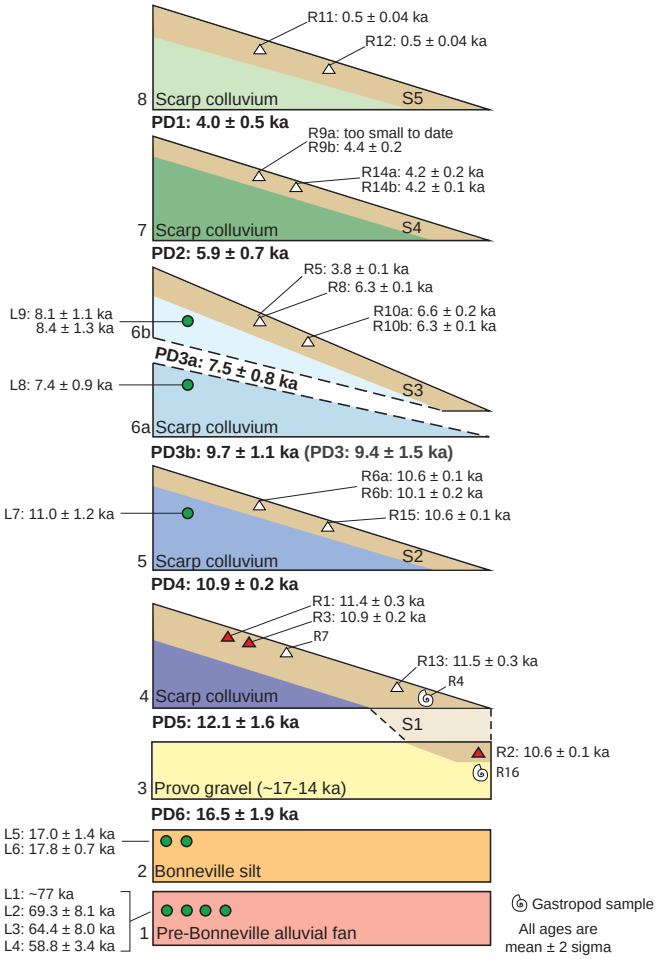

Figure 15. *Surface-faulting earthquake chronology of the Penrose Drive site, showing stratigraphic units, soils, and numerical age control (appendices C and D). White triangles indicate bulk soil-sediment samples; red triangles indicate macrocharcoal samples. Green circles indicate samples dated using optically stimulated luminescence. Earthquake mean ages and 2σ uncertainties based on OxCal models 4b (including earthquakes PD3a and PD3b) and 4c (including earthquake PD3) (appendix E; figure 14).*

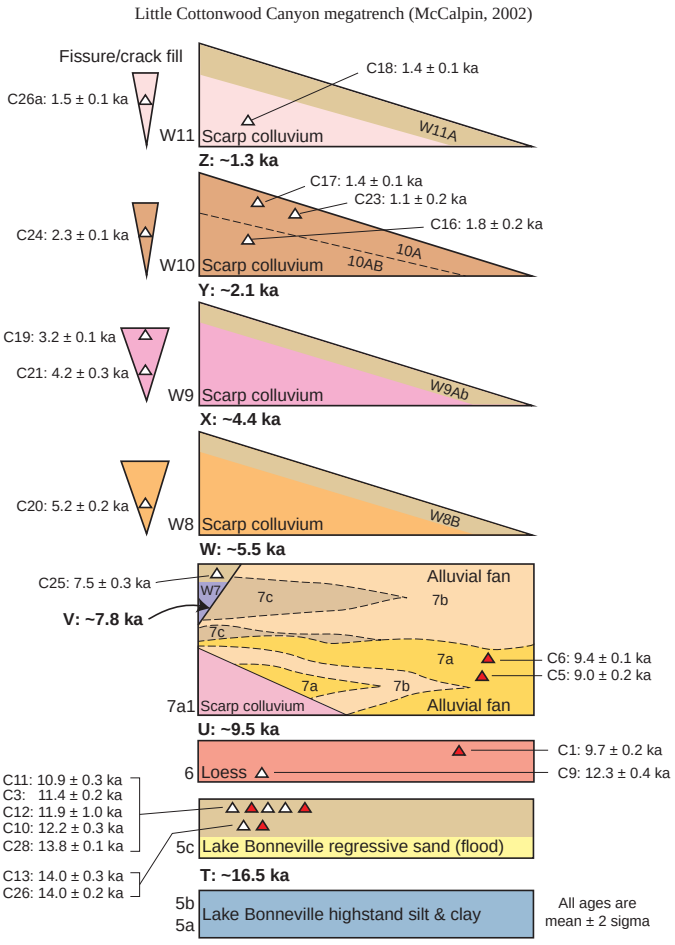

Figure 16. *Chronology of surface-faulting earthquakes at the Little Cottonwood Canyon site, based on stratigraphic units and evidence of surface-faulting earthquakes from McCalpin (2002). White triangles indicate bulk soil-sediment samples; red triangles indicate macrocharcoal samples. Earthquake mean ages and 2σ uncertainties based on OxCal model constructed for the site (this study; appendix E).*

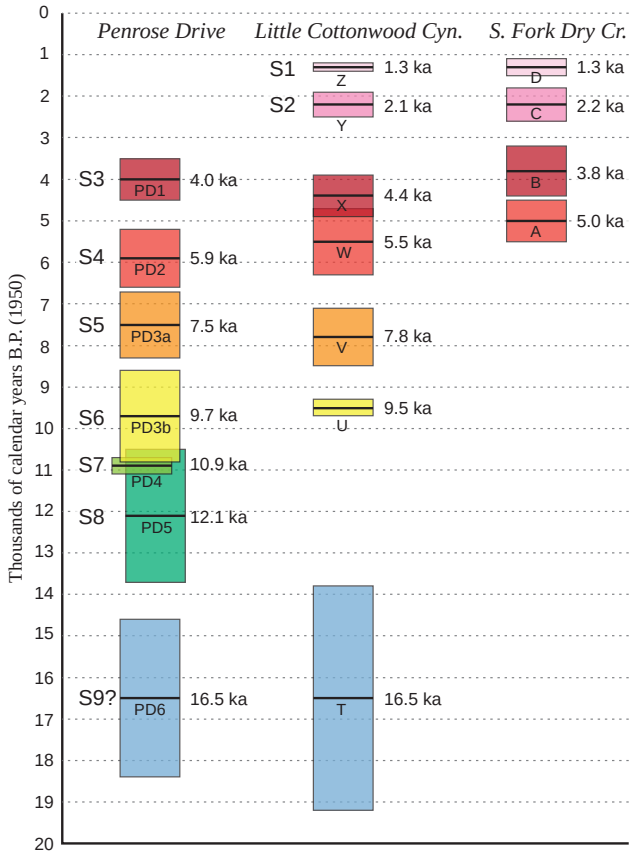

Figure 17. *Correlation of SLCS earthquakes identified at the Penrose Drive, Little Cottonwood Canyon, and South Fork Dry Creek trench sites. Mean earthquake times (black horizontal lines) and 2σ uncertainties (boxes) are derived from our OxCal models (appendix E).*

Penrose Drive earthquake PD6 (~16.5 ka) possibly correlates with the oldest LCC earthquake (T, ~16.5 ka) as SLCS earthquake S9. At LCC, event T postdates Lake Bonneville highstand silt, but possibly predates a regressive sand that McCalpin (2002) interpreted to be contemporaneous with the Bonneville Flood (thus deposited ~17–18 ka) on the basis of its increased thickness within a large graben. However, the regressive sand was only exposed in and along the flanks of the graben, where it could have been eroded during scarp degradation; thus, the thickness outside of the graben is uncertain. In addition, whereas at least one minor fault is truncated at the highstand silt and regressive sand contact, three additional faults terminate at various soil horizons (Ab, AC, C1 and C2; McCalpin, 2002) formed on the regressive sand. Finally, the regressive sand was not dated, and thus uncertainty remains in its age in relation to the flood. Considering these uncertainties, we include two alternative OxCal models for LCC (versions 4 and 4b; appendix E), with event T occurring (1) before deposition of the regressive sand (i.e., before the flood), and (2) after the flood, but before an A horizon developed on the sand over about 10.9–14.0 ka. These models yield earthquake times of 17.9 ± 0.7 ka (event T predates the flood) and 15.2 ± 2.0 ka (event T postdates the flood). To account for both models, we summed the PDFs, yielding a single, broadly constrained earthquake PDF for event T with a mean of 16.5 ka and a possible range of 13.8–19.2 ka (because of the resulting bimodal distribution, we prefer the uncertainty based on the range, ± 2.7 kyr, over the 2σ uncertainty of ± 3.0 kyr). Although we include an alternate model, our mean time of 16.5 ka corresponds well with the 17 ka age interpreted for event T by McCalpin (2002). We correlate LCC earthquake T with Penrose Drive earthquake PD6 considering the striking similarity in faulted highstand silt and unfaulted post-highstand sand or gravel at both sites. However, we recognize that the LCC earthquake T could be a separate, slightly older event than PD6 (which postdates the Bonneville highstand and predates the Provo shoreline) if the earthquake predates the Bonneville flood as interpreted by McCalpin (2002).

The timing of PD6 and LCC event T (SLCS earthquake S9) corresponds well with evidence of surface warping in Lake Bonneville (highstand?) silt and clay at the Dresden Place site (about 2 km southwest of Penrose Drive) on the East Bench fault (Machette and others, 1992). The earthquake at Dresden Place likely occurred between the Lake Bonneville highstand and latest Provo-phase shoreline, about 18–14 ka.

SLCS earthquakes S8 and S7 are based solely on Penrose Drive earthquakes PD5 (12.1 ka) and PD4 (10.9 ka). At LCC, McCalpin (2002) used the absence of earthquakes in the ~8-kyr-long period between earthquakes T (~17 ka) and U (9.5 ka) as evidence of a period of seismic quiescence on the SLCS. This time period is represented by the Lake Bonneville regressive sand (and 11–14-ka soil) and a post-Bonneville loess (and ~10–12-ka soil). McCalpin (2002) discussed the possibility that stratigraphic evidence of events in this time period was removed by alluvial-fan erosion at about 9–10 ka, but considered the scenario unlikely. However, we note that the loess (his unit 6) appears to fill a fault-related depression (graben?), which is possibly evidence of earthquakes postdating the regressive sand and predating the ~9–10 ka alluvial-fan deposits. Evidence of these earthquakes could also have been obscured by the extensive deposition of pedogenic carbonate, which complicated the interpretation of depositional environment (McCalpin, 2002). Considering these uncertainties, we consider it plausible but not certain that PD5 and PD4 ruptured the LCC site (possibly with small displacements?), but were not recognized.

SLCS earthquake S6 is based on the correlation of Penrose Drive earthquake PD3b (9.7 ka) with LCC event U (9.5 ka). Although earthquake PD3b has a larger uncertainty (±1.1 kyr) than event U (±0.2 kyr), both earthquakes postdate soils formed at about 10–11 ka. The larger uncertainty for PD3b stems from the minimum ages of 7–8 ka, whereas charcoal from alluvial-fan deposits postdating event U tightly constrain this event to a minimum of about 9.0–9.4 ka (appendix E). The time of event U is slightly older (~9.8 ka) if the youngest maximum limiting age—C1 at ~9.7 ka (appendix E)—is

excluded due to its position outside the area of burial from event-U colluvium; however, we agree with McCalpin (2002) that the ~9.7-ka age likely represents a reasonable time for event U and thus include it in the OxCal model. Event PD3b had 0.8–1.5 m of vertical displacement, whereas McCalpin (2002) did not estimate displacement for event U.

Penrose Drive earthquake PD3a (7.5 ka) and LCC event V (7.8 ka) define the occurrence of SLCS earthquake S5. PD3a and event V have similar mean times and uncertainties despite differences in the type and quality of their limiting ages. Event V is best constrained (to a minimum) by a soil developed on a fissure-fill deposit and dated at 7.5 ka; charcoal ages of 9.0–9.4 ka for a thick alluvial-fan package provide a poor maximum limit for event V. In contrast, PD3a postdates colluvium deposited about 7.4–8.4 ka, and predates soil ages of 6.3–6.6 ka. Earthquake PD3a produced about 0.8–1.5 m of vertical displacement, whereas the displacement for V is unknown because the colluvial wedge resulting from this event was not exposed.

The timing of SLCS earthquakes S5 and S6 corresponds well with the general timing of surface faulting on the Warm Springs fault, as documented in excavations for an expansion of the Salt Palace Convention Center in downtown Salt Lake City. At the Salt Palace expansion project site, one and possibly two earthquakes occurred between about 7.4 and 9.0 ka (Kleinfelder, 1999; Simon-Bymaster, 1999). However, questions regarding the number of events at the site and the context of the samples reduce our confidence in analyzing potential earthquakes on the Warm Springs fault. Displacements at the Salt Palace are not well constrained because of complex faulting and extensive graben formation.

We correlate Penrose Drive earthquake PD2 (5.9 ka) with LCC event W (5.5 ka) and SFDC earthquake A (5.0 ka) to define earthquake S4 for the SLCS. Earthquake S4 has similar uncertainties (±0.5–0.8 kyr) at the three sites, but slightly different mean ages because of their limiting ages. Event PD2 has maximum ages of 6.3–6.6 ka and minimum ages of 4.2–4.4 ka from soils developed on scarp colluvium. Event W has a presumably poor maximum age from the post-event V soil (7.5 ka), but a better minimum age from event-W fissure fill dated to 5.2 ka. At SFDC, earthquake A occurred after 5.1–5.8 ka, but before ~4 ka based on ages from soils developed on alluvial-fan deposits. Given these limiting ages, S4 likely occurred between 4 and 6 ka. Excluding graben-fill sediments, the colluvial wedge from event W has a maximum thickness of about 0.8 m; however, McCalpin (2002) estimated an average displacement of 1.8 m as discussed above. Black and others (1996) did not report per-event displacement for SFDC events because of an unknown amount of antithetic faulting to the west. Black and Lund (1995) did estimate displacement using colluvial-wedge thickness; however, we do not include these values because of significant back-rotation (tilting) observed in several trenches (e.g., trench DC-1; Black and others, 1996) and because of uncertainties in correlating colluvial wedges exposed in multiple trenches. Our displacement range for Penrose Drive earthquake PD2 is 0.7–1.3 m.

The most recent earthquake at Penrose Drive (PD1, 4.0 ka) likely correlates with LCC event X (4.4 ka) and SFDC earthquake B (3.8 ka) to define SLCS earthquake S3. SFDC event B has close limiting ages of 4.0 ka (maximum) and 3.8–4.0 ka (minimum), which is consistent with the maximum ages of 4.2–4.4-ka for earthquake PD1. An age from fissure fill constrains LCC event X to a minimum of 4.2 ka; however, McCalpin (2002) reported a slightly younger event-X age of 3.5 ka. These limiting ages support a time for earthquake S3 of about 4 ka. Using maximum colluvial-wedge thickness, we estimate 1.0–1.8 m of displacement in event PD1, compared to the average displacement of 1.8 m for event X.

SLCS earthquakes S2 (~2.1–2.2 ka) and S1 (~1.3 ka) did not rupture the Penrose Drive site. Although we cannot rule out the possibility that event PD1 at Penrose Drive—which only has a maximum limiting age of ~4 ka—correlates with one of these events, we consider it unlikely. As discussed above, the ~4-ka soil faulted in PD1 was likely buried by scarp colluvium shortly after the earthquake, whereas a long period of time elapsed after PD1 based on the well-developed soil A horizon formed on scarp colluvium that resulted from the event. Per-event vertical displacements for both S2 and S1 are based on the average displacement of 1.8 m from LCC (McCalpin, 2002) and an average displacement of 2.0 ± 0.5 m at the SFDC site, based on a debris-flow levee that has been faulted during two and possibly three earthquakes (Black and others, 1996).

Earthquake Recurrence

Nine earthquakes (S9–S1) occurred on the SLCS since the latest Pleistocene based on paleoseismic records from Penrose Drive, LCC, and SFDC (table 5; figure 17). Because each site exposed an incomplete SLCS earthquake record, we compare mean recurrence intervals for the individual sites that are based on the number of events that occurred since the (1) latest Pleistocene, using the Bonneville-highstand (~18 ka) and Provo-shoreline (~14 ka) datums, (2) early Holocene (~10–11 ka), and (3) mid-Holocene (~5–6 ka) (table 4). Mean recurrence estimates reported here are simplified, including only the mean earthquake timing results; see DuRoss and Hylland (in review) for a more detailed probabilistic analysis of recurrence (including two-sigma recurrence estimates) that accounts for the full individual earthquake-timing distributions (e.g., DuRoss and others, 2011).

The Penrose Drive and LCC data yield recurrence intervals for the time periods since the Bonneville highstand and Provo shoreline (Provo phase). At Penrose Drive, the post-Bonneville-highstand mean recurrence between earthquakes S9 and S3 is 2.1 kyr, which excludes the long elapsed time (~4 kyr) since the youngest earthquake S3. A comparable mean recurrence for LCC is 2.5 kyr (earthquakes S9–S1); however, this

interval does not account for earthquakes S8 and S7, which were identified at Penrose Drive and possibly could have ruptured the LCC site. Including S8 and S7 reduces the LCC latest Pleistocene recurrence interval to 1.9 kyr. We have relatively low confidence in these recurrence values given the long (~4 kyr) elapsed time between earthquakes S9 and S8 observed at Penrose Drive, and thus, uncertainty regarding the completeness of the SLCS earthquake record prior to about 14 ka. The absence of earthquakes in the 4-kyr period between S9 and S8 could be related to (1) a period of seismic quiescence on the SLCS, (2) difficulty recognizing evidence of earthquakes owing to Provo-phase shoreline erosion and deposition, or (3) the possibility of Penrose Drive earthquake PD6 and LCC event T being two separate earthquakes. Because we cannot fully rule out any of these explanations, we consider the SLCS record poorly constrained (and possibly incomplete) prior to about 14 ka.

A post-Provo-phase mean recurrence estimate for the SLCS is 1.6 kyr based on earthquakes S8–S3 that postdate the Provo shoreline (~14 ka) at Penrose Drive. We have more confidence in this mean recurrence than in the post-Bonneville-highstand mean recurrence because it is similar to Holocene recurrence intervals calculated for both Penrose Drive (1.7–1.9 kyr) and LCC (1.6 kyr) (discussed below). Although the LCC record extends to ~18 ka, SLCS earthquakes S8 and S7, which occurred after abandonment of the Provo shoreline, were not identified at the site, and thus, we do not calculate a post-Provo-shoreline mean recurrence using the LCC data.

Holocene mean recurrence intervals for the SLCS are based on the number of inter-event intervals that occurred after S7 (~10.9 ka at Penrose Drive) and S6 (~9.5–9.7 ka based on Penrose Drive and LCC), whereas late Holocene mean recurrence is based on the intervals postdating S4 (~5.0–5.5 ka based on data from LCC and SFDC). The Holocene mean recurrence is 1.7–1.9 kyr at Penrose Drive and 1.6 kyr at LCC. In contrast, late Holocene mean recurrence intervals are 1.2 kyr at SFDC and 1.4 kyr at LCC; minor differences in these mean estimates relate to the 0.5-kyr difference in the S4 time at LCC (5.5 ka) and SFDC (5.0 ka). We have the most confidence in the ~1.2–1.4-kyr late Holocene mean recurrence estimates as they stem from the best-constrained events, S4–S1, which have been identified at two to three trench sites. Importantly, these late Holocene estimates are reasonably similar to the Penrose Drive post-Provo-phase mean recurrence estimate of 1.6 kyr, possibly indicating that the SLCS earthquake record is complete after ~14 ka. Slightly longer mean recurrence rates for the Holocene (1.7–1.9-kyr at Penrose Drive) likely stem from variability in the inter-event recurrence times (aperiodicity). For example, the longer mean recurrence intervals for the Holocene include relatively long (~2-kyr) inter-event recurrence times for earthquake pairs S6–S5 and S5–S4.

Vertical Slip Rate

Of the three SLCS trench investigations, only the Penrose Drive site yielded vertical-slip-rate information. We have the most confidence in closed-interval slip rates of 0.5–0.9 mm/yr for the Penrose Drive site calculated using various post-Provo time periods (e.g., PD5–PD1; table 3). However, these rates are possibly minima considering the position of the Penrose Drive site on the northernmost East Bench fault. If the along-strike displacement on the East Bench fault and the SLCS follow that for historical normal-faulting earthquakes in the Basin and Range Province (and elsewhere) (Hemphill-Haley and Weldon, 1999; Wesnousky, 2008; Biasi and Weldon, 2009), per-event displacements likely increase south of Penrose Drive, toward the center of the East Bench fault and the center of the SLCS.

We also consider a long-term slip rate calculated using a vertically offset glacial moraine at the mouth of Bells Canyon, south of LCC. Swan and others (1981) profiled the crest of the Bells Canyon moraine and found 14.5 m (11.5–24.5 m range) of vertical surface offset. Using an age of 15.9 ± 0.7 ka derived from two ^{10}Be exposure ages for boulders on the youngest parts of the moraine (Lips, 2005; Lund, 2007), the vertical slip rate is 0.9 mm/yr (0.7–1.6 mm/yr range). However, the UQFPWG (Lund, 2005) preferred a Holocene rate for the SLCS of 1.2 mm/yr (0.6–4.0 mm/yr approximate 5th–95th percentile range) because of the long-term nature of the Bells Canyon rate (and the possible post-Bonneville seismic quiescence) and higher Holocene rates measured for the adjacent Weber and Provo segments.

Rupture Extent

Surface-fault-rupture length (straight-line distance between rupture end points) is important for understanding fault segmentation, such as the persistence of mapped segment boundaries and the relative frequency of single-, partial-, and multi-segment ruptures on a long structure such as the WFZ. Rupture length is also important for estimating and understanding earthquake magnitudes (using magnitude-length empirical regressions), how displacement scales with length, and rupture-propagation direction effects. In essence, do ruptures on WFZ segments have consistent lengths and displacement profiles through time? Or is rupture variability influenced by partial- or multi-segment ruptures or propagation direction?

SLCS earthquake rupture lengths are difficult to assess because the segment consists of the three separate strands, only two of which have robust paleoseismic data (Cottonwood and East Bench faults). In addition, the Penrose Drive site is close to the northern end of the East Bench fault, and thus, it is possible that ruptures could have extended to the East Bench fault, but not ruptured the Penrose Drive site. Thus, we recognize that our length estimates are minimum estimates, and that additional paleoseismic data are necessary to resolve the rupture behavior of the SLCS in more detail.

Of the nine SLCS earthquakes (table 5), four and possibly five have been identified on both the East Bench and Cottonwood faults, with minimum rupture lengths of 25 km for S3 and S4 (Penrose Drive to SFDC) and 21 km for S5 and S6 (Penrose Drive to LCC). Earthquake S5 or S6 may have also ruptured the Warm Springs fault at the Salt Palace site, which would not affect the minimum rupture lengths for these events, but could indicate a full rupture of the SLCS. If LCC event T and Penrose Drive earthquake PD6 correlate in SLCS earthquake S9, surface faulting during this earthquake would have a minimum rupture length of 21 km.

Earthquakes S1 and S2 ruptured the Cottonwood fault (at both LCC and SFDC), but were not identified at Penrose Drive. We consider it unlikely that evidence of these earthquakes was misinterpreted, unrecognized, or disturbed at Penrose Drive because of the length of the west trench and the clear evidence of the most recent earthquake at the site (unfaulted unit 8). However, it is possible that surface ruptures from S1 and S2 extended north of the site on an unidentified strand of the fault, near the active channel of Dry Creek and were later modified by stream processes or obscured during development of the area. Although possible, we do not consider this scenario very likely as the seven previous SLCS earthquakes ruptured the Penrose Drive site (and in fact, the same fault) and had a moderate amount of displacement (~1 m per event), which would likely be evident at the surface if that displacement had occurred on a different fault strand. Alternatively, surface ruptures from these Cottonwood fault earthquakes could have continued on to the East Bench fault, but not as far north as Penrose Drive. The minimum rupture length for S1 and S2 is poorly constrained because of the short distance between the LCC and SFDC sites (3.5 km), but is possibly ~20 km, equal to the length of the Cottonwood fault. Longer rupture lengths are possible if S1 and S2 ruptured part of the East Bench fault south of Penrose Drive. Additional paleoseismic data (particularly for the East Bench fault) are necessary to refine the rupture lengths of earthquakes S1 and S2.

The Penrose Drive data provide new evidence of two earthquakes (S7 and S8) that may have ruptured the East Bench fault, but not the Cottonwood fault. However, as discussed above, the timing of these events corresponds with a part of the LCC stratigraphic record that is difficult to interpret due to complicated faulting from later earthquakes and extensive carbonate soil development. Thus, while S7 and S8 may have been limited to only the East Bench (and Warm Springs?) fault, we cannot completely rule out the possibility that they also ruptured the Cottonwood fault. Separate paleoseismic data confirming that these earthquakes are missing from the Cottonwood fault record are needed. Because earthquakes S7 and S8 have only been identified at one site, their rupture lengths are unknown.

DISCUSSION

Our investigation at Penrose Drive improves the latest Pleistocene to present earthquake history of the SLCS (figure 17). Using our preferred correlation of events, we identify nine earthquakes (S9–S1) on the SLCS that postdate the highstand of Lake Bonneville (~18 ka). Earthquakes PD1 (~4.0 ka) to PD3b (~9.7 ka) provide independent evidence of SLCS earthquakes S3 to S6, which were previously identified at LCC and SFDC, and thus, improve estimates of the event times, displacements, and rupture extents. We identify two additional earthquakes at Penrose Drive that occurred between about 11 and 14 ka (PD4 and PD5), within a previously inferred period of seismic quiescence between ~17 and 9 ka based on the LCC earthquake chronology (McCalpin, 2002). PD4 and PD5 reduce the recurrence time between the earliest two SLCS earthquakes from ~8 kyr to ~4 kyr and show that the apparent lack of earthquakes in this period is likely related to an incomplete geological record rather than a significant change in fault behavior. The earliest earthquake at Penrose Drive (PD6; ~16.5 ka) possibly correlates with the earliest earthquake at LCC (event T; ~16.5 ka); however, these earthquakes have 2–3-kyr timing uncertainties, so we have less confidence in this correlation.

Latest Pleistocene and Holocene mean recurrence intervals for the Penrose Drive, LCC, and SFDC sites range from 1.2 to 2.5 kyr. We have the most confidence in late Holocene mean recurrence estimates of 1.2–1.4 kyr for SFDC and LCC, a post-Provo-phase estimate of 1.6 kyr for Penrose Drive, and a Holocene recurrence estimate of 1.6 kyr for LCC. Penrose Drive data indicate slightly longer Holocene mean recurrence estimates of 1.7–1.9 kyr; however, the two most recent SLCS earthquakes (S1 and S2) did not rupture the site and thus the data are skewed by the ~2-kyr recurrence times for S6–S5 and S5–S4. In contrast, the Holocene mean recurrence interval for LCC, which includes the six most recent SLCS earthquakes, is 1.6 kyr. The similarity in these late Holocene, Holocene, and post-Provo-phase recurrence intervals may indicate that the rate of surface-faulting earthquakes on the SLCS has been fairly constant since the regression of Lake Bonneville from the Provo shoreline (~14 ka). This is similar to paleoseismic results for the Provo segment (Mapleton site), which indicate a fairly constant rate of earthquake recurrence over the Holocene (Olig and others, 2011). The mean recurrence intervals for the SLCS also compare well with the 1.3-kyr (0.5–2.4 kyr approximate 5^{th}–95^{th} percentile range) late Holocene mean recurrence interval estimated for the SLCS (using the LCC and SFDC data) by the UQFPWG (Lund, 2005). We have less confidence in post-Bonneville-highstand mean recurrence estimates of 1.9–2.5 kyr, which include the long (~4-kyr) interval between earthquakes S9 and S8 (18–14 ka). The record of earthquakes in this time interval could be incomplete because of nondeposition or erosion related to the Provo shoreline.

The long-term (since latest Pleistocene) vertical slip rate for the SLCS is about 0.5–0.9 mm/yr based on a Provo-phase closed-seismic-interval slip rate of 0.5–0.9 mm/yr for Penrose Drive and the vertical offset of the Bells Canyon glacial moraine, which yields a slip rate of ~0.9 mm/yr since about ~16 ka. However, we consider this long-term rate only moderately well constrained because of questions regarding the position of the Penrose Drive site in the along-strike displacement profile of the SLCS, and the open-ended nature of the surface-offset-based rate for Bells Canyon. The Holocene rate of slip for the SLCS remains unconstrained.

Although we have refined the latest Pleistocene earthquake record of the SLCS, several questions remain. For example, the extent of individual ruptures along the segment remains uncertain, with minimum distances equal to the actual distance between sites where a specific rupture has been identified. An important question is why did SLCS earthquakes S1 (~1.3 ka) and S2 (~2.2 ka) fail to rupture the Penrose Drive site. Did these earthquakes rupture part of the East Bench fault south of Penrose Drive? Did they rupture the Warm Springs fault? One possibility is that S1 and S2 originated as earthquakes on the Provo segment at 1.5 ± 0.4 ka (earthquake P2 based on the Mapleton trench site; Olig and others, 2011) and 2.2 ± 0.4 ka (earthquake P3 based on the American Fork site; Machette and others, 1992) (S. Olig, written communication, 2013), and thus were spill-over ruptures (across the Provo–Salt Lake City segment boundary) that extended only along the southern part of the SLCS. This would be a similar scenario to that described by DuRoss and others (2012) and Personius and others (2012) where a late Holocene rupture on the Weber segment extended across the Weber–Brigham City segment boundary and onto the southern part of the Brigham City segment. We also note that SLCS earthquakes S7 (~10.9 ka) and S8 (~12.1 ka) ruptured the East Bench fault, but were not identified at LCC. Did S7 and S8 rupture the Cottonwood fault, or only the East Bench fault? If the latter, how do they relate to earthquakes on the Weber segment? Unfortunately, only limited earthquake-timing data are available for the Weber segment prior to about 6 ka (DuRoss and others, 2009).

The correlation of surface-faulting earthquakes at Penrose Drive with earthquakes previously identified at LCC and SFDC highlights important spatial and temporal gaps in paleoseismic data for the SLCS. To improve the resolution of SLCS earthquake rupture extent, additional paleoseismic data are required. Specifically, confirmation of the late Holocene earthquake record of the East Bench fault and the latest Pleistocene record for the Cottonwood fault is needed to determine whether these faults have ruptured independently. Paleoseismic data near the northern and southern boundaries of the SLCS (e.g., on the southern Weber segment or northern Provo segment) would also improve estimates of SLCS rupture lengths and shed light on the possibility of spill-over rupture across mapped segment boundaries. Finally, the earthquake history of the Warm Springs fault and the post-Bonneville highstand (~18–14 ka) earthquake record of the SLCS remain poorly constrained.

SUMMARY AND CONCLUSIONS

The Penrose Drive site provides important information on the timing, displacement, and recurrence of surface-faulting earthquakes on the East Bench fault of the SLCS. At least seven post-Bonneville highstand earthquakes occurred at ~4.0 ka (PD1), ~5.9 ka (PD2), ~7.5 ka (PD3a), ~9.7 ka (PD3b), ~10.9 ka (PD4), ~12.1 ka (PD5), and ~16.5 ka (PD6); earthquakes PD1 to PD5 each had about 1.0–1.4 m of vertical displacement. Where the record is most complete (since ~14 ka), earthquakes PD5–PD1 yield a latest Pleistocene mean recurrence interval of ~1.6 kyr that is similar to Holocene estimates for the site (1.7–1.9 kyr) and late Holocene estimates for the Cottonwood fault (1.2–1.4 kyr). Latest Pleistocene and Holocene vertical slip rates for the Penrose Drive site are 0.5–0.9 mm/yr.

Paleoseismic data from Penrose Drive—when combined with previous results from LCC and SFDC—demonstrate that the SLCS has been a consistently active source of large-magnitude earthquakes since the latest Pleistocene. At least nine surface-faulting earthquakes (S1–S9) have occurred on the SLCS since the Bonneville highstand, including two earthquakes (S7 and S8) that occurred within a previously interpreted ~8-kyr gap in the SLCS paleoseismic record. These data indicate an essentially stable rate of earthquake recurrence since the latest Pleistocene, corroborating similar results for the Provo segment. Refined paleoseismic data for the SLCS demonstrate the difficulty in obtaining a complete latest Pleistocene earthquake record on the WFZ and underscore the importance of having multiple lines of paleoseismic evidence when interpreting a segment-wide earthquake chronology. Although additional paleoseismic data for the SLCS are necessary to address questions of rupture extent and segmentation, our paleoearthquake data are important to understanding the earthquake potential of the SLCS, clarifying the seismogenic relation between the SLCS and WVFZ, and forecasting the probabilities of future large-magnitude earthquakes in the Wasatch Front region.

ACKNOWLEDGMENTS

This paleoseismic study of the Salt Lake City segment was funded by the Utah Geological Survey and U.S. Geological Survey, National Earthquake Hazards Reduction Program, award no. G10AP00068. Rich Giraud (UGS) and Bradley King (USGS) assisted with the fieldwork. Jay Hill, Lori Steadman, and Corey Unger (UGS) helped prepare some of the illustrations in this report. We thank Ian and Annette Cummings for their interest in the project and for granting permission to trench at the Penrose Drive site. Reviews by Steve Bowman, Bill Lund, and Robert Ressetar (UGS) strengthened this report.

REFERENCES

Agricultural Stabilization and Conservation Service, 1937, Aerial photography, Project AAL frames 1-29 to 1-30, dated 9-19-1937, and frames 4-8 to 4-10, dated 9-21-1937, black and white, approximate scale 1:20,000.

Aitken, M.J., 1994, Optical dating—a non-specialist review: Quaternary Geochronology (Quaternary Science Reviews), v. 13, p. 503–508.

Armstrong, P.A., Taylor, A.R., and Ehlers, T.A., 2004, Is the Wasatch fault footwall (Utah, United States) segmented over million-year time scales?: Geology, v. 32, no. 5, p. 385–388, doi:10.1130/G20421.1.

Benson, L.V., Lund, S.P., Smoot, J.P., Rhode, D.E., Spencer, R.J., Verosub, K.L., Louderback, L.A., Johnson, C.A., Rye, R.O., and Negrini, R.M., 2011, The rise and fall of Lake Bonneville between 45 and 10.5 ka: Quaternary International, v. 235, p. 57–69.

Biasi, G.P., and Weldon, R.J., 2009, San Andreas fault rupture scenarios from multiple paleoseismic records—stringing pearls: Bulletin of the Seismological Society of America, v. 99, no. 2A, p. 471–498.

Birkeland, P.W., Machette, M.N., and Haller, K.M., 1991, Soils as a tool for applied Quaternary geology: Utah Geological and Mineral Survey Miscellaneous Publication 91-3, 63 p.

Black, B.D., Hecker, S., Hylland, M.D., Christenson, G.E., and McDonald, G.N., 2003, Quaternary fault and fold database and map of Utah: Utah Geological Survey Map 193DM, scale 1:50,000, CD.

Black, B.D., and Lund, W.R., 1995, Seismic source evaluation of the Salt Lake City segment of the Wasatch fault zone, central Wasatch Front, Utah: Utah Geological Survey Open-File Report 328, 36 p.

Black, B.D., Lund, W.R., Schwartz, D.P., Gill, H.E., and Mayes, B.H., 1996, Paleoseismic investigation on the Salt Lake City segment of the Wasatch fault zone at the South Fork Dry Creek and Dry Gulch sites, Salt Lake County, Utah—Paleoseismology of Utah, Volume 7: Utah Geological Survey Special Study 92, 22 p., 1 plate.

Bowman, S.D., Beisner, K., and Unger, C., 2009, Compilation of 1970s Woodward-Lundgren & Associates Wasatch fault investigation reports and oblique aerial photography, Wasatch Front and Cache Valley, Utah and Idaho: Utah Geological Survey Open-File Report 548, 3 p., 6 plates.

Bronk Ramsey, C., 1995, Radiocarbon calibration and analysis of stratigraphy—the OxCal program: Radiocarbon, v. 37, no. 2, p. 425–430.

Bronk Ramsey, C., 2001, Development of the radiocarbon program OxCal: Radiocarbon, v. 43, no. 2a, p. 355–363.

Bronk Ramsey, C., 2008, Depositional models for chronological records: Quaternary Science Reviews, v. 27, no. 1-2, p. 42–60.

Bronk Ramsey, C., 2009, Bayesian analysis of radiocarbon dates: Radiocarbon, v. 51, no. 4, p. 337–360.

Bruhn, R.L., and Schultz, R.A., 1996, Geometry and slip distribution in normal fault systems—implications for mechanics and fault-related hazards: Journal of Geophysical Research, v. 101, no. B2, p. 3401–3412.

Bruhn, R., Gibler, P., Houghton, W., and Parry, W., 1992, Structure of the Salt Lake segment, Wasatch normal fault zone—implications for rupture propagation during normal faulting, *in* Gori, P.L., and Hays, W.W., editors, Assessment of regional earthquake hazards and risk along the Wasatch Front, Utah: U.S. Geological Survey Professional Paper 1500-A-J, p. H1–H25.

Chang, W.L., and Smith, R.B., 2002, Integrated seismic-hazard analysis of the Wasatch Front, Utah: Bulletin of the Seismological Society of America, v. 92, no. 5, p. 1904–1922.

Chang, W.L., Smith, R.B., Meertens, C.M., and Harris, R.A., 2006, Contemporary deformation of the Wasatch fault, Utah, from GPS measurements with implications for interseismic fault behavior and earthquake hazard—observations and kinematic analysis: Journal of Geophysical Research, v. 111, B11405, 19 p., doi:101029/2006JB004326.

Cluff, L.S., Brogan, G.E., and Glass, C.E., 1970, Wasatch fault, northern portion—earthquake fault investigation and evaluation, a guide to land-use planning: Oakland, California, Woodward-Clyde and Associates, unpublished consultant report for the Utah Geological and Mineralogical Survey, variously paginated.

Currey, D.R., 1982, Lake Bonneville—selected features of relevance to neotectonic analysis: U.S. Geological Survey Open-File Report 82-1070, 30 p., 1 plate, scale 1:500,000.

Currey, D.R., 1990, Quaternary paleolakes in the evolution of semidesert basins, with special emphasis on Lake Bonneville and the Great Basin, U.S.A.: Palaeogeography, Palaeoclimatology, Palaeoecology, v. 76, p. 189–214.

Currey, D.R., Berry, M.S., Douglass, G.E., Merola, J.A., Murchison, S.B., and Ridd, M.K., 1988a, The highest Holocene stage of Great Salt Lake, Utah [abs.]: Geological Society of America Abstracts with Programs, v. 20, no. 6, p. 411.

Currey, D.R., Berry, M.S., Green, S.A., and Murchison, S.B., 1988b, Very late Pleistocene red beds in the Bonneville basin, Utah and Nevada [abs.]: Geological Society of America Abstracts with Programs, v. 20, no. 6, p. 411.

Duller, G.A.T., 2008, Luminescence dating—guidelines on using luminescence dating in archaeology: Swindon, United Kingdom, English Heritage Publishing, 45 p., available online at http://www.aber.ac.uk/en/media/departmental/iges/english_heritage_luminescence_dating.pdf.

DuRoss, C.B., 2008, Holocene vertical displacement on the central segments of the Wasatch fault zone, Utah: Bulletin of the Seismological Society of America, v. 98, no. 6, p. 2918–2933.

DuRoss, C.B., and Hylland, M.D., in review, Latest Pleistocene and Holocene paleoseismicity of the Salt Lake City segment of the Wasatch fault zone and the West Valley fault zone—unraveling the earthquake-rupture behavior of a major graben-forming fault system: Bulletin of the Seismological Society of America.

DuRoss, C.B., Personius, S.F., Crone, A.J., McDonald, G.N., and Lidke, D.J., 2009, Paleoseismic investigation of the northern Weber segment of the Wasatch fault zone at the Rice Creek trench site, North Ogden, Utah—Paleoseismology of Utah, Volume 18: Utah Geological Survey Special Study 130, 37 p., 2 plates, CD.

DuRoss, C.B., Personius, S.F., Crone, A.J., McDonald, G.N., and Briggs, R., 2012, Late Holocene earthquake history of the Brigham City segment of the Wasatch fault zone at the Hansen Canyon, Kotter Canyon, and Pearsons Canyon trench sites, Box Elder County, Utah—Paleoseismology of Utah, Volume 22: Utah Geological Survey Special Study 142, 28 p., 3 plates.

DuRoss, C.B., Personius, S.F., Crone, A.J., Olig, S.S., and Lund, W.R., 2011, Integration of paleoseismic data from multiple sites to develop an objective earthquake chronology—application to the Weber segment of the Wasatch fault zone: Bulletin of the Seismological Society of America, v. 101, no. 6, p. 2765–2781.

Eardley, A.J., 1962, Glauber's salt bed west of Promontory Point, Great Salt Lake: Utah Geological and Mineralogical Survey Special Study 1, 12 p.

Friedrich, A.M., Wernicke, B.P., Niemi, N.A., Bennett, R.A., and Davis, J.L., 2003, Comparison of geodetic and geologic data from the Wasatch region, Utah, and implications for the spectral character of Earth deformation at periods of 10 to 10 million years: Journal of Geophysical Research, v. 108, no. B4, 2199, doi:10.1029/2001JB000682.

Gilbert, G.K., 1890, Lake Bonneville: U.S. Geological Survey Monograph 1, 438 p.

Godsey, H.S., Currey, D.R., and Chan, M.A., 2005, New evidence for an extended occupation of the Provo shoreline and implications for regional climate change, Pleistocene Lake Bonneville, Utah, USA: Quaternary Research, v. 63, no. 2, p. 212–223.

Godsey, H.S., Oviatt, C.G., Miller, D.M., and Chan, M.A., 2011, Stratigraphy and chronology of offshore to nearshore deposits associated with the Provo shoreline, Pleistocene Lake Bonneville, Utah: Palaeogeography, Palaeoclimatology, Palaeoecology, v. 310, no. 3–4, p. 442–450, doi: 10.1016/j.palaeo.2011.08.005.

Hemphill-Haley, M.A., and Weldon, R.J., 1999, Estimating prehistoric earthquake magnitude from point measurements of surface rupture: Bulletin of the Seismological Society of America, v. 89, no. 5, p. 1264–1279.

Huntley, D.J., Godfrey-Smith, D.I., and Thewalt, M.L.W., 1985, Optical dating of sediments: Nature, v. 313, p. 105–107.

Hylland, M.D., DuRoss, C.B., McDonald, G.N., Olig, S.S., Oviatt, C.G., Mahan, S.A., Crone, A.J., and Personius, S.F., 2014, Late Quaternary paleoseismology of the West Valley fault zone, Utah—insights from the Baileys Lake trench site, *in* DuRoss, C.B., and Hylland, M.D., Evaluating surface faulting chronologies of graben-bounding faults in Salt Lake Valley, Utah—new paleoseismic data from the Salt Lake City segment of the Wasatch fault zone and the West Valley fault zone—Paleoseismology of Utah, Volume 24: Utah Geological Survey Special Study 149, p. 41–76, 8 appendices, 1 plate, CD.

Janecke, S.U., and Oaks, R.Q., Jr., 2011, Reinterpreted history of latest Pleistocene Lake Bonneville—geologic setting of threshold failure, Bonneville flood, deltas of the Bear River, and outlets for two Provo shorelines, southeastern Idaho, USA, *in* Lee, J., and Evans, J.P., editors, Geologic field trips to the Basin and Range, Rocky Mountains, Snake River Plain, and terranes of the U.S. Cordillera: Geological Society of America Field Guide 21, p. 195–222, doi:10.1130/2011.0021(09).

Keaton, J.R., and Currey, D.R., 1989, Earthquake hazard evaluation of the West Valley fault zone in the Salt Lake City urban area, Utah: Salt Lake City, Dames & Moore, unpublished final technical report prepared for U.S. Geological Survey, contract no. 14-08-0001-G1397, 69 p. (Subsequently published in 1993 as Utah Geological Survey Contract Report 93-7.)

Keaton, J.R., Currey, D.R., and Olig, S.S., 1987, Paleoseismicity and earthquake hazards evaluation of the West Valley fault zone, Salt Lake City urban area, Utah: Salt Lake City, Dames & Moore and University of Utah Department of Geography, unpublished final technical report prepared for U.S. Geological Survey, contract no. 14-08-0001-22048, 55 p. + 33 p. appendix. (Subsequently published in 1993 as Utah Geological Survey Contract Report 93-8.)

Kleinfelder, Inc., 1999, Geologic investigation; Salt Palace expansion, Phase II; Salt Lake City, Utah: unpublished consultant report prepared for Salt Lake County, 20 p., 7 appendices.

Korbay, S.R., and McCormick, W.V., 1999a, Faults, lateral spreading, and liquefaction features, Salt Palace Convention Center, Salt Lake City [abs.]: Association of Engineering Geologists, 42nd Annual Meeting Program with Abstracts, p. 73.

Korbay, S.R., and McCormick, W.V., 1999b, Supplemental subsurface investigation—fault hazard analysis, Salt Palace expansion site, Salt Lake City, Utah: unpublished consultant letter to Salt Lake City, 7 p.

Leeflang, B.A., 2008, Ground displacement investigations in downtown Salt Lake City, Utah, using the cone penetrometer: Salt Lake City, University of Utah, M.S. thesis, 160 p.

Lienkaemper, J.J., and Bronk Ramsey, C., 2009, OxCal—versatile tool for developing paleoearthquake chronologies—a primer: Seismological Research Letters, v. 80, no. 3, p. 431–434.

Lips, E.W., 2005, Revised chronology of late Pleistocene glaciers, Wasatch Mountains, Utah [abs.]: Geological Society of America Abstracts with Programs, v. 37, no. 7, p. 41.

Lund, W.R., 2005, Consensus preferred recurrence-interval and vertical slip-rate estimates—review of Utah paleoseismic-trenching data by the Utah Quaternary Fault Parameters Working Group: Utah Geological Survey Bulletin 134, CD.

Lund, W.R., 2007, Summary—Utah Quaternary Fault Parameters Working Group Annual Meeting—Wednesday, February 28, 2007: unpublished minutes of the Utah Quaternary Fault Parameters Working Group, 13 p, available at http://geology.utah.gov/ghp/workgroups/pdf/uqfpwg/UQFPWG-2007_Summary.pdf.

Lund, W.R., and Mayes, B.H., 1995, Large earthquakes on the Salt Lake City segment of the Wasatch fault zone—summary of new information from the South Fork Dry Creek site, Salt Lake County, Utah, *in* Lund, W.R., editor, Environmental and engineering geology of the Wasatch Front region: Utah Geological Association Publication 24, p. 11–30.

Machette, M.N., Personius, S.F., and Nelson, A.R., 1992, Paleoseismology of the Wasatch fault zone—a summary of recent investigations, interpretations, and conclusions, *in* Gori, P.L., and Hays, W.W., editors, Assessment of regional earthquake hazards and risk along the Wasatch Front, Utah: U.S. Geological Survey Professional Paper 1500-A-J, p. A1–A71.

McCalpin, J.P., 2002, Post-Bonneville paleoearthquake chronology of the Salt Lake City segment, Wasatch fault zone, from the 1999 "megatrench" site—Paleoseismology of Utah, Volume 10: Utah Geological Survey Miscellaneous Publication 02-7, 37 p.

Miller, D.M., Oviatt, C.G., and McGeehin, J.P., 2013, Stratigraphy and chronology of Provo shoreline deposits and lake-level implications, late Pleistocene Lake Bonneville, eastern Great Basin, USA: Boreas, v. 42, p. 342–361. (Article first published online October 25, 2012, doi: 10.1111/j.1502-3885.2012.00297.x.)

National Aeronautics & Space Administration, 2006, Visible Earth—a catalog of NASA images and animations of our home planet: Online, <http://visibleearth.nasa.gov/>, accessed July 2006.

Nelson, A.R., Lowe, M., Personius, S., Bradley, L.A., Forman, S.L., Klauk, R., and Garr, J., 2006, Holocene earthquake history of the northern Weber segment of the Wasatch fault zone, Utah—Paleoseismology of Utah, Volume 13: Utah Geological Survey Miscellaneous Publication 05-8, 39 p., 2 plates.

Olig, S.S., McDonald, G., Black, B.D., DuRoss, C.B., Lund, W.R., Hylland, M., Simon, D.B., Giraud, R.E., and Christenson, G.E., 2011, Extending the paleoseismic record of the Provo segment of the Wasatch fault zone, Utah: Final Technical Report to the U.S. Geological Survey contract no. 02HQGR0109, variously paginated.

Oviatt, C.G., 1997, Lake Bonneville fluctuations and global climate change: Geology, v. 25, p. 155–158.

Oviatt, C.G., Currey, D.R., and Sack, D., 1992, Radiocarbon chronology of Lake Bonneville, eastern Great Basin, USA: Palaeogeography, Palaeoclimatology, Palaeoecology, v. 99, p. 225–241.

Oviatt, C.G., Miller, D.M., McGeehin, J.P., Zachary, C., and Mahan, S., 2005, The Younger Dryas phase of Great Salt Lake, Utah, USA: Palaeogeography, Palaeoclimatology, Palaeoecology, v. 219, p. 263–284.

Parry, W.T., and Bruhn, R.L., 1987, Fluid inclusion evidence for minimum 11 km vertical offset on the Wasatch fault, Utah: Geology, v. 15, no. 1, p. 67–70, doi: 10.1130/0091-7613(1987).

Personius, S.F., DuRoss, C.B., and Crone, A.J., 2012, Holocene behavior of the Brigham City segment—implications for forecasting the next large-magnitude earthquake on the Wasatch fault zone, Utah: Bulletin of the Seismological Society of America, v. 102, no. 6, p. 2265–2281.

Personius, S.F., and Scott, W.E., 1992, Surficial geologic map of the Salt Lake City segment and parts of adjacent segments of the Wasatch fault zone, Davis, Salt Lake, and Utah Counties, Utah: U.S. Geological Survey Miscellaneous Investigations Series Map I-2106, scale 1:50,000.

Personius, S.F., and Scott, W.E., 2009 (digital release), Surficial geologic map of the Salt Lake City segment and parts of adjacent segments of the Wasatch fault zone, Davis, Salt Lake, and Utah Counties, Utah (digitized from U.S. Geological Survey Miscellaneous Investigations Series Map I-2106 [1992]): Utah Geological Survey Map 243DM, GIS data, scale 1:50,000.

Prescott, J.R., and Hutton, J.T., 1994, Cosmic ray contributions to dose rates for luminescence and ESR dating—large depths and long-term time variations: Radiation Measurements, v. 23, p. 497–500.

Puseman, K., and Cummings, L.S., 2005, Separation and identification of charcoal and organics from bulk sediment samples for improved radiocarbon dating and stratigraphic correlations, *in* Lund, W.R., editor, Western States Seis-

mic Policy Council, Proceedings Volume of the Basin and Range Province Seismic Hazards Summit II: Utah Geological Survey Miscellaneous Publication 05-2, 10 p., CD.

Reimer, P.J., Baillie, M.G.L., Bard, E., Bayliss, A., Beck, J.W., Blackwell, P.G., Bronk Ramsey, C., Buck, C.E., Burr, G.S., Edwards, R.L., Friedrich, M., Grootes, P.M., Guilderson, T.P., Hajdas, I., Heaton, T.J., Hogg, A.G., Hughen, K.A., Kaiser, K.F., Kromer, B., McCormac, F.G., Manning, S.W., Reimer, R.W., Richards, D.A., Southon, J.R., Talamo, S., Turney, C.S.M., van der Plicht, J., and Weyhenmeyer, C.E., 2009, IntCal09 and Marine09 radiocarbon age calibration curves, 0–50,000 years cal BP: Radiocarbon, v. 51, no. 4, p. 1111–1150.

Rhodes, E.J., 2011, Optically stimulated luminescence dating of sediments over the past 200,000 years: Annual Review of Earth and Planetary Sciences, v. 39, p. 461–488, doi: 10.1146/annurev-earth-040610-133425.

Robison, R.M., and Burr, T.N., 1991, Fault-rupture hazard analysis using trenching and borings—Warm Springs fault, Salt Lake City, Utah, *in* McCalpin, J.P., editor, Proceedings of the 27th Symposium on Engineering Geology and Geotechnical Engineering: Boise, Idaho Department of Transportation, p. 26-1–26-13.

Schwartz, D.P., and Coppersmith, K.J., 1984, Fault behavior and characteristic earthquakes—examples from the Wasatch and San Andreas fault zones: Journal of Geophysical Research, v. 89, p. 5681–5698.

Schwartz, D.P., and Lund, W.R., 1988, Paleoseismicity and earthquake recurrence at Little Cottonwood Canyon, Wasatch fault zone, Utah, *in* Machette, M.N., editor, In the footsteps of G.K. Gilbert—Lake Bonneville and neotectonics of the eastern Basin and Range Province: Utah Geological and Mineral Survey Miscellaneous Publication 88-1, p. 82–85.

Scott, W.E., and Shroba, R.R., 1985, Surficial geologic map of an area along the Wasatch fault zone in the Salt Lake Valley, Utah: U.S. Geological Survey Open-File Report 85-448, 18 p, 2 plates.

Simon-Bymaster, Inc., 1999, Report of geologic investigation—Salt Palace Convention Center expansion project, 100 South West Temple Street, Salt Lake City: Salt Lake City, unpublished consultant report prepared for Salt Lake County, 27 p.

Simon, D.B., and Shlemon, R.J., 1999, The Holocene "Downtown fault" in Salt Lake City, Utah [abs.]: Association of Engineering Geologists, 42nd Annual Meeting Program with Abstracts, p. 85.

Solomon, B.J., 1998, New evidence for the age of faulting on the West Valley fault zone: Utah Geological Survey, Survey Notes, v. 30, no., 3, p. 8 and 13.

Swan, F.H., III, Schwartz, D.P., and Cluff, L.S., 1980, Recurrence of moderate to large magnitude earthquakes produced by surface faulting on the Wasatch fault zone, Utah: Bulletin of the Seismological Society of America, v. 70, p. 1431–1462.

Swan, F.H., III, Schwartz, D.P., Hanson, K.L., Knuepfer, P.L., and Cluff, L.S., 1981, Study of earthquake recurrence intervals on the Wasatch fault at the Kaysville site, Utah: U.S. Geological Survey Open-File Report 81-228, 30 p.

U.S. Department of Agriculture, 2012, Aerial Photography Field Office, National Agriculture Imagery Program: Online, <http://www.fsa.usda.gov/FSA/apfoapp?area=home&subject=prog&topic=nai>, accessed January 2012.

Utah Automated Geographic Reference Center, 2012, Utah GIS Portal: Online, http://agrc.its.state.ut.us/, accessed January 2012.

Van Horn, R., and Crittenden, M.D., Jr., 1987, Map showing surficial units and bedrock geology of the Fort Douglas quadrangle and parts of the Mountain Dell and Salt Lake City North quadrangles, Davis, Salt Lake, and Morgan Counties, Utah: U.S. Geological Survey Miscellaneous Investigations Series Map I-1762, scale 1:24,000.

Wesnousky, S.G., 2008, Displacement and geometrical characteristics of earthquake surface ruptures—Issues and implications for seismic-hazard analysis and the process of earthquake rupture: Bulletin of the Seismological Society of America, v. 98, no. 4, p. 1609–1632, doi: 10.1785/0120070111.

Wheeler, R.L., and Krystinik, K.B., 1992, Persistent and nonpersistent segmentation of the Wasatch fault zone, Utah—statistical analysis for evaluation of seismic hazard, *in* Gori, P.L., and Hays, W.W., editors, Assessment of regional earthquake hazards and risk along the Wasatch Front, Utah: U.S. Geological Survey Professional Paper 1500-A-J, p. B1–B47.

APPENDIX A

DESCRIPTION OF STRATIGRAPHIC UNITS IN TRENCHES AT THE PENROSE DRIVE TRENCH SITE

Unit, genesis[1]	Station no. (trench)[2]	Textural name[3]	Texture (%)[4]				Clasts		Plast-icity	Density/ consistency	Cemen-tation	HCL reaction	Clast ang.	Bedding	Structure	Sorting	Lower bound.[5]	Color[6] dry (moist)	Notes
			F	S	G	C/B	Largest (cm)	Average (cm)											
Stratigraphic Units																			
1, S & DF	10.8, 8.9 (W)	silty gravel with sand & cobbles	15	15	60	10	46	1-5	low	med-high	weak-mod	mod-strong	ang.-subang.	mod. well strat.	variable	variable	not exp.	*7.5YR6/4 (7.5YR4/6)*	Pre-Bonneville alluvial-fan deposits
2, L	32.7, 1.4 (W)	slightly sandy silt with minor clay and rare pebbles	95	4	<1	0	2	0.5	med	firm	none	mod	subang-subround	mottled & bioturbated	matrix	well	not exp.	*10YR6/6 (10YR5/6)*	Lake Bonneville highstand silt; slightly sticky when wet
3, L	29.6, 1.8 (W)	boulder gravel with minor sand	1	6	18	75	40-50	20-25	none	med	mod-strong	strong	subround-round	massive	clast	variable	abrupt, smooth	*10YR5/4 (10YR4/5)*	Provo-phase shorezone deposits
4, C	7.6, 2.1 (E)	boulder gravel with silt and sand	25	15	20	40	65	5-15	low	low-high	none-weak	mod-strong	subround-round	variable	variable	poor	clear	*10YR6/4 (10YR4/5)*	Scarp-derived colluvium
5, C	22.3, 4.4 (W)	sandy silty gravel with cobbles	32	8	40	20	25-30	3-5	med	med	none	mod	subang-subround	variable	maxtrix	poor	clear	*7.5YR6/4 (7.5YR4/6)*	Scarp-derived colluvium; clast-supported near fault zone
6, C	22.6, 4.8 (W)	sandy silty gravel with cobbles	30	10	35	25	10-15	5-8	med	med	none	mod	subang-subround	variable	matrix	poor	gradual	*7.5YR6/3 (7.5YR4/6)*	Scarp-derived colluvium. Near fault zone: clast supported with aligned cobbles
7, C	22.9, 5.5 (W)	sandy silt with gravel	40	15	35	10	10-15	4-6	med	low-med	none	mod	ang-subround	variable	matrix	poor	gradual	*7.5YR6/3 (7.5YR4.5/4)*	Scarp-derived colluvium
8, C	21.9, 6.2 (W)	sandy silt with gravel and rare cobbles	45	10	35	10	24	2-5	med	low-med	none	mod	ang-subround	variable	matrix	poor	gradual	*7.5YR7/3 (7.5YR5/4)*	Scarp-derived colluvium
9, F	25.3, 5.8 (W)	gravelly silt with sand and cobbles	40	15	40	5	40	2-6	med	loose-low	none	mod-strong	subang-subround	nonstrat-poorly strat.	matrix	poor	clear, smooth	*7.5YR5/4 (7.5YR4/3.5)*	Cultural fill with metal fragments
Soils																			
S1(3)	27.6, 2.5 (W)	sand with gravel and silt	5	65	20	10	25	5	low	med	none-weak	mod	subang-round	nonstrat	matrix	poor	clear-gradual	*(7.5YR3/2-3)**	A horizon with weak granular structure; local carbonate filaments; minor bioturbation; developed in Provo shoreline gravel (unit 3)
S1(4)	6.75, 2.25 (E)	sand with gravel and fines	10	45	35	10	16	4-5	none-low	med	none	strong	subang	nonstrat	matrix	poor	clear-gradual	*(7.5YR3/3)**	A horizon developed on unit 4 (scarp colluvium); locally contains carbonate filaments
S2	6.5, 2.7 (E)	sand with gravel and silt	10	50	30	10	13	3	low	med-high	none	mod-strong	subang-subround	nonstrat	matrix	poor	gradual	*(7.5YR3/4)**	A horizon with granular structure developed on unit 5; minor carbonate filaments; locally very fine grained.
S3	23.9, 4.7 (W)	silty sand with gravel	15	55	20	10	15	5	med	low	none	mod	ang-subang	nonstrat	matrix	poor	gradual-diffuse	*(7.5YR3/4)**	A horizon with weak granular structure developed on unit 6; abundant carbonate filaments.
S4	7.5, 5.05 (E)	gravel with sand and silt	25	30	40	5	8	2	med	low-med	none	mod-strong	ang-subang	nonstrat	matrix	poor	diffuse	*(7.5YR3/4)**	Weak A horizon (no soil structure) developed on unit 8; locally bioturbated and overprinted by S5

S5	26.15, 4.6 (W)	gravel with fines and sand	25	25	45	5	17	1-2	med	low	none	none-weak	ang-subang	nonstrat	matrix	poor	clear-diffuse	*(7.5YR2/2)**	A horizon with granular structure developed on several units; carbonate accumulation at 10-20 cm; locally very organic
S6(9)	26.85, 5.75 (W)	gravel with sand and silt	10	40	45	5	10	1-2	med	loose	none	mod	ang	nonstrat	variable	poor	gradual-diffuse	*(7.5YR3/4)**	A horizon with granular structure developed on unit 9 (hanging wall); bioturbated
S6(1)	5.9, 10.95 (W)	silty sand with gravel and organic debris	18	50	30	2	7	2	low	loose	none	weak	ang-subround	nonstrat	matrix	poor	abrupt	*(7.5YR2/2)**	A horizon with granular structure developed on unit 1 (footwall); biotrubated
S6(1) 2Bk	5.9, 10.75 (W)	sand with gravel and silt	5	55	30	10	15	2-3	low	med-high	mod	strong	subang-subround	nonstrat	matrix	poor	clear-diffuse	*(7.5YR4/4)**	Carbonate soil horizon (stage II-III?) developed on unit 1; carbonate throughout matrix--though variable; locally well cemented with weak horizonatal laminations; most clasts completely coated; rinds <2 mm thick and diffuse (poorly laminated)

[1] Units correspond with plate 1. Genesis: S - stream, DF - debris flow, L - lacustrine, C - colluvium, F - fill. For soils (S1-S6), number in parentheses is unit soil is developed on (where described).

[2] Horizontal and vertical meters correspond to plate 1; (W) - west trench, (E) - east trench.

[3] Texture terms based on the Unified Soil Classification System (density/consistency after Birkeland and others [1991]). Textural information may not be representative of entire unit due to vertical and horizontal heterogeneity in units.

[4] Percentages of clast-size fractions (based on area) are field estimates. We used a U.S. Standard #10 (2 mm) sieve to separate matrix from gravel.

[5] Lower boundary modified from Birkeland and others (1991). Distinctness: abrupt (1mm-2.5 cm), clear (2.5-6 cm), gradual (6-12.5 cm). Not exp. - base of unit not exposed.

[6] Munsell color of matrix (year 2000 revised version). * indicates dry color not recorded.

Appendix B

Examination of Bulk Soil for Radiocarbon Datable Material and Extraction of Microcharcoal from the Penrose Drive Trench Site, East Bench Fault, Salt Lake City, Utah

By

Kathryn Puseman

with assistance from
Peter Kovacik and R.A. Varney

PaleoResearch Institute
Golden, Colorado

PaleoResearch Institute Technical Report 10-85

Prepared For

United States Geological Survey
Golden, Colorado

October 2010

INTRODUCTION

A total of eleven bulk soil samples, three charcoal samples, and two shell samples were examined for the presence of organic material suitable for radiocarbon analysis. These samples were recovered from two trenches at the Penrose Drive site in Salt Lake City, Utah. Botanic components and detrital charcoal were identified, and potentially radiocarbon datable material was separated. Dating of material from the trenches will be used to help develop detailed information on the timing and recurrence of paleoearthquakes on the Salt Lake City segment of the Wasatch Fault zone. Samples for AMS radiocarbon dating will be submitted to Woods Hole Institute.

METHODS

Flotation and Identification

The macrofloral samples were floated using a modification of the procedures outlined by Matthews (1979). Each sample was added to approximately 3 gallons of water, then stirred until a strong vortex formed. The floating material (light fraction) was poured through a 150 micron mesh sieve. Additional water was added and the process repeated until all floating material was removed from the sample (a minimum of five times). The material that remained in the bottom (heavy fraction) was poured through a 0.5-mm mesh screen. The floated portions were allowed to dry.

The light fractions were weighed, then passed through a series of graduated screens (US Standard Sieves with 2-mm, 1-mm, 0.5-mm and 0.25-mm openings) to separate charcoal debris and to initially sort the remains. The contents of each screen then were examined. Charcoal pieces larger than 2-mm, 1-mm, or 0.5-mm in diameter were separated from the rest of the light fraction and the total charcoal weighed. A representative sample of charcoal pieces was broken to expose fresh cross, radial, and tangential sections. Charcoal fragments were examined under a binocular microscope at a magnification of 70x and under a Nikon Optiphot 66 microscope at magnifications of 320-800x. The weights of each charcoal type within the representative sample also were recorded. The material that remained in the 2-mm, 1-mm, 0.5-mm, and 0.25-mm sieves was scanned under a binocular stereo microscope at a magnification of 10x, with some identifications requiring magnifications of up to 70x. The material that passed through the 0.25-mm screen was not examined. The heavy fractions were scanned at a magnification of 2x for the presence of botanic remains. Remains from the light and heavy fractions were recorded as charred and/or uncharred, whole and/or fragments. The term "seed" is used to represent seeds, achenes, caryopses, and other disseminules.

Charcoal fragments in the three charcoal samples were broken to expose fresh cross, radial, and tangential sections, then examined under a binocular microscope at a magnification of 70x and under a Nikon Optiphot 66 microscope at magnifications of 320-800x. The weights of each charcoal type were recorded. The two shell samples were water-screened through a 250 micron mesh and allowed to dry. Shell fragments were separated from the rest of the sample matrix and weighed. Macrofloral remains, including charcoal, are identified using manuals (Carlquist 2001; Hoadley 1990; Martin and Barkley 1961; Musil 1963; Panshin and de Zeeuw 1980; Schopmeyer 1974) and by comparison with modern and archaeological

references. Because charcoal and possibly other botanic remains were to be submitted for radiocarbon dating, clean laboratory conditions were used during flotation and identification to avoid contamination. All instruments were washed between samples, and samples were protected from contact with modern charcoal.

Microcharcoal Recovery

Now it is possible to recover microscopic charcoal (microcharcoal) from sediments for the purpose of obtaining an AMS radiocarbon age. Microscopic charcoal fragments are far superior to humates because they provide dates with the same precision as those obtained from larger pieces of charcoal, with the single exception that the individual pieces of microscopic charcoal are not identified to taxon.

A chemical extraction technique based on that used for pollen, and relying upon heavy liquid extraction, has been modified to recover microcharcoal for the purpose of obtaining an AMS radiocarbon age. After removing calcium carbonates and iron with hydrochloric acid (10%), the samples were screened through 150 micron mesh. The material remaining in the screen was examined for the presence of macroscopic charcoal. Since an the amount of macroscopic charcoal was insufficient for obtaining a radiocarbon date, the screened samples then were rinsed until neutral, and a small quantity of sodium hexametaphosphate was added. Samples then were filled with reverse osmosis, deionized (RODI) water and allowed to settle according to Stoke's Law. After two hours the supernatant, containing clay, was poured off and the sample was rinsed with RODI water three more times, being allowed to settle according to Stoke's Law after each rinse to remove more clays. Once the clays had been removed, the samples were freeze-dried using a vacuum system, freezing out all moisture at -98 °C. Sodium polytungstate (SPT), with a density of 1.8, was used for the flotation process. The samples were mixed with SPT and centrifuged at 1500 rpm for 10 minutes to separate organic from inorganic remains. The supernatant containing pollen, organic remains, and microcharcoal was decanted. Sodium polytungstate again was added to the inorganic fraction to repeat the separation process until all visible microcharcoal had been recovered. The microcharcoal was recovered from the sodium polytungstate and rinsed thoroughly with RODI water. Following this step, the samples were examined using a binocular microscope at a magnification of up to 30x to check the matrix for microscopic charcoal and other debris. Each sample received a treatment with hot nitric acid (30%) for 30 minutes to remove extraneous debris. RODI water rinses followed, with another examination with the binocular microscope. The nitric acid treatments continued until examination of the samples using the binocular microscope indicated that all that remained was microcharcoal and feldspar. Feldspar and other microminerals cannot be removed from microcharcoal samples, however, the presence of these minerals will not affect the date that is obtained.

DISCUSSION

The two trenches at the Penrose Drive trench site crossed the East Bench fault of the Salt Lake City segment of the Wasatch fault zone. The trench site is noted to lie below the highest shoreline of Lake Bonneville and at the approximate elevation of the of the Provo shoreline. The trenches exposed pre-Bonneville alluvial-fan deposits, fine-grained Lake

Bonneville sediments related to the Bonneville highstand, a boulder gravel at the Provo shoreline, and fault-scarp-derived colluvium (Christopher DuRoss, personal communication, June 3, 2010). Excavation of the trenches yielded evidence for five (P1-P5) and possibly six surface-faulting earthquakes that occurred after abandonment of the Provo shoreline at around 14,000 B.P. The bulk soil samples and two of the charcoal samples were recovered from soils (S1-S5) developed between earthquakes on the fault-scarp-derived colluvium. One of the charcoal samples and the two shell samples were recovered from soils developed on the Provo boulder gravel.

Bulk samples PD-R12 and PD-R11 were recovered from soil S5 developed on distal P2 and P1 colluvium (Table 1). Sample PD-R12 contained three small fragments of *Artemisia* charcoal weighing 0.0010 g, three small fragments of hardwood charcoal too small for further identification weighing 0.0006 g, and unidentified charcoal weighing 0.0033 g (Table 2, Table 3). A few charred Poaceae C caryopses and unidentified seeds also were noted. Poaceae C caryopses reflect grasses with small seeds, such as *Agrostis* (bentgrass), *Muhlenbergia* (muhly grass), *Poa* (bluegrass), etc. Four pieces of charred, vitrified tissue weighing 0.0002 g may represent charcoal or other charred plant tissue with a shiny, glassy appearance due to fusion by heat. A few uncharred seeds and an uncharred hardwood wood fragment represent modern plants in the area. In addition, the sample contained several insect chitin fragments and a single snail shell with a depressed (flat) shape where the width is much bigger than the height.

A single piece of *Quercus* charcoal weighing 0.0010 g was present in sample PD-R11, as well as several fragments of hardwood charcoal too small for further identification weighing 0.0005 g. Components of the local vegetation are represented by a single uncharred *Descurainia* seed, a few root fragments, and several rootlets. Non-floral remains include an uncharred bone fragment, a few insect chitin fragments, and a few insect puparium fragments.

Samples PD-R14 and PD-R9 were collected from soil S4 developed on P2 colluvium in Unit 7. Seven fragments of hardwood charcoal too small for identification and weighing 0.0004 g were present in sample PD-R14. The sample also contained a single piece of charred vitrified tissue weighing 0.0001 g. In addition, the sample contained a few depressed snail shells and several snail shell fragments. Due to the small weight of charred material recovered in the sample, additional sediment was processed to recover microscopic charcoal for dating. Examination of the microcharcoal screen contents yielded an additional 0.0002 g of unidentified hardwood charcoal. A total of 0.0102 g of microcharcoal with about 30% feldspar was extracted (Table 4).

Sample PD-R9 yielded four fragments of hardwood charcoal too small for further identification weighing 0.0003 g. Additional sediment was processed to recover microcharcoal, resulting in 0.0022 g of microscopic charcoal (with about 60% feldspar) for dating. The sample also yielded a few uncharred rootlets from modern plants, an insect chitin fragment, an insect egg fragment, and a few depressed snail shells.

Samples PD-R10, PD-R8, and PD-R5 were taken from soil S3 developed on P3 colluvium in Unit 6. Sample PD-R10 contained a charred *Prunus*-type seed fragment weighing 0.0005 g suggesting the presence of a wild cherry in the area. In addition, the sample contained three fragments of charred parenchymous tissue weighing 0.0006 g and eight pieces of hardwood charcoal too small for further identification weighing 0.0002 g. Parenchyma is the botanical term for relatively undifferentiated tissue, composed of many similar thin-walled cells.

Parenchyma occurs in many different plant organs in varying amounts, especially large fleshy organs such as roots and stems. The vegetative storage parenchyma in roots and stems stores starch and other carbohydrates and sugars (Hather 2000:1). Recovery of charred parenchymous tissue might reflect burned root or stem tissue. Non-floral remains include an uncharred bone fragment, a moderate amount of insect eggs, a few depressed snail shells, and several snail shell fragments. Additional sediment also was processed to recover microcharcoal, and a total of 0.0029 g of microcharcoal (containing about 30% feldspar) was recovered.

A total of six pieces of hardwood charcoal too small for further identification weighing 0.0002 g were present in sample PD-R8, as well as a few uncharred rootlets from modern plants and a snail shell fragment. Additional soil was processed to recover microscopic charcoal, and an additional 0.0017 g of microcharcoal was obtained. Of this amount, about 30% was feldspar.

Sample PD-R5 contained several fragments of hardwood charcoal too small for further identification weighing 0.0005 g, as well as three small pieces of charred parenchymous tissue weighing 0.0001 g. A few uncharred rootlets from modern plants, an insect chitin fragment, a moderate amount of insect eggs, several snail shells with a depressed shape, and a moderate amount of snail shell fragments also were noted. Additional soil processed to recover microscopic charcoal yielded only 0.0003 g of microcharcoal, 50% of which was feldspar.

Samples PD-R15 and PD-R6 represent soil S2 developed on P4 colluvium in Unit 5. Pieces of hardwood charcoal too small for further identification and weighing 0.0012 g were present in sample PD-R15. A piece of charred parenchymous tissue weighing 0.0003 g and three fragments of charred vitrified tissue weighing 0.0002 g also were recovered. In addition, the sample contained several snail shells with a depressed shape and a moderate amount of snail shell fragments.

Sample PD-R6 yielded several fragments of unidentified hardwood charcoal weighing 0.0029 g and six pieces of small, vitrified charcoal from a twig fragment weighing 0.0031 g. The sample also yielded a few charred seeds and several uncharred *Celtis* seed fragments. Uncharred seeds normally are interpreted to represent components of modern or historic vegetation. However, *Celtis* seeds undergo natural mineralization (biomineralization) over time and contain large quantities of calcium carbonate, which makes them resilient to decomposition. As a result, uncharred *Celtis* seeds can survive in old deposits without other means of outside preservation, such as charring (Zohary and Hopf 2000). Non-floral remains in this sample include two uncharred bone fragments, fifteen depressed snail shells, a moderate amount of snail shell fragments, and an oblong snail shell where the height is much bigger than the width.

A charcoal sample and two snail shell samples were collected from soil S1 developed on the Provo boulder gravel. Charcoal sample PD-R2 yielded two fragments of probable Rosaceae charcoal weighing 0.0037 g and eight pieces of unidentified hardwood charcoal weighing 0.0012 g. Numerous snail shell fragments weighing 0.076 g were present in sample PD-R4. Sample PD-R16 contained several oblong snail shells and shell fragments weighing 0.757 g.

Bulk sample PD-R7 and charcoal samples PD-R1 and PD-R3 were recovered from soil S1 developed on P5 colluvium in Unit 4. Sample PD-R7 contained several fragments of hardwood charcoal too small for further identification weighing 0.0012 g, a vitrified piece of hardwood root charcoal weighing 0.0010 g, two fragments of vitrified hardwood twig fragments weighing 0.0007 g, and a small fragment of charcoal too vitrified for identification weighing less than 0.0001 g. In addition, the sample yielded two charred fragments of parenchymous tissue weighing 0.0005 g, a small charred and vitrified monocot/herbaceous dicot stem fragment weighing less than 0.0001 g, and a charred unidentified seed endosperm fragment. The sample also contained two uncharred bone fragments, an insect puparium, two depressed snail shells, and numerous snail shell fragments.

Eight fragments of hardwood charcoal too small and friable for further identification and weighing 0.0040 g were present in sample PD-R1. Pieces of hardwood charcoal weighing 0.0035 g also were noted in sample PD-R3.

Bulk sample PD-R13 from soil S1 possibly was developed on distal P5 colluvium in Unit 4. This sample contained seven fragments of hardwood charcoal too small for further identification weighing 0.0002 g and several fragments of charred parenchymous tissue weighing 0.0111 g. Non-floral remains include an insect chitin fragment, a depressed snail shell, and a moderate amount of snail shell fragments.

SUMMARY AND CONCLUSIONS

Flotation of sediment samples and identification of charcoal samples from two trenches at the Penrose Drive site in the Salt Lake City segment of the Wasatch Fault zone, Utah, resulted in recovery of charcoal and other charred botanic remains that can be submitted for radiocarbon analysis. Several samples contained charcoal or charred botanic remains in sufficient quantities for AMS radiocarbon dating. Five samples did not contain sufficient macroscopic charcoal for dating; therefore, the samples were processed to recover microscopic charcoal. Four of these samples yielded sufficient microcharcoal for dating. The majority of the charcoal fragments recovered from these samples consisted of hardwood charcoal too small for further identification. Fragments of identifiable *Artemisia* and *Quercus* charcoal in samples from the youngest S5 soil reflect sagebrush and oak in the area. A charred *Prunus*-type seed fragment in sample PD-R10 from soil S3 and pieces of probable Rosaceae charcoal in sample PD-R2 from the oldest S1 soil suggest the presence of a woody member of the rose family, such as chokecherry. Several samples contained pieces of charred parenchymous tissue, likely from burned root or stem tissue.

TABLE 1
PROVENIENCE DATA FOR SAMPLES FROM THE PENROSE DRIVE TRENCH SITE,
SALT LAKE CITY, UTAH

Sample No.	Trench	Unit No.	Sample Location (horiz., vert.)	Provenience/ Description	Analysis
PD-R12	West	7, 8	28.9 m, 3.6 m	Bulk sample from soil S5 developed on distal P2 and P1 colluvium; minimum for P1	Macrofloral
PD-R11	West	7, 8	26.9 m, 4.2 m	Bulk sample from soil S5 developed on distal P2 and P1 colluvium; minimum for P1	Macrofloral
PD-R14	West	7	23.4 m, 5.5 m	Bulk sample from soil S4 developed on P2 colluvium; minimum for P2, maximum for P1	Macrofloral Microcharcoal
PD-R9	West	7	22.9 m, 5.6 m	Bulk sample from soil S4 developed on P2 colluvium; minimum for P2, maximum for P1	Macrofloral Microcharcoal
PD-R10	West	6	23.6 m, 4.8 m	Bulk sample from soil S3 developed on P3 colluvium; minimum for P3, maximum for P2	Macrofloral Microcharcoal
PD-R8	East	6	6.2 m, 3.5 m (west wall)	Bulk sample from soil S3 developed on P3 colluvium; minimum for P3, maximum for P2	Macrofloral Microcharcoal
PD-R5	East	6	5.6 m, 3.6 m	Bulk sample from soil S3 developed on P3 colluvium; minimum for P3, maximum for P2	Macrofloral Microcharcoal
PD-R15	West	5	25.1 m, 3.4 m	Bulk sample from soil S2 developed on P4 colluvium; minimum for P4, maximum for P3	Macrofloral
PD-R6	East	5	6.7 m, 2.8 m	Bulk sample from soil S2 developed on P4 colluvium; minimum for P4, maximum for P3	Macrofloral
PD-R2	West	3	31.2 m, 2.2 m	Charcoal from soil S1 developed on Provo boulder gravel; possible minimum age for P5	Charcoal ID
PD-R16	West	3	26.0 m, 2.6 m to 29.6 m, 2.0 m	Gastropod shells from Provo boulder gravel	Shell

TABLE 1 (Continued)

Sample No.	Trench	Unit No.	Sample Location (horiz., vert.)	Provenience/ Description	Analysis
PD-R4	West	3	24.9 m, 2.8 m	Gastropod shell fragments from soil S1 developed on Provo boulder gravel; possible minimum age for P5	Shell
PD-R7	East	4	6.6 m, 2.2 m	Bulk sample from soil S1 developed on P5 colluvium; minimum age for P5	Macrofloral
PD-R1	East	4	6.3 m, 2.0 m	Charcoal fragment from soil S1 developed on P5 colluvium; minimum age for event P5	Charcoal ID
PD-R3	East	4	7.4 m, 2.4 m	Charcoal from soil S1 developed on P5 colluvium; minimum age for P5	Charcoal ID
PD-R13	West	4	24.8 m, 3.0 m	Bulk sample from soil S1 possibly developed on distal P5 colluvium; possible minimum age for P5	Macrofloral

horiz. = horizontal
vert. = vertical
S1 = oldest soil
S5 = youngest soil
P1 = youngest prehistoric surface-faulting earthquake
P5 = oldest prehistoric surface-faulting earthquake

TABLE 2
MACROFLORAL REMAINS FROM THE PENROSE DRIVE TRENCH SITE, SALT LAKE CITY, UTAH

Sample No.	Identification	Part	Charred		Uncharred		Weights/ Comments
			W	F	W	F	
PD-R12	Liters Floated						0.85 L
Unit 7, 8	Light Fraction Weight						1.44 g
Soil S5	FLORAL REMAINS:						
	Poaceae C	Caryopsis	1				0.0001 g
	cf. Poaceae C	Caryopsis	1	2			0.0002 g
	Unidentified N	Seed	4	1			0.0004 g
	Vitrified tissue			4			0.0002 g
	Cheno-am	Seed				1	< 0.0001 g
	Medicago	Seed			1		0.0017 g
	Sambucus					1	0.0007 g
	Rootlets					X	Few
	CHARCOAL/WOOD:						
	Artemisia	Charcoal		3			0.0010 g
	Unidentified hardwood - small	Charcoal		3			0.0006 g
	Unidentified	Charcoal		X			0.0033 g
	Unidentified hardwood	Wood				1	0.0004 g
	NON-FLORAL REMAINS:						
	Insect	Chitin				18	
	Rock/Gravel					X	Moderate
	Snail shell - depressed				1		0.0014 g

TABLE 2 (Continued)

Sample No.	Identification	Part	Charred W	Charred F	Uncharred W	Uncharred F	Weights/ Comments
PD-R11	Liters Floated						0.70 L
Unit 7, 8	Light Fraction Weight						0.84 g
Soil S5	FLORAL REMAINS:						
	Descurainia	Seed			1		< 0.0001 g
	Roots					X	Few
	Rootlets					X	Moderate
	CHARCOAL/WOOD:						
	Quercus	Charcoal		1			0.0010 g
	Unidentified hardwood	Charcoal		21			0.0005 g
	NON-FLORAL REMAINS:						
	Bone - 0.05 mm					1	0.0018 g
	Insect	Insect				5	
	Insect	Puparium				3	
	Rock/Gravel					X	Moderate
PD-R14	Liters Floated						1.00 L
Unit 7	Light Fraction Weight						1.74 g
Soil S4	Microcharcoal Screen Content Weight						151.48 g
	FLORAL REMAINS:						
	Vitrified tissue > 0.25 mm			1			0.0001 g
	Rootlets					X	Moderate
	CHARCOAL/WOOD:						
	Unidentified hardwood - small	Charcoal		X			0.0006 g
	NON-FLORAL REMAINS:						
	Rock/Gravel					X	Moderate
	Snail shell - depressed, 0.05 mm				4	2	0.006 g
	Snail shell in heavy fraction					X	Moderate

TABLE 2 (Continued)

Sample No.	Identification	Part	Charred W	Charred F	Uncharred W	Uncharred F	Weights/ Comments
PD-R9	Liters Floated						0.50 L
Unit 7	Light Fraction Weight						1.10 g
Soil S4	Microcharcoal Screen Content Weight						120.23 g
	FLORAL REMAINS:						
	Rootlets					X	Few
	CHARCOAL/WOOD:						
	Total charcoal ≥ 2 mm						
	Unidentified hardwood - small	Charcoal		4			0.0003 g
	NON-FLORAL REMAINS:						
	Insect	Chitin				1	
	Insect	Egg			1		
	Rock/Gravel					X	Moderate
	Snail shell - depressed				4	1	0.0050 g
PD-R10	Liters Floated						0.80 L
Unit 6	Light Fraction Weight						0.82 g
Soil S3	Microcharcoal Screen Content Weight						107.30 g
	FLORAL REMAINS:						
	Parenchymous tissue			3			0.0006 g
	Prunus-type	Seed		1			0.0005 g
	Rootlets					X	Few
	CHARCOAL/WOOD:						
	Total charcoal ≥ 0.25 mm						0.0002 g
	Unidentified hardwood	Charcoal		8			0.0002 g
PD-R10	NON-FLORAL REMAINS:						
Unit 6	Bone					1	0.008 g
Soil S3	Insect	Egg			X		Moderate
	Rock/Gravel					X	Moderate
	Snail shell - depressed ≥ 1 mm					3	0.002 g
	Snail shell in heavy fraction				1	X	Moderate

TABLE 2 (Continued)

Sample No.	Identification	Part	Charred W	Charred F	Uncharred W	Uncharred F	Weights/ Comments
PD-R8	Liters Floated						1.00 L
Unit 6	Light Fraction Weight						3.63 g
Soil S3	Microcharcoal Screen Content Weight						101.76 g
	FLORAL REMAINS:						
	Rootlets					X	Few
	CHARCOAL/WOOD:						
	Unidentified hardwood - small	Charcoal		6			0.0002 g
	NON-FLORAL REMAINS:						
	Rock/Gravel					X	Moderate
	Snail shell					1	0.005 g
PD-R5	Liters Floated						1.20 L
Unit 6	Light Fraction Weight						1.06 g
Soil S3	Microcharcoal Screen Content Weight						136.27 g
	FLORAL REMAINS:						
	Parenchymous tissue > 0.25 mm			3			0.0001 g
	Rootlets					X	Few
	CHARCOAL/WOOD:						
	Unidentified hardwood - small	Charcoal		24			0.0005 g
	NON-FLORAL REMAINS:						
	Insect	Chitin				1	
	Insect	Egg			X		Moderate
	Rock/Gravel					X	Moderate
	Snail shell - depressed > 1 mm				5		0.006 g
	Snail shell - depressed > 0.5 mm				8	2	
	Snail shell in heavy fraction					X	Moderate

TABLE 2 (Continued)

Sample No.	Identification	Part	Charred W	Charred F	Uncharred W	Uncharred F	Weights/ Comments
PD-R15	Liters Floated						1.20 L
Unit 5	Light Fraction Weight						1.62 g
Soil S2	FLORAL REMAINS:						
	Parenchymous tissue > 0.25 mm			1			0.0003 g
	Vitrified tissue > 0.25 mm			3			0.0002 g
	Rootlets					X	Few
	CHARCOAL/WOOD:						
	Unidentified hardwood - small	Charcoal		11			0.0012 g
	NON-FLORAL REMAINS:						
	Snail shell - depressed $\geq$ 1 mm				2	3	0.009 g
	Snail shell - depressed < 1 mm					10	
	Snail shell in heavy fraction					X	Moderate
PD-R6	Liters Floated						1.20 L
Unit 5	Light Fraction Weight						10.67 g
Soil S2	FLORAL REMAINS:						
	Cheno-am	Perisperm		2			< 0.0001 g
	Unidentified P	Seed	1				< 0.0001 g
	Celtis - outer	Seed coat				26	0.2692 g
	Celtis - inner	Seed coat			1		0.0213 g
	Rootlets					X	Few
	CHARCOAL/WOOD:						
	Total charcoal $\geq$ 0.5 mm						0.0080 g
	Unidentified hardwood	Charcoal		14			0.0029 g
	Unidentified twig - small, vitrified	Charcoal		6			0.0031 g
	NON-FLORAL REMAINS:						
	Bone					2	0.0035 g
	Rock/Gravel					X	Moderate
	Snail shell - depressed				15		0.0089 g
	Snail shell - oblong					1	0.0010 g
	Snail shell < 1 mm					X	Moderate

TABLE 2 (Continued)

Sample No.	Identification	Part	Charred W	Charred F	Uncharred W	Uncharred F	Weights/ Comments
PD-R2	Sample Weight						0.04 g
Unit 3	CHARCOAL/WOOD:						
Soil S1	cf. Rosaceae	Charcoal		2			0.0037 g
	Unidentified hardwood	Charcoal		8			0.0012 g
PD-R16	Water-screened Sample Weight						2.61 g
Unit 3	NON-FLORAL REMAINS:						
	Snail shell - oblong				13	65	0.757 g
	Sediment					X	1.853 g
PD-R4	Water-screened Sample Weight						0.43 g
Unit 3	NON-FLORAL REMAINS:						
	Snail shell					X	0.076 g
PD-R7	Liters Floated						0.80 L
Unit 4	Light Fraction Weight						7.05 g
Soil S1	Microcharcoal Screen Content Weight						122.24 g
	FLORAL REMAINS:						
	Unidentified	Endosperm		1			0.0001 g
	Monocot/Herbaceous dicot - vitrified	Stem		1			< 0.0001 g
	Parenchymous tissue $\geq$ 0.5 mm			2			0.0005 g
	Rootlets					X	Few
	CHARCOAL/WOOD:						
	Unidentified hardwood	Charcoal		21			0.0012 g
	Unidentified hardwood root - vitrified	Charcoal		1			0.0010 g
	Unidentified hardwood twig - small, vitrified	Charcoal		2			0.0007 g
	Unidentifiable - vitrified	Charcoal		1			< 0.0001 g

Sample No.	Identification	Part	Charred		Uncharred		Weights/ Comments
			W	F	W	F	
	NON-FLORAL REMAINS:						
	Bone > 0.5 mm					2	0.003 g
	Insect	Puparium			1		
	Rock/Gravel					X	Few
	Snail shell - depressed > 1 mm				2	1	0.008 g
	Snail shell < 1 mm					X	Numerous
	Snail shell in heavy fraction					X	Numerous
PD-R1	Sample Weight						0.53 g
Unit 4	CHARCOAL/WOOD:						
Soil S1	Total charcoal $\geq$ 2 mm						
	Unidentified hardwood - small, friable	Charcoal		8			0.0040 g
PD-R3	Sample Weight						2.27 g
Unit 4	CHARCOAL/WOOD:						
Soil S1	Unidentified hardwood	Charcoal		18			0.0035 g
PD-R13	Liters Floated						0.90 L
Unit 4	Light Fraction Weight						2.45 g
Soil S1	FLORAL REMAINS:						
	Parenchymous tissue > 0.25 mm - vitrified			74			0.0111 g
	CHARCOAL/WOOD:						
	Unidentified hardwood - small	Charcoal		7			0.0002 g
	NON-FLORAL REMAINS:						
	Insect	Chitin				1	
	Rock/Gravel					X	Moderate
	Snail shell - depressed > 1 mm				1		0.001 g
	Snail shell in heavy fraction					X	Moderate

W = Whole
F = Fragment
X = Presence noted in sample
g = grams
mm = millimeters
L = liters

TABLE 3
INDEX OF MACROFLORAL REMAINS RECOVERED FROM THE PENROSE DRIVE TRENCH SITE, SALT LAKE CITY, UTAH

Scientific Name	Common Name
FLORAL REMAINS:	
Celtis	Hackberry
Cheno-am	Includes goosefoot and amaranth families
Descurainia	Tansy mustard, Flixweed
Monocot/Herbaceous dicot	A member of the Monocotyledonae class of Angiosperms, which include grasses, sedges, lilies, and palms/A non-woody member of the Dicotyledonae class of Angiosperms
Medicago	Burclover, Alfalfa
Poaceae C	Members of the grass family with small caryopses, such as *Agrostis* (bentgrass), *Muhlenbergia* (muhly grass), *Poa* (bluegrass), etc.
Prunus-type	Similar to Cherry
Sambucus	Elderberry
Parenchymous tissue	Relatively undifferentiated tissue composed of many similar thin-walled cells–occurs in different plant organs in varying amounts, especially large fleshy organs such as roots and stems
Vitrified tissue	Charred material with a shiny, glassy appearance due to fusion by heat
CHARCOAL/WOOD:	
Artemisia	Sagebrush
Quercus	Oak
Rosaceae	Rose family
Unidentified hardwood	Wood from a broad-leaved flowering tree or shrub
Unidentified hardwood - small	Wood from a broad-leaved flowering tree or shrub, fragments too small for further identification
Unidentified hardwood - vitrified	Wood from a broad-leaved flowering tree or shrub, exhibiting a shiny, glassy appearance due to fusion by heat
Unidentifiable - vitrified	Charcoal exhibiting a shiny, glassy appearance due to fusion by heat

TABLE 3 (Continued)

Scientific Name	Common Name
NON-FLORAL REMAINS:	
Insect puparium	A rigid outer shell made from tough material that includes chitin (a natural polymer found in insect exoskeleton and crab shells) and hardens from a larva's skin to protect the pupa as it develops into an adult insect

TABLE 4
DATABLE CHARCOAL, CHARRED ORGANIC MATERIAL, AND MICROCHARCOAL RECOVERED IN SAMPLES FROM THE PENROSE DRIVE TRENCH SITE, SALT LAKE CITY, UTAH

Sample No.	Provenience/ Description	Charred organic material/ Charcoal and Weight	Microcharcoal Weight
PD-R12	Bulk sample from soil S5 developed on distal P2 and p1 colluvium; minimum for P1	*Artemisia* charcoal 0.0010 g Unidentified charcoal 0.0033 g Unid. hardwood charcoal 0.0006 g	
PD-R11	Bulk sample from soil S5 developed on distal P2 and p1 colluvium; minimum for P1	*Quercus* charcoal 0.0010 g Unidentified hardwood charcoal 0.0005 g	
PD-R14	Bulk sample from soil S4 developed on P2 colluvium; minimum for P2, maximum for P1	Unidentified hardwood charcoal 0.0006 g	0.0102 g
PD-R9	Bulk sample from soil S4 developed on P2 colluvium; minimum for P2, maximum for P1	Unidentified charcoal 0.0003 g	0.0022 g
PD-R10	Bulk sample from soil S3 developed on P3 colluvium; minimum for P3, maximum for P2	*Prunus*-type seed 0.0005 g Parenchymous tissue 0.0006 g Unid. hardwood charcoal 0.0002 g	0.0029 g
PD-R8	Bulk sample from soil S3 developed on P3 colluvium; minimum for P3, maximum for P2	Unidentified hardwood charcoal 0.0002 g	0.0017 g
PD-R5	Bulk sample from soil S3 developed on P3 colluvium; minimum for P3, maximum for P2	Parenchymous tissue 0.0001 g Unidentified hardwood charcoal 0.0005 g	0.0003 g (do not use)
PD-R15	Bulk sample from soil S2 developed on P4 colluvium; minimum for P4, maximum for P3	Parenchymous tissue 0.0003 g Unidentified hardwood charcoal 0.0012 g	
PD-R6	Bulk sample from soil S2 developed on P4 colluvium; minimum for P4, maximum for P3	Unid. twig charcoal 0.0029 g Unidentified hardwood charcoal 0.0031 g	
PD-R16	Gastropod shells from Provo boulder gravel	Snail shell 0.757 g	
PD-R4	Gastropod shell fragments from soil S1 developed on Provo boulder gravel; possible minimum age for P5	Snail shell 0.076 g	
PD-R2	Charcoal from soil S1 developed on Provo boulder gravel; possible minimum age for P5	cf. Rosaceae charcoal 0.0037 g Unidentified hardwood charcoal 0.0012 g	

TABLE 4 (Continued)

Sample No.	Provenience/ Description	Charred organic material/ Charcoal and Weight	Microcharcoal Weight
PD-R13	Bulk sample from soil S1 possibly developed on distal P5 colluvium; possible minimum age for P5	Parenchymous tissue 0.0111 g Unidentified hardwood charcoal 0.0002 g	
PD-R7	Bulk sample from soil S1 possibly developed on distal P5 colluvium; possible minimum age for P5	Unid. hardwood charcoal 0.0012 g Unid. hardwood twig - vitrified 0.0007 g	
PD-R3	Charcoal from soil S1 developed on P5 colluvium; minimum age for P5	Unidentified hardwood charcoal 0.0035 g	
PD-R1	Charcoal fragment from soil S1 developed on P5 colluvium; minimum age for event P5	Unidentified hardwood charcoal 0.0040 g	

Unid. = Unidentified

REFERENCES CITED

Carlquist, Sherwin
2001 *Comparative Wood Anatomy: Systematic, Ecological, and Evolutionary Aspects of Dicotyledon Wood*. Springer Series in Wood Science. Springer, Berlin.

Hather, Jon G.
2000 *Archaeological Parenchyma*. Archetype Publications Ltd., London.

Hoadley, R. Bruce
1990 *Identifying Wood: Accurate Results with Simple Tools*. The Taunton Press, Inc., Newtown, Connecticut.

Martin, Alexander C. and William D. Barkley
1961 *Seed Identification Manual*. University of California, Berkeley.

Matthews, Meredith H.
1979 Soil Sample Analysis of 5MT2148: Dominguez Ruin, Dolores, Colorado. Appendix B. In *The Dominguez Ruin: A McElmo Phase Pueblo in Southwestern Colorado*, edited by A. D. Reed. Bureau of Land Management Cultural Resource Series. vol. 7. Bureau of Land Management, Denver, Colorado.

Musil, Albina F.
1963 *Identification of Crop and Weed Seeds*. Agricultural Handbook no. 219. U.S. Department of Agriculture, Washington D.C.

Panshin, A. J. and Carl de Zeeuw
1980 *Textbook of Wood Technology*. McGraw-Hill Book, Co., New York.

Schopmeyer, C. S.
1974 *Seeds of Woody Plants in the United States*. Agricultural Handbook No. 450. U.S. Department of Agriculture, Washington, D.C.

Zohary, Daniel and Maria Hopf
2000 *Domestication of Plants in the Old World: The Origin and Spread of Cultivated Plants in West Asia, Europe, and the Nile Valley*. Third ed. Oxford University Press, New York.

APPENDIX C

SUMMARY OF RADIOCARBON DATING, PENROSE DRIVE SITE

Sample No.	NOSAMS[1] Accession No.	Trench	Station[2] (m)	Depth (m)	Unit Sampled[3]	Material Sampled		Organic Material Dated[4]	Sample Weight (mg)	Pre-Treatment Method	$\delta^{13}C$[5]	Relation to Earthquake[6]	Age[7] (^{14}C yr B.P., ± 1σ)	Age[8] (cal yr B.P., ± 2σ)
						Soil/sediment sampled	Notes							
PD-R1	OS-84833	East	6.28, 2.02	4.1	S1	Charcoal from S1 on scarp-colluvium unit 4	Macro-charcoal sample	8 fragments unidentified hardwood charcoal	4	Acid-base-acid	-26.4	Min - PD5, Max - PD4	9940 ± 65	11,410 ± 260
PD-R2	OS-84840	West	31.15, 2.20	2.3	S2 (top)	Charcoal from top of S2 on boulder gravel unit 3	Macro-charcoal sample	2 fragments *Rosaceae* charcoal	3.7	Acid-base-acid	-24.21	Min - PD5, Max - PD4	9390 ± 45	10,620 ± 120
PD-R3	OS-84846	East	7.14, 2.35	4.0	S1	Charcoal from S1 on scarp-colluvium unit 4	Macro-charcoal sample	18 fragments unidentified hardwood charcoal	3.5	Acid-base-acid	-25.61	Min - PD5	9550 ± 55	10,910 ± 240
PD-R4	*Sample not dated*	West	24.93, 2.75	3.8	S1	Shell from S1 on boulder gravel unit 3	-	Gastropod shell	76	Acid-base-acid	-		-	-
PD-R5	OS-85007	East	5.60, 3.55	2.2	S3	Soil sediment from S3 on scarp-colluvial unit 6b	~22-cm wide, 8-cm high sample area	24 fragments unidentified hardwood charcoal	0.5	Acid-base-acid	-25†	Max - PD2	3560 ± 45	3850 ± 140
PD-R6a	OS-85006	East	6.65, 2.75	3.4	S2	Soil sediment from S2 on scarp-colluvial unit 5	~22-cm wide, 8-cm high sample area	14 fragments unidentified hardwood charcoal	2.9	Acid-base-acid	-25.99	Max PD3/PD3b	9350 ± 50	10,570 ± 140
PD-R6b	OS-84835	East	6.65, 2.75	3.4	S2	Soil sediment from S2 on scarp-colluvial unit 5	~22-cm wide, 8-cm high sample area	6 fragments unidentified twig, vitrified	3.1	Acid-base-acid	-25.85	Max PD3/PD3b	8990 ± 55	10,120 ± 200
PD-R7	*Sample not dated*	East	6.58, 2.23	4.0	S1	Soil sediment from S1 on scarp colluvial unit 4	~16-cm wide, 8-cm high sample area	Many fragments unidentified hardwood charcoal	1.2	-	-	-	-	-
PD-R8	OS-87068	East (west wall)	6.17, 3.52	2.1	S3	Soil sediment from S3 on scarp-colluvial unit 6b (same position as R5)	~22-cm wide, 6-cm high sample area	Microcharcoal	1.7	Acid-base-acid	-28.9	Max - PD2	5480 ± 50	6280 ± 120
PD-R9a	*Sample too small to date*	West	22.94, 5.56	1.5	S4	Soil sediment from S4 on scarp-colluvial unit 7	~18-cm wide, 8-cm high sample area	4 fragments unidentified hardwood charcoal	0.3	Acid-base-acid	-	-	-	-
PD-R9b	OS-87069	West	22.94, 5.56	1.5	S4	Soil sediment from S4 on scarp-colluvial unit 7	~18-cm wide, 8-cm high sample area	Microcharcoal	2.2	Acid-base-acid	-29.14	Max - PD1	3960 ± 45	4420 ± 160
PD-R10a	OS-85121	West	23.6, 4.80	2.0	S3	Soil sediment from S3 on scarp-colluvial unit 6b	~25-cm wide, 8-cm high sample area	1 fragment *Prunus*-type seed, charred	0.5	Acid-base-acid	-25†	Max - PD2	5800 ± 75	6600 ± 180
PD-R10b	OS-87060	West	23.6, 4.80	2.0	S3	Soil sediment from S3 on scarp-colluvial unit 6b	~25-cm wide, 8-cm high sample area	Microcharcoal	2.9	Acid-base-acid	-28.64	Max - PD2	5470 ± 40	6270 ± 80
PD-R11	OS-84850	West	26.85, 4.20	1.7	S1	Soil sediment from base of S1, developed on scarp colluvium	~16-cm wide, 6-cm high sample area	1 fragment *Quercus* charcoal	1.0	Acid-base-acid	-24.84	Min - PD1	490 ± 35	530 ± 40
PD-R12	OS-84847	West	28.85, 3.55	1.6	S1	Soil sediment from base of S1, developed on scarp colluvium	~16-cm wide, 7-cm high sample area	3 fragments *Artemisia* charcoal	1.0	Acid-base-acid	-25.42	Min - PD1	495 ± 30	530 ± 40
PD-R13	OS-85008	West	24.83, 3.03	3.5	S1	Soil sediment from near top of S1 on boulder gravel unit 3	~20-cm wide, 6-cm high sample area	7 fragments unidentified hardwood charcoal	0.2	Acid-base-acid	-25†	Min - PD5, Max - PD4	10,000 ± 75	11,510 ± 320
PD-R14a	OS-85124	West	23.41, 5.46	1.5	S4	Soil sediment from S4 on scarp-colluvial unit 7	12-cm high, 8-cm wide sample area	Many fragments unidentified hardwood charcoal	0.6	Acid-base-acid	-25†	Max - PD1	3790 ± 65	4180 ± 220
PD-R14b	OS-87000	West	23.41, 5.46	1.5	S4	Soil sediment from S4 on scarp-colluvial unit 7	12-cm high, 8-cm wide sample area	Microcharcoal	10.2	Acid-base-acid	-28.89	Max - PD1	3790 ± 40	4170 ± 140
PD-R15	OS-84849	West	25.00, 3.40	3.1	S2	Soil sediment from S2 on scarp-colluvial unit 5	~22-cm wide, 7-cm high sample area	11 fragments unidentified hardwood charcoal	1.2	Acid-base-acid	-25.95	Max PD3/PD3b	9400 ± 50	10,630 ± 140
PD-R16	*Sample not dated*	West	26.0, 3.0 to 29.6, 2.0	3.5–2.8	S1	Shells from S1 and boulder-gravel unit 3; location not shown on log	-	Many gastropod shells	757	-	-	-	-	-

[1] National Ocean Sciences Accelerator Mass Spectrometry Facility, Woods Hole Oceanographic Institution (Woods Hole, Massachusetts).
[2] Station coordinates are horizontal and vertical meter marks along arbitrary reference grid for trench site (see plate 1).
[3] See appendix A for descriptions of stratigraphic units.
[4] Separation and identification by Paleo Research Institute (Golden, Colorado).
[5] Measured delta ^{13}C values. † Assumed value.
[6] Min (max) indicates minimum (maximum) limiting time constraint for a surface-faulting earthquake (e.g., PD1).
[7] Laboratory-reported radiocarbon age with one standard deviation uncertainty. B.P. is before present (AD 1950).
[8] Mean calendar-calibrated age and two-sigma uncertainty, rounded to nearest decade, determined using OxCal calibration software (v. 4.1; Bronk Ramsey, 2009) and the IntCal09 atmospheric data set (Reimer and others, 2009).

APPENDIX D

SUMMARY OF LUMINESCENCE DATING, PENROSE DRIVE SITE

Sample No.[1]	Trench	Station[2] (m)	Depth (m)	Unit Sampled[3]	Material Sampled	Stratigraphic Position	Water Content[4] (%)	K[5] (ppm)	U[5] (ppm)	Th[5] (ppm)	Cosmic Dose Additions[6] (Gy/ka)	Total Dose Rate OSL[7] (IRSL)[8] (Gy/ka)	Equivalent Dose OSL[7] (IRSL)[8] (Gy)	n[9]	Relation to Earthquake[10]	Laboratory Age OSL[7] (IRSL)[8] ± 1σ (yr before 2010)
PD-L1	West	9.15, 9.40	1.0	1	Fine to medium sand laminae	Upper part of pre-Bonneville alluvial fan	1 (35)	1.42 ± 0.03	2.12 ± 0.08	4.60 ± 0.13	0.25 ± 0.02	2.37 ± 0.04 (3.36 ± 0.05)f	>180 (452 ± 9.04)	16 (20)	-	>76,990 ± 3920 (134,730 ± 6850)
PD-L2	West	10.11, 9.33	0.9	1	Fine sand laminae	Same stratigraphic position as L1	11 (38)	1.36 ± 0.03	2.18 ± 0.08	5.14 ± 0.13	0.25 ± 0.02	2.35 ± 0.04	163 ± 9.13	23 (24)	-	69,310 ± 4040
PD-L3	West	11.84, 9.35	0.6	1	Medium-fine sand lense	Similar stratigraphic position as L1 & L2	10 (31)	1.39 ± 0.03	2.10 ± 0.08	4.89 ± 0.13	0.25 ± 0.02	2.39 ± 0.04	154 ± 9.24	25 (25)	-	64,370 ± 3980
PD-L4	West	18.93, 7.66	0.5	1	Sandy gravel horizon	Slightly lower stratigraphic position than L1-L3	8 (37)	1.33 ± 0.03	1.80 ± 0.08	4.25 ± 0.12	0.26 ± 0.02	2.21 ± 0.04 (3.08 ± 0.05)f	130 ± 2.99 (680 ± 9.72)	24 (25)	-	58,790 ± 1700 (220,780 ± 9880)
PD-L5	West	28.24, 1.77	3.6	2	Bonneville silty sand	Immediately below boulder gravel (Provo stage)	12 (31)	1.61 ± 0.03	1.54 ± 0.07	5.22 ± 0.13	0.21 ± 0.01	2.48 ± 0.04	42.1 ± 1.56	25 (25)	Max - PD6	16,990 ± 680
PD-L6	West	30.96, 1.59	3.0	2	Bonneville silty sand	Immediately below boulder gravel (Provo stage)	10 (37)	1.60 ± 0.03	1.44 ± 0.07	4.95 ± 0.13	0.19 ± 0.01	2.38 ± 0.04 (3.24 ± 0.05)f	42.3 ± 2.98 (50.2 ± 0.60)	32 (33)	Max - PD6	17,770 ± 340 (15,490 ± 610)
PD-L7	East	7.10, 2.75	3.5	5	Scarp colluvium	Upper part of unit 5 colluvial wedge	14 (31)	1.22 ± 0.03	1.72 ± 0.07	3.72 ± 0.11	0.18 ± 0.01	2.00 ± 0.03 (2.83 ± 0.05)f	21.9 ± 1.14 (63.2 ± 1.92)	22 (25)	Max - PD3b/PD3, Min - PD4	10,950 ± 600 (22,340 ± 1560)
PD-L8	East	7.03, 3.52	2.7	6a	Scarp colluvium	Upper part of 6a colluvial wedge	9 (35)	1.30 ± 0.03	2.16 ± 0.08	5.41 ± 0.13	0.20 ± 0.01	2.27 ± 0.04	16.7 ± 0.97	18 (20)	Max - PD3a, Min - PD3b/PD3	7360 ± 440
PD-L9	East	5.88, 3.44	2.4	6b	Scarp colluvium	Upper-middle part of 6b colluvial wedge	10 (37)	1.40 ± 0.08	1.45 ± 0.11	5.00 ± 0.21	0.20 ± 0.01	2.21 ± 0.06	18.5 ± 0.91 (23.9 ± 0.51)	19 (20)	Max - PD2, Min - PD3a/PD3	8390 ± 640 (8140 ± 570)

[1] Analyses by U.S. Geological Survey Luminescence Dating Laboratory (Denver, Colorado).
[2] Station coordinates are horizontal and vertical meter marks along arbitrary reference grid for trench (see plate 1).
[3] See appendix A for descriptions of stratigraphic units.
[4] Field moisture; complete sample saturation percent in parentheses.
[5] Analyses obtained using laboratory gamma spectrometry (high-resolution Ge detector) and readings are delayed after 21 days of being sealed in the planchet (used for dose rates).
[6] Cosmic doses and attenuation with depth were calculated using the methods of Prescott and Hutton (1994); Gy – gray.
[7] Dose rate and optically stimulated luminescence (OSL) age for fine-grained (90–125 microns) quartz sand; linear + exponential fit used on equivalent dose, single aliquot regeneration; ages rounded to nearest decade, errors to one sigma.
[8] Dose rate and infrared stimulated luminescence (IRSL) age for fine grains (4–11 microns) of polymineral silt; exponential fit used for equivalent dose, multiple aliquot additive dose; ages rounded to nearest decade, errors to one sigma; fade tests indicate no correction.
[9] Number of replicated equivalent dose (De) estimates used to calculate the mean; total number of measurements made, including failed runs with unusable data, in parentheses.
[10] Min (max) indicates minimum (maximum) limiting time constraint for a surface-faulting earthquake (e.g., PD6).

APPENDIX E

OXCAL MODELS FOR THE SALT LAKE CITY SEGMENT

OxCal models for the Penrose Drive, Little Cottonwood Canyon, and South Fork Dry Creek (SFDC) sites were created using OxCal calibration and analysis software (version 4.1; Bronk Ramsey, 1995, 2001; using the IntCal09 calibration curve of Reimer and others, 2009). The models include *C_Date* for luminescence ages, *R_Date* for radiocarbon ages, and *Boundary* for undated events (paleoearthquakes). For the SFDC model, *Delta_R* accounts for the bulk-soil residence time following DuRoss and others (2011). These components are arranged into ordered sequences based on the relative stratigraphic positions of the samples. The sequences may contain *phases*, or groups where the relative stratigraphic ordering information for the individual radiocarbon ages is unknown. The models are presented here in reverse stratigraphic order, following the order in which the ages and events are evaluated in OxCal.

OxCal Input

Penrose Drive Version 4b – 7 Events (preferred)

```
Plot()
 {
  Sequence("SLCS_Penrose_v4b_post_Bonneville.oxcal")
  {
   Boundary("start");
   Phase("Unit 2 - Bonn. silt")
   {
    C_Date("L6, 17.8+/-0.7 ka",-15760,340);
    C_Date("L5, 17.0+/-1.4 ka",-14980,680);
   };
   Boundary("P6");
   C_Date("Godsey et al., 2005", -13619,1360);
   Boundary("P5");
   Phase("Soil S1")
   {
    R_Date("R13, 10000+/-75",10000,75);
    R_Date("R1, 9940+/-65",9940,65);
    //R_Date("R2, 9390+/-45",9390,45);
    R_Date("R3, 9550+/-55",9550,55);
   };
   Boundary("P4");
   C_Date("L7, 11.0+/-1.2 ka",-8940,600);
   Phase("Soil S2")
   {
    R_Date("R15, 9400+/-50",9400 ,50 );
    R_Date("R6a, 9350+/-50",9350 ,50 );
```

```
   R_Date("R6b, 8990+/-55",8990 ,55 );
  };
  Boundary("P3b");
  C_Date("L8, 7.4+/-0.9 ka",-5350,440);
  Boundary("P3a");
  C_Combine("L9")
  {
   C_Date("R9-OSL, 8.4 ka", -6380, 640);
   C_Date("R9-IRSL, 8.1 ka", -6130, 570);
  };
  Phase("Soil S3")
  {
   R_Date("R8, 5480+/-50", 5480, 50);
   R_Date("R10a, 5800+/-75", 5800, 75);
   R_Date("R10b, 5470+/-40", 5470, 40);
  };
  Boundary("P2");
  Zero_Boundary("Unit 7");
  Phase("Soil S4")
  {
   R_Date("R9b, 3960+/-45", 3960,45);
   R_Date("R14a, 3790+/-65", 3790, 65);
   R_Date("R14b, 3790+/-40", 3790, 40);
  };
  Boundary("P1");
  Zero_Boundary("Unit 8");
  Phase("Soil S5")
  {
   R_Date("R11, 490+/-35", 490,35);
   R_Date("R12, 495+/-30", 495,30);
  };
  Boundary("Begin Historical Record",1847 AD);
 };
};
```

Penrose Drive Version 4c – 6 Events

```
Plot()
 {
  Sequence("SLCS_Penrose_v4c_post_Bonneville.oxcal")
  {
   Boundary("start");
   Phase("Unit 2 - Bonn. silt")
   {
    C_Date("L6, 17.8+/-0.7 ka",-15760,340);
    C_Date("L5, 17.0+/-1.4 ka",-14980,680);
```

```
};
Boundary("P6");
C_Date("Godsey et al., 2005", -13619,1360);
Boundary("P5");
Phase("Soil S1")
{
 R_Date("R13, 10000+/-75",10000,75);
 R_Date("R1, 9940+/-65",9940,65);
 //R_Date("R2, 9390+/-45",9390,45);
 R_Date("R3, 9550+/-55",9550,55);
};
Boundary("P4");
C_Date("L7, 11.0+/-1.2 ka",-8940,600);
Phase("Soil S2")
{
 R_Date("R15, 9400+/-50",9400 ,50 );
 R_Date("R6a, 9350+/-50",9350 ,50 );
 R_Date("R6b, 8990+/-55",8990 ,55 );
};
Boundary("P3b");
C_Date("L8, 7.4+/-0.9 ka",-5350,440);
C_Combine("L9")
{
 C_Date("R9-OSL, 8.4 ka", -6380, 640);
 C_Date("R9-IRSL, 8.1 ka", -6130, 570);
};
Phase("Soil S3")
{
 R_Date("R8, 5480+/-50", 5480, 50);
 R_Date("R10a, 5800+/-75", 5800, 75);
 R_Date("R10b, 5470+/-40", 5470, 40);
};
Boundary("P2");
Zero_Boundary("Unit 7");
Phase("Soil S4")
{
 R_Date("R9b, 3960+/-45", 3960,45);
 R_Date("R14a, 3790+/-65", 3790, 65);
 R_Date("R14b, 3790+/-40", 3790, 40);
};
Boundary("P1");
Zero_Boundary("Unit 8");
Phase("Soil S5")
{
 R_Date("R11, 490+/-35", 490,35);
 R_Date("R12, 495+/-30", 495,30);
```

```
  };
  Boundary("Begin Historical Record",1847 AD);
 };
};
```

Little Cottonwood Canyon

```
Plot()
 {
  Sequence("SLCS LCC ver . 4; ET predates Flood")
  {
   Boundary("Sequence start ");
   R_Date("Bonneville reaches trench elev.", 16800, 250);
   R_Date("Bonneville highstand", 15000, 250);
   Boundary("ET");
   R_Date("Bonneville Flood", 14500, 250);
   (Boundary("ET"); –ET postdates Bonneville Flood in version 4b)
   R_Date("C13; 5cACb5", 12150, 70);
   R_Date("C26; 5cAC", 12160, 60);
   Phase("Soil on upper 5c")
   {
    R_Date("C28; 5cAkb5", 11980, 50);
    R_Date("C10; 5cAkb5", 10320, 60);
    R_Date("C12; 5cAb5", 10260, 330);
    R_Date("C3; 5cAb5", 9960, 50);
    R_Date("C11; 5cAb5", 9540, 60);
    R_Date("C1; 6btb4", 8680, 60);
   };
   Boundary("EU");
    R_Date("C5; 7c lower", 8350, 50);
   R_Date("C6; 7c upper", 8070, 50);
   //ZB: Min age (C25) closer constraint on EV time
   Zero_Boundary("V");
   Boundary("EV");
   R_Date("C25; W7fAb4", 6640, 180);
   //ZB: Min age (C20) closer constraint on EW time
   Zero_Boundary("W");
   Boundary("EW");
   R_Date("C20; E8Ab2", 4560, 40);
   //ZB: Min ages (C19,C21) closer constraint on EX time
   Zero_Boundary("X");
   Boundary("EX");
   R_Date("C21; E9bABb1", 3820, 120);
   R_Date("C19; E9bAb1", 3000, 40);
   R_Date("C24; W9Ab2", 2280, 40);
   Boundary("EY");
```

```
  //ZB: Max age (C24) closer constraint on EY time
  Zero_Boundary("Y");
  R_Date("C16; E10a", 1890, 80);
  Phase("EY colluv./EZ fissure")
  {
   R_Date("C26a; younger FF", 1570, 70);
   R_Date("C17; E10b", 1440, 70);
   R_Date("C23; W10Ab1", 1130, 70);
  };
  Boundary("EZ");
  R_Date("C18; E11", 1540, 40);
  C_Date("Historic constraint AD 1850", 1850, 5);
  Boundary("Sequence end");
 };
};
```

South Fork Dry Creek/Dry Gulch

```
Plot()
 {
  Sequence("SLCS SFDC ver. 6f ")
  {
   Boundary("Sequence start ");
   Phase("Soil on fan deposits; DC-1, DC-2")
   {
    Delta_R("MRT-200yr1", 200, 200);
    R_Date("DC-1-R1", 5230, 160);
    R_Date("DC-1-R2", 4910, 200);
    R_Date("DC-2-R1", 4710, 180);
    Delta_R("MRT-0yr", 0, 100);
    R_Date("DC-1-R6", 4520, 120);
   };
   Boundary("EW");
   //ZB: Max ages closer constraint on EW time
   Zero_Boundary("W");
   Delta_R("MRT-150yr1", 150, 75);
   R_Date("DC2-2-R1", 3810, 180);
   Boundary("EX");
   Phase("post EX deposits; DC2-4")
   {
    Delta_R("MRT-300yr1", 300, 300);
    R_Date("DC2-4-R3", 3910, 140);
    R_Date("DC2-4-R4", 3760, 160);
   };
   Phase("Soil on fan - pre EY; DC2-5, DG")
   {
```

```
 Delta_R("MRT-200yr2", 200, 200);
 R_Date("DC2-5-R3", 3090, 120);
 Delta_R("MRT-100yr2", 100, 50);
 R_Date("APST-BS2", 2370, 140);
 R_Date("APST-BS3", 2410, 120);
 };
 Boundary("EY");
 //ages removed - stratigraphically out of place
 #Delta_R("MRT-200yr", 200, 200);
 #R_Date("DC2-5-R1", 2570, 140);
 #R_Date("DC2-1-R1", 3000, 160);
 //ZB: Max ages closer constraint on EY time
 Zero_Boundary("Y");
 Phase("soil on fan/colluvium pre EZ");
 {
 Delta_R("MRT-200yr3", 200, 200);
 R_Date("DC-1-R4", 2310, 140);
 R_Date("DC-1-R3", 1830, 160);
 Delta_R("MRT-150yr2", 150, 150);
 R_Date("DC2-1-R2", 1850, 120);
 Delta_R("MRT-200yr4", 200, 200);
 R_Date("DC-2-R3", 1640, 100);
 Delta_R("MRT-100yr3", 100, 50);
 R_Date("APST-BS1", 1770, 120);
 R_Date("DC2-3-R2", 1420, 160);
 //These ages removed as per discussion in Black et al.
 #Delta_R("MRT-0yr", 0, 0);
 #R_Date("DC-2-R2", 1170, 120);
 #R_Date("DC-1-R5", 930, 120);
 };
 Boundary("EZ");
 Phase("Post EZ deposits");
 {
 Delta_R("MRT-300yr2", 300, 300);
 R_Date("DC2-4-R2", 1620, 100);
 R_Date("DC2-2-R2", 1570, 120);
 Delta_R("MRT-100yr5", 100, 50);
 R_Date("DC2-3-R1", 1240, 140);
 Delta_R("MRT-200yr5", 200, 200);
 R_Date("DC2-3-R3", 1160, 160);
 };
 C_Date("Historic constraint AD 1850", 1850, 5);
 Boundary("Sequence end");
 };
};
```

Penrose Drive Version 4b (7 event model)	**Unmodelled (BP)** Mean	1s	**Modelled (BP)** Mean	1s	**Agreement**
Boundary start			18350	1090	
Phase Unit 2 - Bonn. silt					
C_Date L6, 17.8±0.7 ka	17710	340	17590	320	98.9
C_Date L5, 17.0±1.4 ka	16930	680	17240	530	103.4
Boundary P6			**16480**	**960**	
C_Date Godsey et al., 2005	15570	1360	14970	1100	104.3
Boundary P5			**12080**	**810**	
Phase Soil S1					
R_Date R13, 10000±75	11510	160	11460	140	103.7
R_Date R1, 9940±65	11410	130	11390	120	105.4
R_Date R3, 9550±55	10910	120	11000	100	99.1
Boundary P4			**10870**	**120**	
C_Date L7, 11.0±1.2 ka	10890	600	10750	100	135.5
Phase Soil S2					
R_Date R15, 9400±50	10630	70	10610	60	100.4
R_Date R6a, 9350±50	10570	70	10560	70	101.6
R_Date R6b, 8990±55	10120	100	10150	90	111.6
Boundary P3b			**9700**	**560**	
C_Date L8, 7.4±0.9 ka	7300	440	7820	360	72.4
Boundary P3a			**7520**	**380**	
C_Combine L9	8190	430	7330	350	32.3
Phase Soil S3					
R_Date R8, 5480±50	6280	60	6280	50	100.5
R_Date R10a, 5800±75	6600	90	6600	90	100.2
R_Date R10b, 5470±40	6270	40	6270	40	99.8
Boundary P2			**5890**	**350**	
Zero_Boundary Unit 7			4840	410	
Phase Soil S4					
R_Date R9b, 3960±45	4420	80	4380	80	86.4
R_Date R14a, 3790±65	4180	110	4210	100	104
R_Date R14b, 3790±40	4170	70	4190	70	98.5
Boundary P1			**4000**	**260**	
Zero_Boundary Unit 8			1770	870	
Phase Soil S5					
R_Date R11, 490±35	530	20	520	20	99.7
R_Date R12, 495±30	530	20	530	20	99.5
Boundary Historical Record, 1847	100	0	100	0	100

Penrose Drive Version 4c (6 event model)	**Unmodelled (BP)** Mean	1s	**Modelled (BP)** Mean	1s	**Agreement**
Boundary start			18420	1180	
Phase Unit 2 - Bonn. silt					
C_Date L6, 17.8±0.7 ka	17710	340	17600	330	99.1
C_Date L5, 17.0±1.4 ka	16930	680	17240	530	103.2
Boundary P6			**16460**	**970**	
C_Date Godsey et al., 2005	15570	1360	14960	1100	104.1
Boundary P5			**12070**	**810**	
Phase Soil S1					
R_Date R13, 10000±75	11510	160	11460	140	103.6
R_Date R1, 9940±65	11410	130	11390	120	105.7
R_Date R3, 9550±55	10910	120	11000	100	98.7
Boundary P4			**10880**	**120**	
C_Date L7, 11.0±1.2 ka	10890	600	10750	110	135.7
Phase Soil S2					
R_Date R15, 9400±50	10630	70	10610	60	100.7
R_Date R6a, 9350±50	10570	70	10560	70	101.5
R_Date R6b, 8990±55	10120	100	10140	90	107.4
Boundary P3			**9370**	**770**	
C_Date L8, 7.4±0.9 ka	7300	440	7860	340	67.7
C_Combine L9	8190	430	7600	330	61.1
Phase Soil S3					
R_Date R8, 5480±50	6280	60	6280	50	100.2
R_Date R10a, 5800±75	6600	90	6600	90	100
R_Date R10b, 5470±40	6270	40	6270	40	99.7
Boundary P2			**5770**	**410**	
Zero_Boundary Unit 7			4820	390	
Phase Soil S4					
R_Date R9b, 3960±45	4420	80	4380	80	85.7
R_Date R14a, 3790±65	4180	110	4210	90	104.1
R_Date R14b, 3790±40	4170	70	4190	70	98.5
Boundary P1			**4010**	**250**	
Zero_Boundary Unit 8			1770	870	
Phase Soil S5					
R_Date R11, 490±35	530	20	520	20	99.8
R_Date R12, 495±30	530	20	530	20	99.6
Boundary Historical Record, 1847	100	0	100	0	100

Little Cottonwood Canyon	**Unmodelled (BP)**		**Modelled (BP)**		**Agreement**
Version 4	Mean	1s	Mean	1s	
Boundary Sequence start			20720	1110	
R_Date Bonneville reaches trench elev.	19980	310	19840	290	99.2
R_Date Bonneville highstand	18210	280	18320	240	103.5
Boundary ET			**17880**	**340**	
R_Date Regression to Provo shoreline	17650	350	17460	280	100.1
R_Date C13; 5cACb5	14010	130	14080	140	93.2
R_Date C26; 5cAC	14010	110	13970	70	108
Version 4b					
Boundary Sequence start			*20880*	*1200*	
R_Date Bonneville reaches trench elev.	*19980*	*310*	*19870*	*290*	*100.5*
R_Date Bonneville highstand	*18210*	*280*	*18250*	*250*	*103.4*
R_Date Regression to Provo shoreline	*17650*	*350*	*17600*	*310*	*105.2*
Boundary ET			***15220***	***1000***	
R_Date C13; 5cACb5	*14010*	*130*	*14070*	*120*	*97.3*
R_Date C26; 5cAC	*14010*	*110*	*13970*	*70*	*107.6*
Version 4 (and 4b) continued					
Phase Soil on upper 5c					
R_Date C28; 5cAkb5	13840	70	13830	60	104.5
R_Date C10; 5cAkb5	12170	140	12170	140	100
R_Date C12; 5cAb5	11930	460	11940	460	100
R_Date C3; 5cAb5	11420	120	11420	120	100
R_Date C11; 5cAb5	10900	130	10900	130	99.9
R_Date C1; 6btb4	9660	90	9680	100	94.4
Boundary EU			**9470**	**120**	
R_Date C5; 7c lower	9360	70	9340	80	94.3
R_Date C6; 7c upper	8960	100	9010	100	101.4
Zero_Boundary V			8490	360	
Boundary EV			**7830**	**330**	
R_Date C25; W7fAb4	7530	160	7520	160	100.4
Zero_Boundary W			6720	610	
Boundary EW			**5530**	**400**	
R_Date C20; E8Ab2	5200	100	5210	100	99.4
Zero_Boundary X			4860	270	
Boundary EX			**4440**	**270**	
R_Date C21; E9bABb1	4220	170	4140	160	95.8
R_Date C19; E9bAb1	3200	70	3200	70	99.7
R_Date C24; W9Ab2	2270	60	2280	60	105.9
Boundary EY			**2110**	**140**	

Zero_Boundary Y			1890	150	
R_Date C16; E10a	1830	100	1720	100	74.1
Phase EY colluv./EZ fissure					
R_Date C26a; younger FF	1470	70	1460	60	105.8
R_Date C17; E10b	1360	70	1390	50	92.1
R_Date C23; W10Ab1	1060	80	1350	20	
Boundary EZ			**1340**	**20**	
R_Date C18; E11	1440	50	1330	20	15.8
C_Date Historic constraint AD 1850	100	10	100	10	92.6
Boundary Sequence end			-310	350	

South Fork Dry Creek/Dry Gulch	**Unmodelled (BP)**		**Modelled (BP)**		**Agreement**
Version 6f	Mean	1s	Mean	1s	
Boundary Sequence start			5560	360	
Phase Soil on fan deposits; DC-1, DC-2					
Delta_R MRT-200yr1	200	200	333.386	162.56	94.7
R_Date DC-1-R1	5780	300	5410	270	65.6
R_Date DC-1-R2	5370	350	5270	250	109.4
R_Date DC-2-R1	5140	340	5190	240	115.3
Delta_R MRT-0yr	-1.82E-07	100	-8.88798	92.0309	104
R_Date DC-1-R6	5170	210	5220	190	102
Boundary EW			**4980**	**280**	
Zero_Boundary W			4410	360	
Delta_R MRT-150yr1	150	75	151.566	73.6144	100.9
R_Date DC2-2-R1	4020	270	3990	230	106.2
Boundary EX			**3760**	**300**	
Phase post EX deposits; DC2-4					
Delta_R MRT-300yr1	300	300	580.637	222.109	86
R_Date DC2-4-R3	3970	430	3510	290	81.1
R_Date DC2-4-R4	3780	440	3400	290	91.6
Phase Soil on fan - pre EY; DC2-5, DG					
Delta_R MRT-200yr2	200	200	250.972	178.804	104.5
R_Date DC2-5-R3	3050	280	2960	240	102.8
Delta_R MRT-100yr2	100	50	75.4261	49.7092	93.9
R_Date APST-BS2	2310	200	2470	180	86
R_Date APST-BS3	2360	190	2480	170	92.6
Boundary EY			**2250**	**210**	
Zero_Boundary Y			1980	230	
Phase soil on fan/colluvium pre EZ					
Delta_R MRT-200yr3	200	200	280.756	135.383	110.5
R_Date DC-1-R4	2110	300	1800	180	82.3
R_Date DC-1-R3	1580	280	1640	120	123.8
Delta_R MRT-150yr2	150	150	172.553	108.534	113.6
R_Date DC2-1-R2	1640	210	1570	100	121.5
Delta_R MRT-200yr4	200	200	66.1274	110.7	104.4
R_Date DC-2-R3	1360	240	1500	90	111.7
Delta_R MRT-100yr3	100	50	101.061	48.0054	102
R_Date APST-BS1	1590	140	1460	90	95.1
R_Date DC2-3-R2	1230	170	1390	100	82.4
Boundary EZ			**1350**	**110**	
Phase Post EZ deposits					
Delta_R MRT-300yr2	300	300	342.961	136.187	127.6
R_Date DC2-4-R2	1250	320	1220	120	131.6

R_Date DC2-2-R2	1210	320	1120	130	129.5
Delta_R MRT-100yr5	100	50	106.959	48.9048	100.6
R_Date DC2-3-R1	1060	150	990	120	102.1
Delta_R MRT-200yr5	200	200	271.902	169.895	105.1
R_Date DC2-3-R3	920	230	780	160	107
C_Date Historic constraint AD 1850	100	10	100	10	92.5
Boundary Sequence end			-100	230	

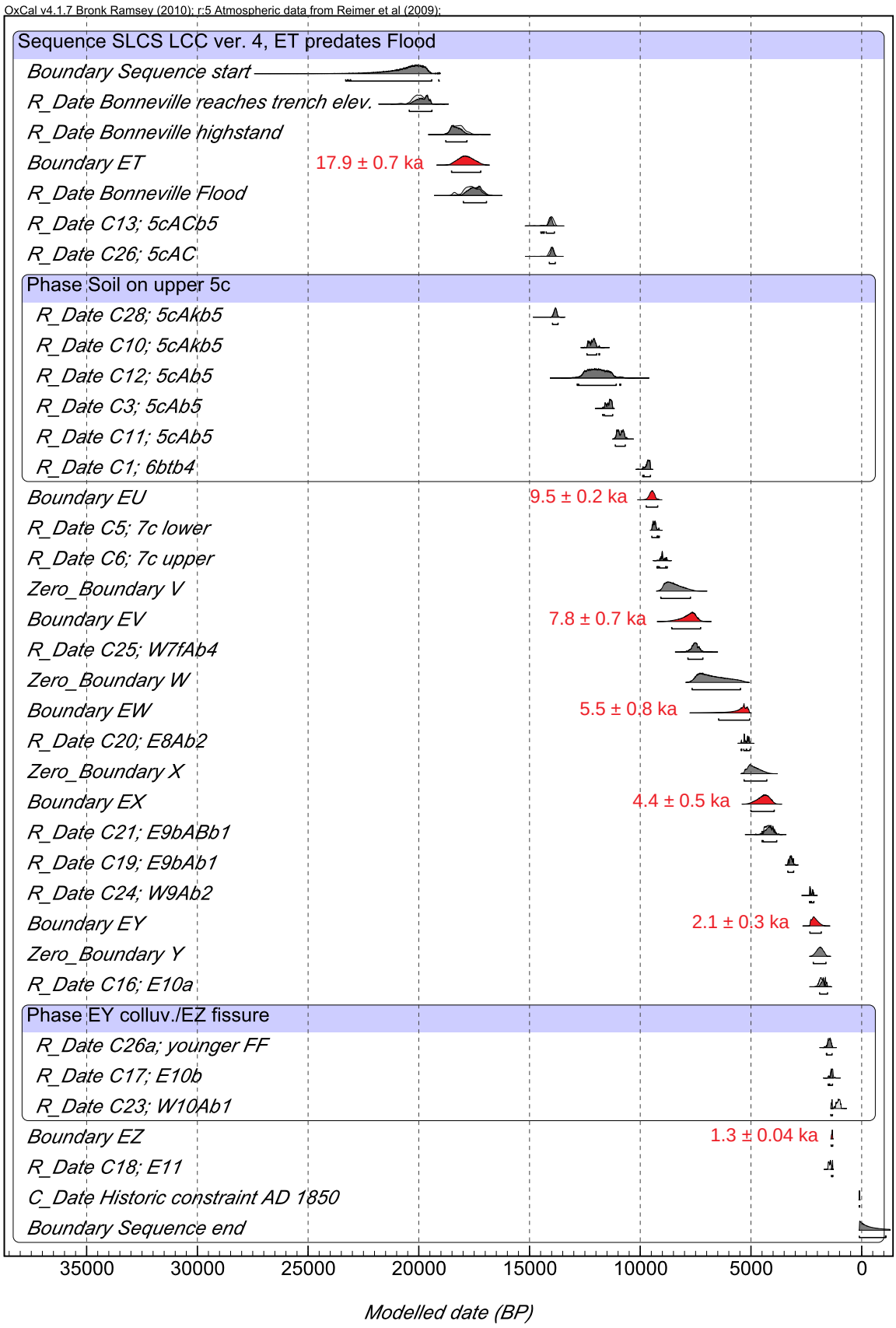
OxCal v4.1.7 Bronk Ramsey (2010); r:5 Atmospheric data from Reimer et al (2009);
Sequence SLCS LCC ver. 4, ET predates Flood
Boundary Sequence start
R_Date Bonneville reaches trench elev.
R_Date Bonneville highstand
Boundary ET
17.9 ± 0.7 ka
R_Date Bonneville Flood
R_Date C13; 5cACb5
R_Date C26; 5cAC
Phase Soil on upper 5c
R_Date C28; 5cAkb5
R_Date C10; 5cAkb5
R_Date C12; 5cAb5
R_Date C3; 5cAb5
R_Date C11; 5cAb5
R_Date C1; 6btb4
Boundary EU
9.5 ± 0.2 ka
R_Date C5; 7c lower
R_Date C6; 7c upper
Zero_Boundary V
Boundary EV
7.8 ± 0.7 ka
R_Date C25; W7fAb4
Zero_Boundary W
Boundary EW
5.5 ± 0.8 ka
R_Date C20; E8Ab2
Zero_Boundary X
Boundary EX
4.4 ± 0.5 ka
R_Date C21; E9bABb1
R_Date C19; E9bAb1
R_Date C24; W9Ab2
Boundary EY
2.1 ± 0.3 ka
Zero_Boundary Y
R_Date C16; E10a
Phase EY colluv./EZ fissure
R_Date C26a; younger FF
R_Date C17; E10b
R_Date C23; W10Ab1
Boundary EZ
1.3 ± 0.04 ka
R_Date C18; E11
C_Date Historic constraint AD 1850
Boundary Sequence end
35000
30000
25000
20000
15000
10000
5000
0
Modelled date (BP)

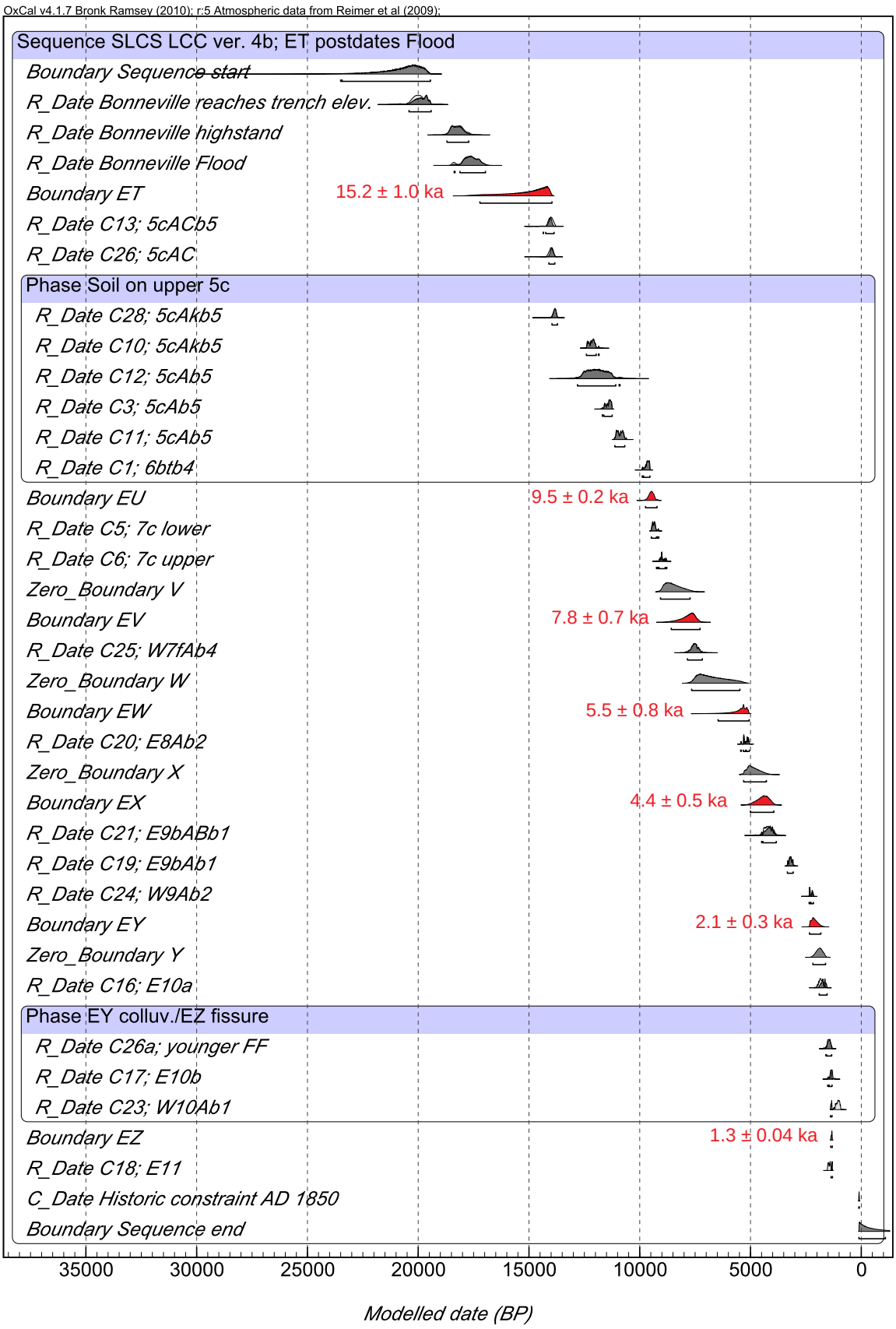
OxCal v4.1.7 Bronk Ramsey (2010); r:5 Atmospheric data from Reimer et al (2009);
Sequence SLCS LCC ver. 4b; ET postdates Flood
Boundary Sequence start
R_Date Bonneville reaches trench elev.
R_Date Bonneville highstand
R_Date Bonneville Flood
Boundary ET
15.2 ± 1.0 ka
R_Date C13; 5cACb5
R_Date C26; 5cAC
Phase Soil on upper 5c
R_Date C28; 5cAkb5
R_Date C10; 5cAkb5
R_Date C12; 5cAb5
R_Date C3; 5cAb5
R_Date C11; 5cAb5
R_Date C1; 6btb4
Boundary EU
9.5 ± 0.2 ka
R_Date C5; 7c lower
R_Date C6; 7c upper
Zero_Boundary V
Boundary EV
7.8 ± 0.7 ka
R_Date C25; W7fAb4
Zero_Boundary W
Boundary EW
5.5 ± 0.8 ka
R_Date C20; E8Ab2
Zero_Boundary X
Boundary EX
4.4 ± 0.5 ka
R_Date C21; E9bABb1
R_Date C19; E9bAb1
R_Date C24; W9Ab2
Boundary EY
2.1 ± 0.3 ka
Zero_Boundary Y
R_Date C16; E10a
Phase EY colluv./EZ fissure
R_Date C26a; younger FF
R_Date C17; E10b
R_Date C23; W10Ab1
Boundary EZ
1.3 ± 0.04 ka
R_Date C18; E11
C_Date Historic constraint AD 1850
Boundary Sequence end
35000
30000
25000
20000
15000
10000
5000
0
Modelled date (BP)

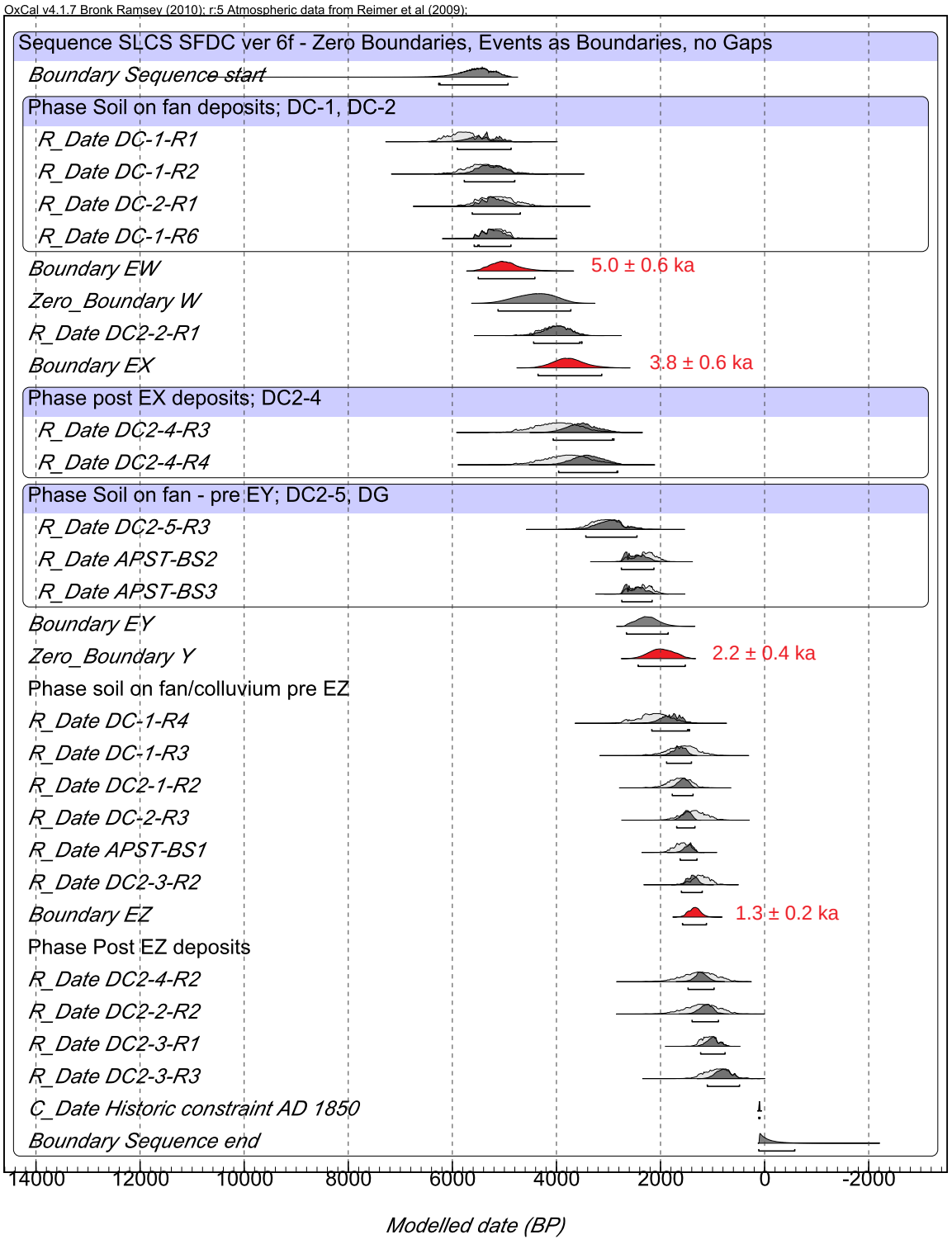
OxCal v4.1.7 Bronk Ramsey (2010); r:5 Atmospheric data from Reimer et al (2009);
Sequence SLCS SFDC ver 6f - Zero Boundaries, Events as Boundaries, no Gaps
Boundary Sequence start
Phase Soil on fan deposits; DC-1, DC-2
R_Date DC-1-R1
R_Date DC-1-R2
R_Date DC-2-R1
R_Date DC-1-R6
Boundary EW
5.0 ± 0.6 ka
Zero_Boundary W
R_Date DC2-2-R1
Boundary EX
3.8 ± 0.6 ka
Phase post EX deposits; DC2-4
R_Date DC2-4-R3
R_Date DC2-4-R4
Phase Soil on fan - pre EY; DC2-5, DG
R_Date DC2-5-R3
R_Date APST-BS2
R_Date APST-BS3
Boundary EY
Zero_Boundary Y
2.2 ± 0.4 ka
Phase soil on fan/colluvium pre EZ
R_Date DC-1-R4
R_Date DC-1-R3
R_Date DC2-1-R2
R_Date DC-2-R3
R_Date APST-BS1
R_Date DC2-3-R2
Boundary EZ
1.3 ± 0.2 ka
Phase Post EZ deposits
R_Date DC2-4-R2
R_Date DC2-2-R2
R_Date DC2-3-R1
R_Date DC2-3-R3
C_Date Historic constraint AD 1850
Boundary Sequence end
14000
12000
10000
8000
6000
4000
2000
0
-2000
Modelled date (BP)

APPENDIX F

SUMMARY OF OXCAL MODELING RESULTS FOR THE SALT LAKE CITY SEGMENT

	Mean[1] (cal yr B.P.)	**2σ**[1] (yr)	**RMS**[2] (yr)	**5th**[3] (cal yr B.P.)	**50th**[3] (cal yr B.P.)	**95th**[3] (cal yr B.P.)	**Mode**[3] (cal yr B.P.)
Penrose Drive (PD)							
PD1	3998	497	260	3530	4070	4245	4095
PD2	5888	705	353	5135	6005	6250	6205
PD3	7515	760	381	6890	7515	8150	7520
PD4	9705	1113	559	8385	9910	10,185	10,155
PD5	10,866	239	119	10,675	10,870	11,055	10,920
PD6	12,081	1587	808	11,400	11,805	13,830	11,620
PD7	16,468	1912	964	14,580	16,680	17,655	17,140
Little Cottonwood Canyon (LCC)							
LCC1 (Z)	1339	39	19	1315	1340	1375	1325
LCC2 (Y)	2105	284	142	1845	2125	2310	2155
LCC3 (X)	4440	545	272	4035	4420	4935	4370
LCC4 (W)	5532	806	404	5130	5410	6410	5315
LCC5 (V)	7826	665	333	7380	7765	8480	7655
LCC6 (U)	9473	243	121	9285	9470	9680	9460
LCC7 (T)[4]	16,547	3048	1525	14,175	17,285	18,325	17,915
South Fork Dry Creek (SFDC)							
SFDC1 (D)	1347	227	113	1165	1345	1530	1330
SFDC2 (C)	2247	414	207	1890	2255	2580	2300
SFDC3 (B)	3756	604	301	3230	3775	4230	3830
SFDC4 (A)	4984	548	275	4490	5010	5400	5050

[1] Mean and two-sigma earthquake times based on exported probability density functions (PDFs) from the OxCal models (appendix E). See DuRoss and others (2011) for discussion of methods.

[2] RMS is square root of the sum of the squared deviations from the mean, using the OxCal timing PDFs.

[3] 5th, 50th, and 95th percent values and modal earthquake times are based on exported OxCal earthquake-timing PDFs.

[4] LCC event T is based on the summed results of two separate OxCal models (see text for discussion).

UTAH GEOLOGICAL SURVEY
a division of
Utah Department of Natural Resources

Plate 1
Utah Geological Survey Special Study 149
Holocene and Latest Pleistocene Paleoseismology of the
Salt Lake City Segment of the Wasatch Fault Zone, Utah,
at the Penrose Drive Trench Site

Explanation

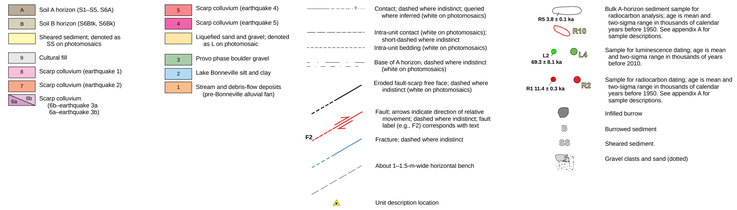

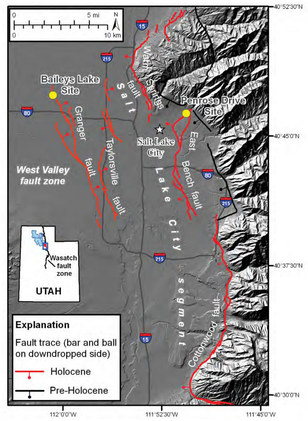

The West Valley fault zone (Granger and Taylorsville faults) and Salt Lake City segment (SLCS) of the Wasatch fault zone (Warm Springs, East Bench, and Cottonwood faults); traces from Black and others (2003). Yellow circles indicate locations of the Baileys Lake trench site at the north end of the Granger fault, and the Penrose Drive trench site at the north end of the East Bench fault. Shaded-relief base is from 2-m posting LiDAR data (2006; Utah Automated Geographic Reference Center) illuminated from the northwest.

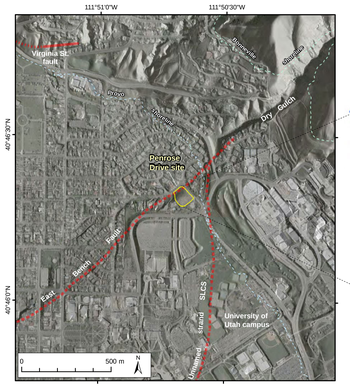

Penrose Drive trench site on the northern East Bench fault of SLCS. Bonneville-highstand and Provo shorelines approximated using mean shoreline elevations. Trace of the SLCS from Black and others (2003). Basemap is 2009 National Agriculture Imagery Program (NAIP; U.S. Department of Agriculture, 2012) aerial photography draped over 1-m-posting digital elevation model (LiDAR; Utah Automated Geographic Reference Center, 2010) illuminated from the east.

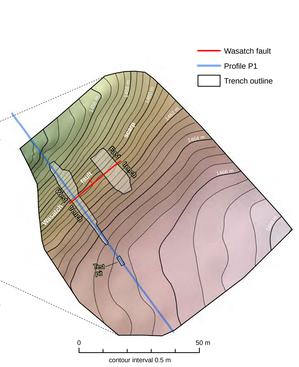

Contour map of the Penrose Drive site, showing the West and East trench locations and trace of the East Bench fault where projected to the surface (ball and bar on downthrown side). Elevations are relative to mean sea level, based on high-precision GPS data measured in 2010 (figure 8). Blue line shows location of profile P1 (figure 8).

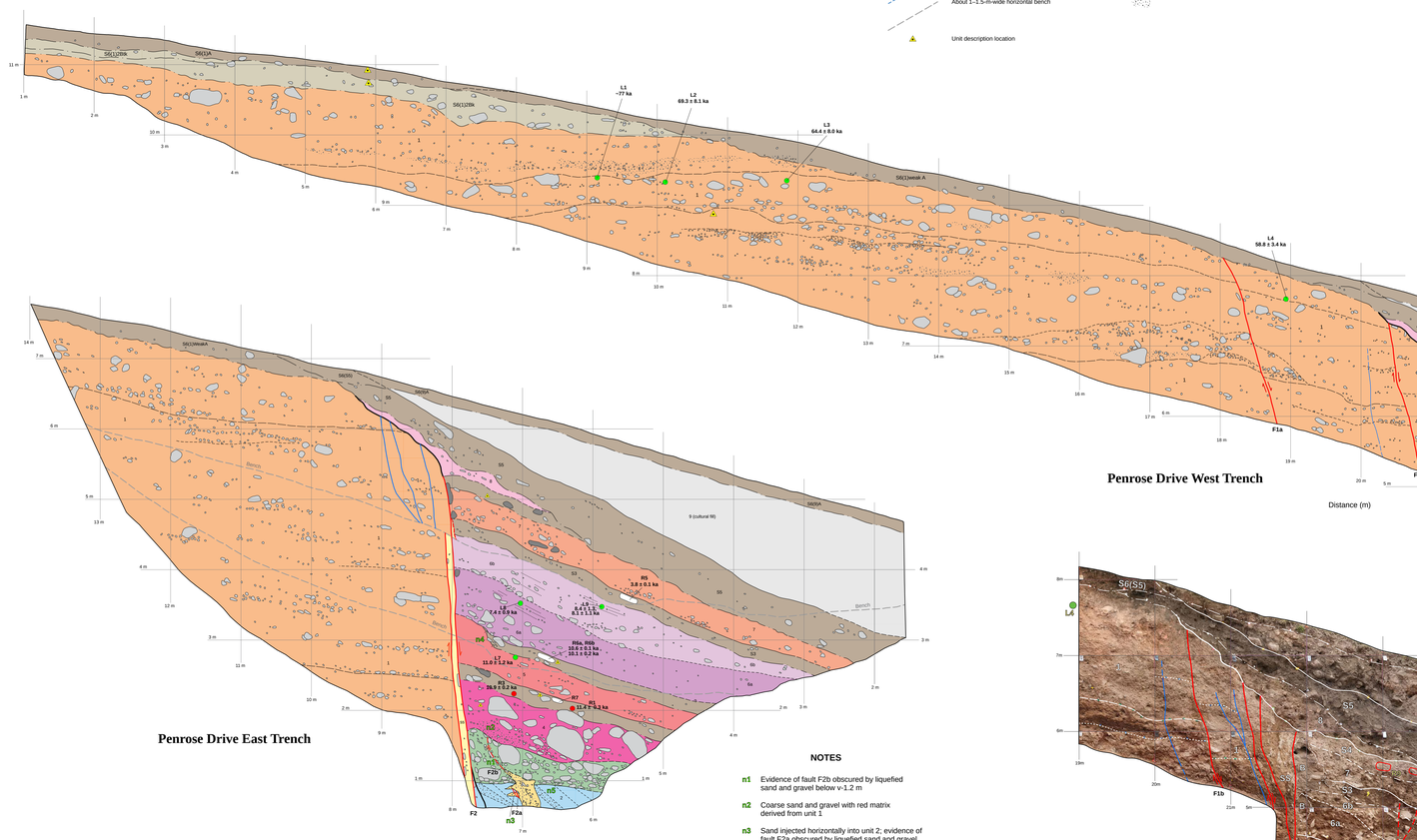

Penrose Drive West Trench

Distance (m)

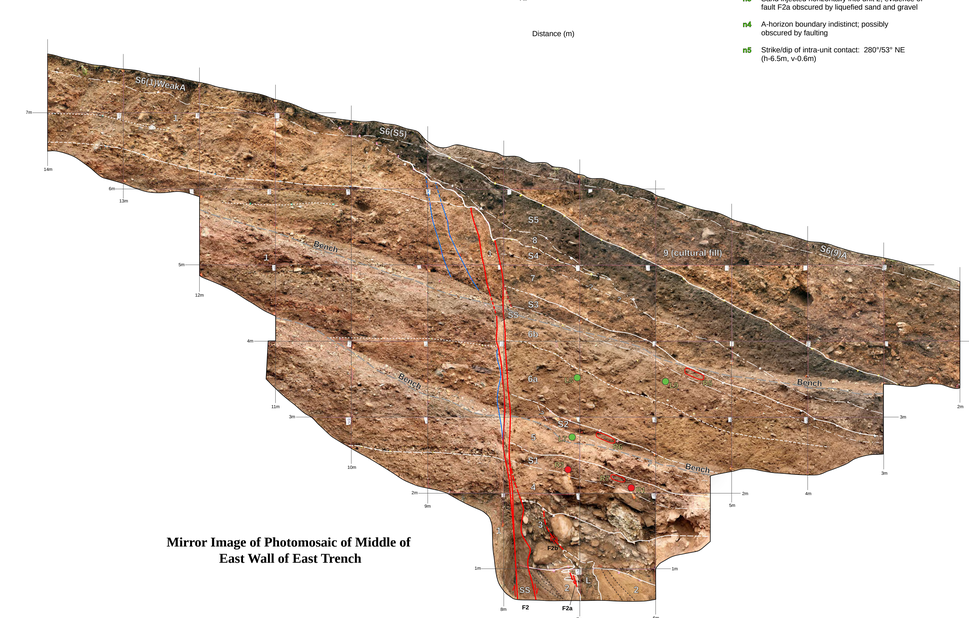

Penrose Drive East Trench

Distance (m)

NOTES

n1 Evidence of fault F2b obscured by liquefied sand and gravel below v-1.2 m

n2 Coarse sand and gravel with red matrix derived from unit 1

n3 Sand injected horizontally into unit 2; evidence of fault F2a obscured by liquefied sand and gravel

n4 A-horizon boundary indistinct; possibly obscured by faulting

n5 Strike/dip of intra-unit contact: 280°/53° NE (h-6.5m, v-0.6m)

Mirror Image of Photomosaic of Middle of East Wall of East Trench

Distance (m)

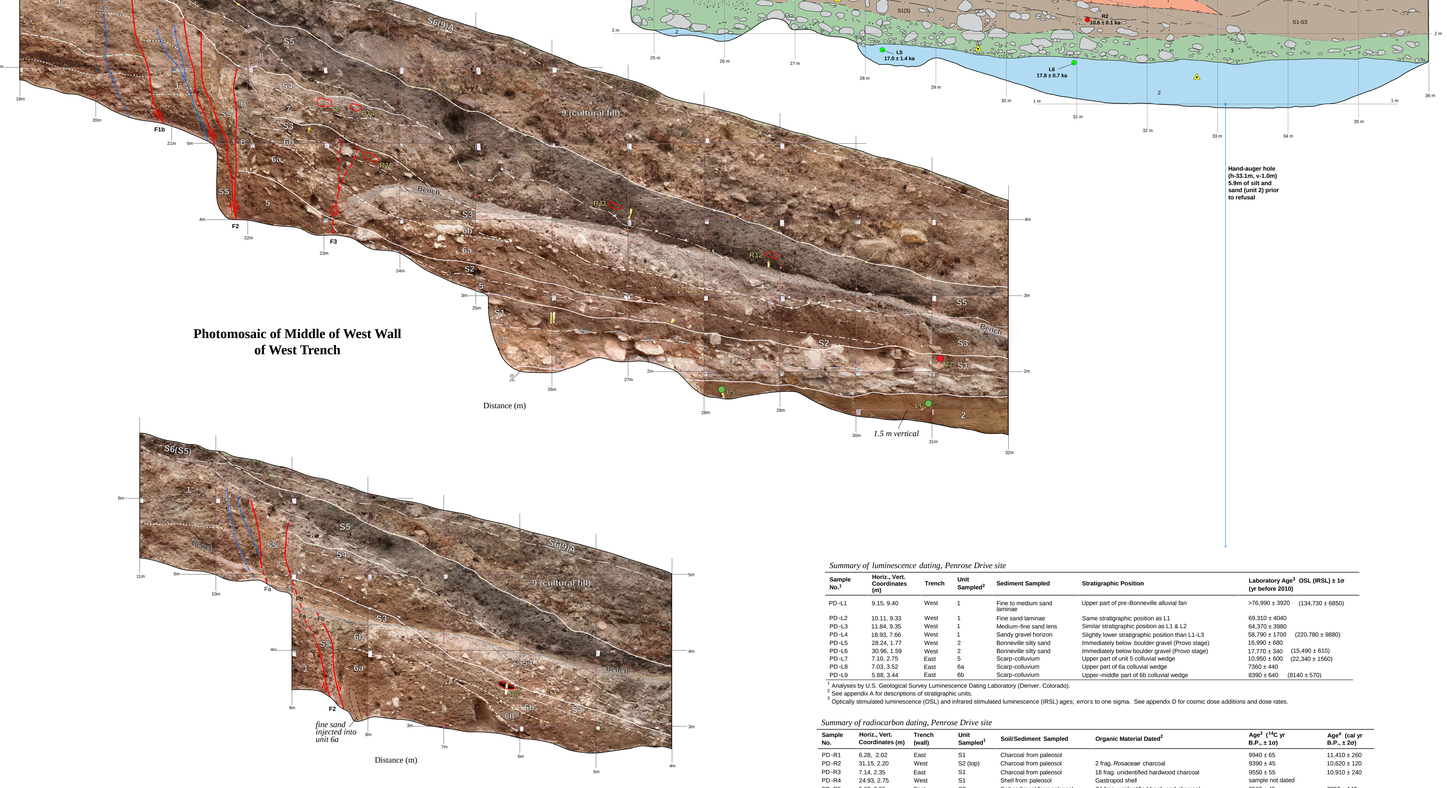

Photomosaic of Middle of West Wall of West Trench

Distance (m)

1.5 m vertical

Photomosaic of Middle of West Wall of East Trench

Distance (m)

Summary of luminescence dating, Penrose Drive site

Sample No.[1]	Horiz., Vert. Coordinates (m)	Trench	Unit Sampled[2]	Sediment Sampled	Stratigraphic Position	Laboratory Age[3] OSL (IRSL) ± 1σ (yr before 2010)
PD -L1	9.15, 9.40	West	1	Fine to medium sand laminae	Upper part of pre–Bonneville alluvial fan	>76,990 ± 3920 (134,730 ± 6850)
PD -L2	10.11, 9.33	West	1	Fine sand laminae	Same stratigraphic position as L1	69,310 ± 4040
PD -L3	11.84, 9.35	West	1	Medium–fine sand lens	Similar stratigraphic position as L1 & L2	64,370 ± 3980
PD -L4	18.93, 7.66	West	1	Sandy gravel horizon	Slightly lower stratigraphic position than L1-L3	58,790 ± 1700 (220,780 ± 9880)
PD -L5	28.24, 1.77	West	2	Bonneville silty sand	Immediately below boulder gravel (Provo stage)	16,990 ± 680
PD -L6	30.96, 1.59	West	2	Bonneville silty sand	Immediately below boulder gravel (Provo stage)	17,770 ± 340 (15,490 ± 610)
PD -L7	7.10, 2.75	East	5	Scarp-colluvium	Upper part of unit 5 colluvial wedge	10,950 ± 600 (22,340 ± 1560)
PD -L8	7.03, 3.52	East	6a	Scarp-colluvium	Upper part of 6a colluvial wedge	7360 ± 440
PD -L9	5.88, 3.44	East	6b	Scarp-colluvium	Upper–middle part of 6b colluvial wedge	8390 ± 640 (8140 ± 570)

[1] Analyses by U.S. Geological Survey Luminescence Dating Laboratory (Denver, Colorado).
[2] See appendix A for descriptions of stratigraphic units.
[3] Optically stimulated luminescence (OSL) and infrared stimulated luminescence (IRSL) ages; errors to one sigma. See appendix D for cosmic dose additions and dose rates.

Summary of radiocarbon dating, Penrose Drive site

Sample No.	Horiz., Vert. Coordinates (m)	Trench (wall)	Unit Sampled[1]	Soil/Sediment Sampled	Organic Material Dated[2]	Age[3] (^{14}C yr B.P., ± 1σ)	Age[4] (cal yr B.P., ± 2σ)
PD -R1	6.28, 2.02	East	S1	Charcoal from paleosol		9940 ± 65	11,410 ± 260
PD -R2	31.15, 2.20	West	S2 (top)	Charcoal from paleosol	2 frag. *Rosaceae* charcoal	9390 ± 45	10,620 ± 120
PD -R3	7.14, 2.35	East	S1	Charcoal from paleosol	18 frag. unidentified hardwood charcoal	9550 ± 55	10,910 ± 240
PD -R4	24.93, 2.75	West	S1	Shell from paleosol	Gastropod shell	sample not dated	
PD -R5	5.60, 3.55	East	S3	Soil sediment from paleosol	24 frag. unidentified hardwood charcoal	3560 ± 45	3850 ± 140
PD -R6a	6.65, 2.75	East	S2	Soil sediment from paleosol	14 frag. unidentified hardwood charcoal	9350 ± 50	10,570 ± 140
PD -R6b	6.65, 2.75	East	S2	Soil sediment from paleosol	6 frag. unidentified twig, vitrified	8990 ± 55	10,120 ± 200
PD -R7	6.58, 2.23	East	S1	Soil sediment from paleosol	Many frag. unidentified hardwood charcoal	sample not dated	
PD -R8	6.17, 3.52	East (west)	S3	Soil sediment from paleosol	Microcharcoal	5480 ± 50	6280 ± 120
PD -R9a	22.94, 5.56	West	S4	Soil sediment from paleosol	4 frag. unidentified hardwood charcoal	sample too small to date	
PD -R9b	22.94, 5.56	West	S4	Soil sediment from paleosol	Microcharcoal	3960 ± 45	4420 ± 160
PD -R10a	23.6, 4.80	West	S3	Soil sediment from paleosol	1 frag. *Prunus*-type seed, charred	5800 ± 75	6600 ± 180
PD -R10b	23.6, 4.80	West	S1	Soil sediment from paleosol	Microcharcoal	5470 ± 40	6270 ± 80
PD -R11	26.85, 4.20	West	S1 (base)	Soil sediment from paleosol	1 fragment *Quercus* charcoal	490 ± 35	530 ± 40
PD -R12	28.85, 3.55	West	S1 (base)	Soil sediment from paleosol	3 fragments *Artemisia* charcoal	495 ± 30	530 ± 40
PD -R13	24.83, 3.03	West	S1	Soil sediment from paleosol	7 fragments unidentified hardwood charcoal	10,000 ± 75	11,510 ± 320
PD -R14a	23.41, 5.46	West	S4	Soil sediment from paleosol	Many frag. unidentified hardwood charcoal	3790 ± 65	4180 ± 220
PD -R14b	23.41, 5.46	West	S4	Soil sediment from paleosol	Microcharcoal	3790 ± 40	4170 ±140
PD -R15	25.00, 3.40	West	S2	Soil sediment from paleosol	11 frag. unidentified hardwood charcoal	9400 ± 50	10,630 ±140
PD -R16	26.0, 3.0 to 29.6, 2.0	West	S1	Shells from paleosol and unit 3	Many gastropod shells	sample not dated	

[1] See appendix A for descriptions of stratigraphic units.
[2] Separation and identification by Paleo Research Institute (Golden, Colorado). See appendix C for additional sample notes.
[3] Laboratory-reported radiocarbon age with one standard deviation uncertainty. B.P. is before present (AD 1950).
[4] Mean calendar–calibrated age and two–sigma uncertainty, rounded to nearest decade, determined using OxCal calibration software (v. 4.1; Bronk Ramsey, 2009) and the IntCal09 atmospheric data set (Reimer and others, 2009).

STRATIGRAPHIC AND STRUCTURAL RELATIONS AT THE PENROSE DRIVE TRENCH SITE, SALT LAKE CITY SEGMENT, WASATCH FAULT ZONE

by

Christopher B. DuRoss, Michael D. Hylland, Greg N. McDonald, Anthony J. Crone, Stephen F. Personius, Ryan D. Gold, and Shannon A. Mahan

2014